A THREE-DIMENSIONAL MODEL OF ATMOSPHERIC CO_2 TRANSPORT BASED ON OBSERVED WINDS: 2. MODEL DESCRIPTION AND SIMULATED TRACER EXPERIMENTS

Martin Heimann

Max-Planck-Institut für Meteorologie, Bundesstrasse 55
D-2000 Hamburg 13, FRG

Charles D. Keeling

Scripps Institution of Oceanography, La Jolla, California, 92093, U.S.A.

Abstract. The three-dimensional atmospheric transport model developed at the Goddard Institute of Space Sciences (GISS) has been modified in its coarse-grid version ($7.83° \times 10.00°$ horizontal resolution, 9 layers in vertical direction) by replacing the original model-generated wind fields with observed winds of the Global Weather Experiment, covering the period December 1978 through November 1979. The parameterization of subgridscale vertical convection was retained from the earlier model version, except that all intensities were reduced by 50 percent. To simulate atmospheric CO_2 and its $^{13}C/^{12}C$ ratio, sources and sinks of carbon at the earth's surface were prescribed. The net primary productivity of the terrestrial biosphere was computed from vegetation index (NDVI) data representing the greenness of the land as recorded by the AVHRR instrument flown on satellites of the U.S. National Oceanic and Atmospheric Administration. The productivity for a given greenness was assumed to be proportional to the amount of photosynthetically active radiation reaching the plant canopy as computed from estimates of solar insolation under clear sky conditions with an allowance for attenuation caused by the presence of clouds. Estimates of cloud cover were based on satellite data of daily albedo. The respiration of terrestrial plant detritus and soils was assumed to be dependent on temperature but was globally adjusted to achieve an optimal fit of the model prediction of the seasonal cycle of atmospheric CO_2 to that observed at four northern hemisphere stations. The oceanic exchange of CO_2 was prescribed from rough estimates of the CO_2 partial pressure of sea water, assuming a constant air-sea exchange rate. The mean annual partial pressure field was afterwards adjusted to achieve an optimal fit with respect to broad geographic features of the observed mean annual atmospheric CO_2 field. The seasonal variation in partial pressure was assumed to depend on sea-surface temperature, but the variation was reduced poleward of 35° in both hemispheres to account, at least crudely, for marine plant activity. Perturbations of the global carbon cycle arising from industrial CO_2 production and anthropogenic changes in land use were also modeled, as well as a postulated net annual uptake of CO_2 by the terrestrial biosphere in recent years attributed to enhanced plant activity. The $^{13}C/^{12}C$ of atmospheric CO_2 was predicted by the model taking into account the degree to which these stable isotopes were fractionated by the sources and sinks prescribed for the CO_2 concentration. Purely isotopic source components arising from temperature dependency of the air-sea exchange of CO_2 and resulting from the carbon-13 Suess effect were also taken into account. In addition the transport properties of the model were tested by simulating the dispersal of two radioactive tracers having simple source/sink configurations: krypton-85 and radon-222. The model gives satisfactory predictions of the meridional concentration gradient of krypton-85 and of the seasonally changing vertical gradient of radon-222 over the continents.

1. Introduction

Taking full advantage of the available data on the concentration and isotopic ratios of atmospheric CO_2 requires that transport within the atmosphere be accounted for, since the three-dimensional circulation greatly modifies the distribution of CO_2 produced by the local release and uptake of CO_2 gas by the oceans and the land. Thus, as the distribution of CO_2 in the air has become better documented, the need has increased for a realistic representation of the atmospheric circulation and the associated transport of CO_2.

We describe here a study in modeling the temporal and spatial distribution of atmospheric CO_2 by means of an atmospheric transport model based on observed three-dimensional, time-varying wind fields coupled with specifications of the gas exchange fluxes of atmospheric CO_2 with the oceans and the land. The portrayed oceanic exchanges are driven by the action of the carbon cycle through variations in the CO_2 pressure difference across the air-sea boundary. The portrayed exchanges on land are controlled by the terrestrial biosphere, that is, by the photosynthesis and respiration of land plants, the decay of their litter, and processes within soils.

237

The burning of fossil fuels and man-induced disturbances of the terrestrial biosphere are taken into account through appropriate specification of the locations and strengths of their sources and sinks.

The ultimate goal of this study is to predict the observed distribution of atmospheric CO_2 and its $^{13}C/^{12}C$ ratio in space and time as closely as possible. This allows us to draw conclusions regarding the behavior of the oceanic and biospheric components of the carbon cycle by estimating the source/sink configurations which result in predictions that compare best with the observations.

The more limited goal of this article is to establish a methodology for predicting the distribution of atmospheric CO_2 by means of a set of components representing the most important oceanic and terrestrial exchanges of CO_2 with the atmosphere. We do not deal exhaustively with all known aspects of these exchanges, however. Rather, we strive to produce predictions which can be tested against direct observations of atmospheric CO_2 in a manner conducive to devising more realistic models in the future. Given the complexity of the carbon cycle, and our limited knowledge of its transport behavior, we are obliged to invoke a considerable number of assumptions in the course of formulating our model. We do not attempt here to justify all of these assumptions in detail, but rely on subsequent sensitivity tests of the model to challenge the most critical ones. These are discussed in the final article by Keeling et al. [this volume, b].

In this article we first describe the structure of the atmospheric tracer model, the data used in constructing the transport terms, and an attempt to validate the model by simulating the distribution of the radioactive tracers ^{85}Kr and ^{222}Rn. Afterwards we describe the source/sink components that were used to simulate the concentration and the $^{13}C/^{12}C$ ratio of atmospheric CO_2. The results of the model study in terms of the seasonal cycle of CO_2 are presented by Heimann et al. [this volume] and the analysis of the mean annual concentration fields is discussed by Keeling et al. [this volume, b]. Each of these subsequent articles briefly summarizes the properties of the model now to be presented. Readers interested mainly in the results of the model, rather than the details of its formulation, may at this point turn directly to these articles.

2.   Model Description

The three-dimensional tracer model used in our study originally was developed by Russell and Lerner [1981] and has been used to study the global scale dispersion of gaseous atmospheric tracers with moderate to long lifetimes, such as CO_2 [Fung et al., 1983, 1986; Heimann et al., 1986], halocarbons [Prather et al., 1987] and krypton-85 [Jacob et al., 1987]. The model numerically solves the continuity equation for the concentration $C(\mathbf{x},t)$ of a tracer

$$\frac{d}{dt}(\rho(\mathbf{x},t)\,C(\mathbf{x},t)) = Q(\mathbf{x},t) \tag{2.1}$$

on a three-dimensional grid spanning the whole global atmosphere. Here $\rho(\mathbf{x},t)$ denotes the density of air and $Q(\mathbf{x},t)$ a source term specified according to the physics and chemistry of the tracer under consideration. The concentration, $C(\mathbf{x},t)$, is expressed as a volume mixing ratio, i.e., a mole fraction. The quantities, ρ, C, and Q, all vary with the three space coordinates, $\mathbf{x} \equiv x,y,z$, and with the time, t.

In addition to equation (2.1) tracer specific boundary conditions have to be imposed at the top of the model atmosphere located at 10 hPa (= 10 mb) and at the surface of the earth. For the simulation of the inert CO_2 gas and its $^{13}C/^{12}C$ ratio, $Q(\mathbf{x},t)$ is set to zero and the CO_2 exchange fluxes between the atmosphere and the other carbon reservoirs are specified as boundary fluxes at the surface of the earth. By assumption no CO_2 flux crosses the top of the model atmosphere.

The total time derivative following the motion of the air is written as

$$\frac{d}{dt}(\_) = \frac{\partial}{\partial t}(\_) + \nabla \cdot \mathbf{v} \cdot (\_) + CONVEC\,(\_) \tag{2.2}$$

The advective term has been split into one part that is explicitly resolved on the grid of the model with wind velocities $\mathbf{v}(\mathbf{x},t)$ and another part, termed CONVEC, which represents the effects of subgridscale motions in the vertical dimension.

The model grid, identical to the grid of climate model II of Hansen et al. [1983, Figure 1], has a horizontal spacing of approximately 7.83° latitude (180°/23) by exactly 10° longitude (midpoints of boxes at 0°, 10°, etc.). The specific latitudes of the midpoints and southern latitudinal boundaries of the boxes are shown in Table 1. There are 9 layers in the vertical, of which the topmost

TABLE 1. Latitudinal Coordinates of the
Three-Dimensional Atmospheric
CO_2 Transport Model

Zonal Index No.	Mid-Zone	Southern Boundary
24	90.00 N.	86.09 N.
23	82.17 N.	78.26 N.
22	74.35 N.	70.43 N.
21	66.52 N.	62.61 N.
20	58.70 N.	54.78 N.
19	50.87 N.	46.96 N.
18	43.04 N.	39.13 N.
17	35.22 N.	31.30 N.
16	27.39 N.	23.48 N.
15	19.57 N.	15.65 N.
14	11.74 N.	7.83 N.
13	3.91 N.	0.00
12	3.91 S.	7.83 S.
11	11.74 S.	15.65 S.
10	19.57 S.	23.48 S.
9	27.39 S.	31.30 S.
8	35.22 S.	39.13 S.
7	43.04 S.	46.96 S.
6	50.87 S.	54.78 S.
5	58.70 S.	62.61 S.
4	66.52 S.	70.43 S.
3	74.35 S.	78.26 S.
2	82.17 S.	86.09 S.
1	90.00 S.	

Note

Model grid boxes each have an extent of 180/23 degrees latitudinally, except the polar boxes, which are centered on the poles and have a meridional extent of 180/46 degrees.

TABLE 2. Vertical Coordinates of the Three Dimensional Atmospheric Transport Model

Model Level	Model levels (σ coordinate) Boundary	Delta	Global mean pressure levels (hPa)[a] Boundary	Delta	"Mean level"	Geopotential Height (km)[b]
	0.000000		10			26.2
9		0.0616		60	27	22.3
	0.061602		70			17.8
8		0.0821		80	103	15.7
	0.143737		150			13.6
7		0.1078		105	201	11.8
	0.251540		255			10.2
6		0.1386		145	321	8.7
	0.390144		390			7.3
5		0.1643		160	468	5.9
	0.554415		550			4.7
4		0.1745		170	634	3.6
	0.728953		720			2.6
3		0.1376		134	786	1.9
	0.866530		854			1.2
2		0.0821		80	894	0.8
	0.948665		934			0.4
1		0.0513		50	959	0.2
	1.000000		984			0.0

[a]Boundaries of global mean pressure levels are computed from corresponding σ values using $p = p_{top} + \sigma(p_s - p_{top})$, where p_s, the global average surface pressure, is taken to be 984 hPa and the topmost boundary of the model, P_{top}, is fixed at 10 hPa. The global "mean levels" of the model layers are from Hansen et al. [1983].

[b]Approximate heights above sea level are computed from the global mean pressure levels assuming a uniform lapse rate, γ, of 6.5 K km^{-1}, and using the equation from Holton [1979, p. 24]:

$$Z = \frac{T_o}{\gamma}\left[1 - (\frac{p_o}{p_1})^{-R\frac{\gamma}{g}}\right]$$

where Z denotes the geopotential height in km; T_o and p_o are estimates of the global average surface temperature and pressure, 293 K and 984 hPa, respectively; R, the gas constant, is 287 m^2 s^{-2} K^{-1} and g, the acceleration of gravity, is 9.81 m s^{-2}.

2 are in the stratosphere (centered at 27 and 103 hPa). Table 2 lists the global average pressures and approximate heights of the vertical boundaries and midpoint heights. The lowermost 2 layers are centered at global averages of 959 hPa and 894 hPa, thus resolving the surface boundary layer with slightly more detail than the rest of the troposphere. The model uses reduced pressure (sigma) coordinates in the vertical [Holton, 1979, p. 199; Hansen et al. 1983, p. 612]. The tracer is advected by a three-dimensional, time-dependent wind field and is mixed vertically by convection.

The wind fields used in the original tracer model were obtained from the three-dimensional general circulation climate model of the atmosphere (climate GCM) developed by Hansen et al. [1983] at the Goddard Institute for Space Studies (GISS). Using this original tracer model to study the mean annual gradients of atmospheric CO_2, we noticed that the model predicted too small an interhemispheric exchange [Heimann et al., 1986]. Since this feature is of primary importance in interpreting global scale atmospheric concentration gradients in terms of sources and sinks, and since, a priori, one would expect directly observed wind data to be superior to simulated winds, we replaced in the present study the GISS climate model wind fields by wind fields derived from the

meteorological fields analyzed during the GWE (Global Weather Experiment, formerly called "FGGE") from December 1978 through November 1979. These fields were derived from practically all available meteorological observations of the GWE time period by means of the four-dimensional assimilation system in operation at the European Center for Medium-Range Weather Forecast (ECMWF) [Bengtsson et al., 1982; Hollingsworth et al., 1985]. This data set has been widely used. Possible problems with these data have been discussed, for example, by Julian [1983] and Lambert [1983] and more recently by Trenberth [1987, 1988]; nevertheless it represents one of the most comprehensive assessments of the state of the global troposphere currently available.

The use of observed winds to drive the tracer model results in a further advantage. Model predictions may be directly compared to observations pertaining to the specific time period of the wind fields. This comparison provides a much more stringent test than merely to compare the model results to observations in a climatological sense.

We converted geopotential data and horizontal wind data of the 1.825° by 1.825° grid GWE data set to the tracer model grid by transforming the data into the sigma coordinate system and then

integrating the mass fluxes over the sides of the grid boxes of the tracer model as described in Appendix A. In a second step, mass conservation in each grid column was achieved by adjusting the horizontal wind fields so that the vertically integrated air mass convergence matched the rate of change of the surface pressure during each time step of 12 hours for which the data were available, as described in Appendix B. The needed adjustment was found to be small; it amounted typically to 4 percent of the interpolated and integrated mass flux fields.

Figure 1 displays the zonally averaged meridional circulation based on the GWE data set, as resolved on the transport model grid, by means of a mass stream function averaged for each of the four seasons. These displays permit a direct comparison of the present transport model, based on the GWE wind fields, with the simulated wind fields of the original transport model (see Fung et al. [1983], Figure 1). The zonally averaged meridional circulations in the two tracer models are substantially different. The present model compared to the GISS climate model, exhibits about 20 percent weaker Hadley cells (see, for example, Holton [1979], p. 273) in the tropics but stronger Ferrel cells [loc. cit] poleward, more prominently in the southern hemisphere. Further differences exist in the extent and position of the meridional circulation cells of the two models.

The parameterization of the vertical convection was retained from the previously used GISS climate GCM, in which dry and moist convection are modeled at each time step through air mass exchange between vertical layers that are conditionally unstable. The monthly average frequencies of vertical convection in each grid column, obtained from the climate GCM in the form of a transition matrix, M_c, are used in the tracer model to determine the
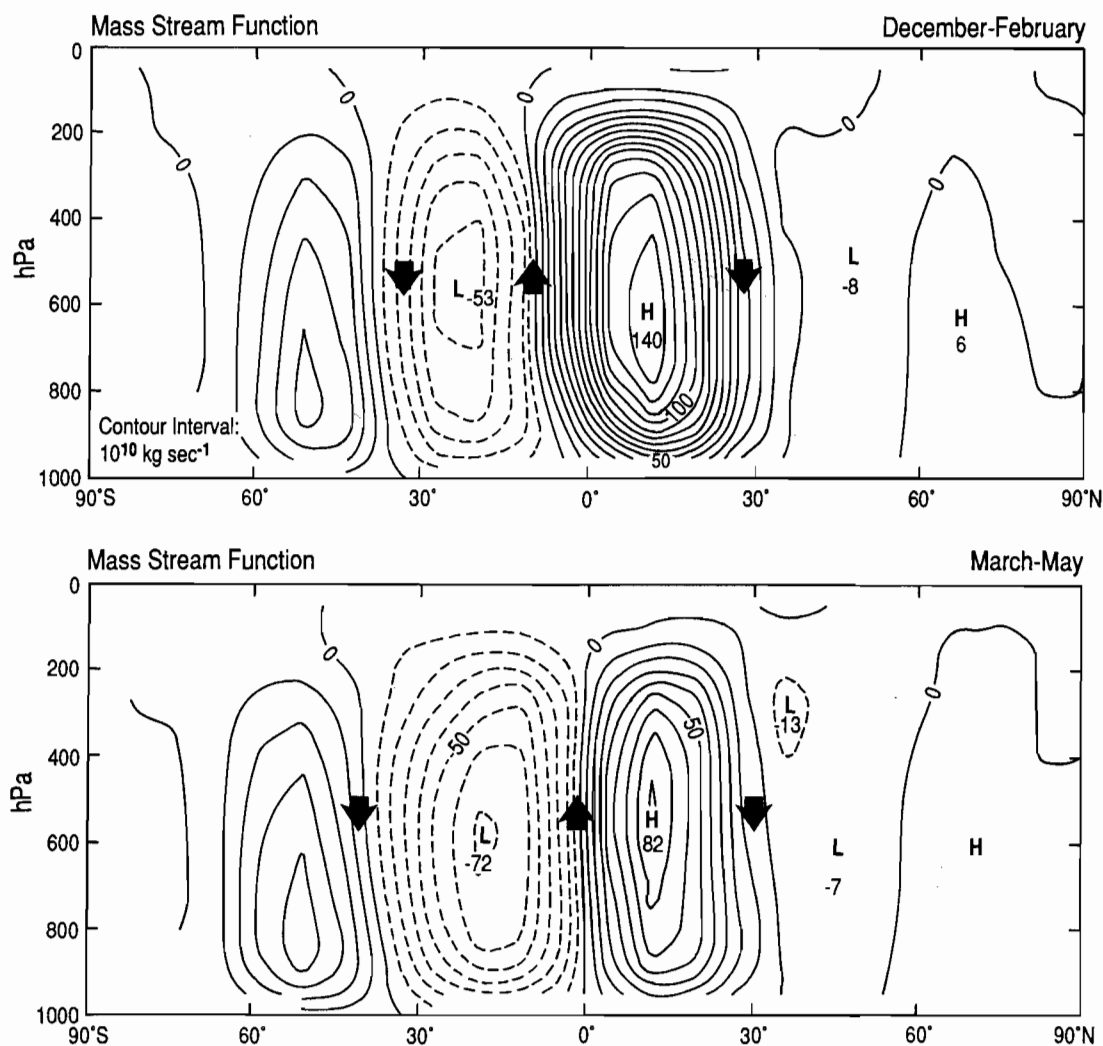

Fig. 1. Latitude-height display of the zonally averaged mass stream function of the meridional circulation used in the three-dimensional model averaged for each season as indicated on the separate panels. Contour labels are expressed in units of 10^9 kg sec^{-1}. Solid contour lines indicate positive stream function. Negative lines indicate negative stream function.

Mass Stream Function   June-August

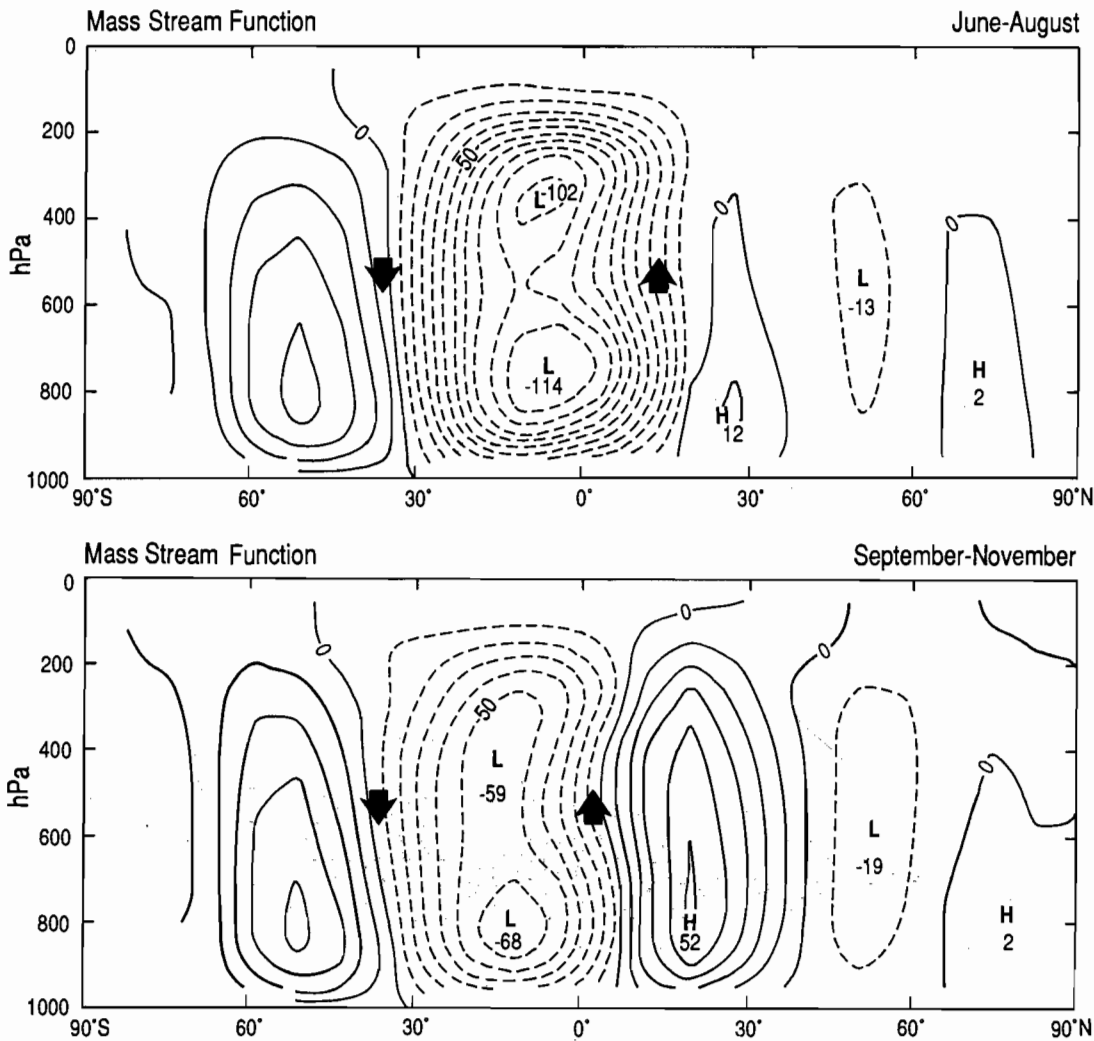Mass Stream Function   September-November

Fig. 1. -- continued

amount of air exchanged in each time step between the various layers [Hansen et al. 1983, p. 621; Prather et al., 1987].

In a preliminary investigation it was found that the simulated seasonal CO_2 cycles were not enough attenuated with height as compared to the CO_2 data from aircraft of Keeling et al. [1968]. We therefore reduced the vertical convection to a fraction ζ of the original value by replacing the transition matrix M_c with

$$M_c^* = (1-\zeta)I + \zeta M_c \qquad (2.3)$$

where I denotes the identity matrix.

By setting the parameter ζ equal to 0.50 we obtained reasonable agreement with the aircraft data, although a reduction to 0.25 of the original value would have been preferable in higher latitudes. All model runs were carried out with both 0.25 and 0.50 of the original convective parameterization in order to assess the sensitivity of the results to this particular model feature. All the presented results refer to the $\zeta = 0.50$ case unless quoted otherwise.

The use of a convective parameterization from a particular run of a climate GCM in conjunction with the GWE wind fields is not entirely consistent. Ideally, subgridscale vertical mixing processes should be calculated by means of a convective model which is driven by the large scale atmospheric structure as resolved on the model grid. Such a model is included in the ECMWF's weather forecast general circulation model which was used in assimilating the GWE wind fields. A recalculation of individual convective events and their vertical mixing characteristics from the GWE meteorological fields, however, was beyond the scope of this study.

The approach chosen in the present study is to use only monthly averaged convection matrices based on the GISS climate model run. We assume that these represent an acceptable approximation to a climate average, at least with respect to geographic structure and seasonality.

In order to illustrate the effect of the transport process owing to vertical convection we display in Figure 2, for winter and summer, the vertical displacement of a unit tracer mass injected into the lowest model layer at each grid location. Shown are the vertical position, in sigma units, of the center of gravity of the tracer mass

Dec, Jan and Feb   Convective Transport
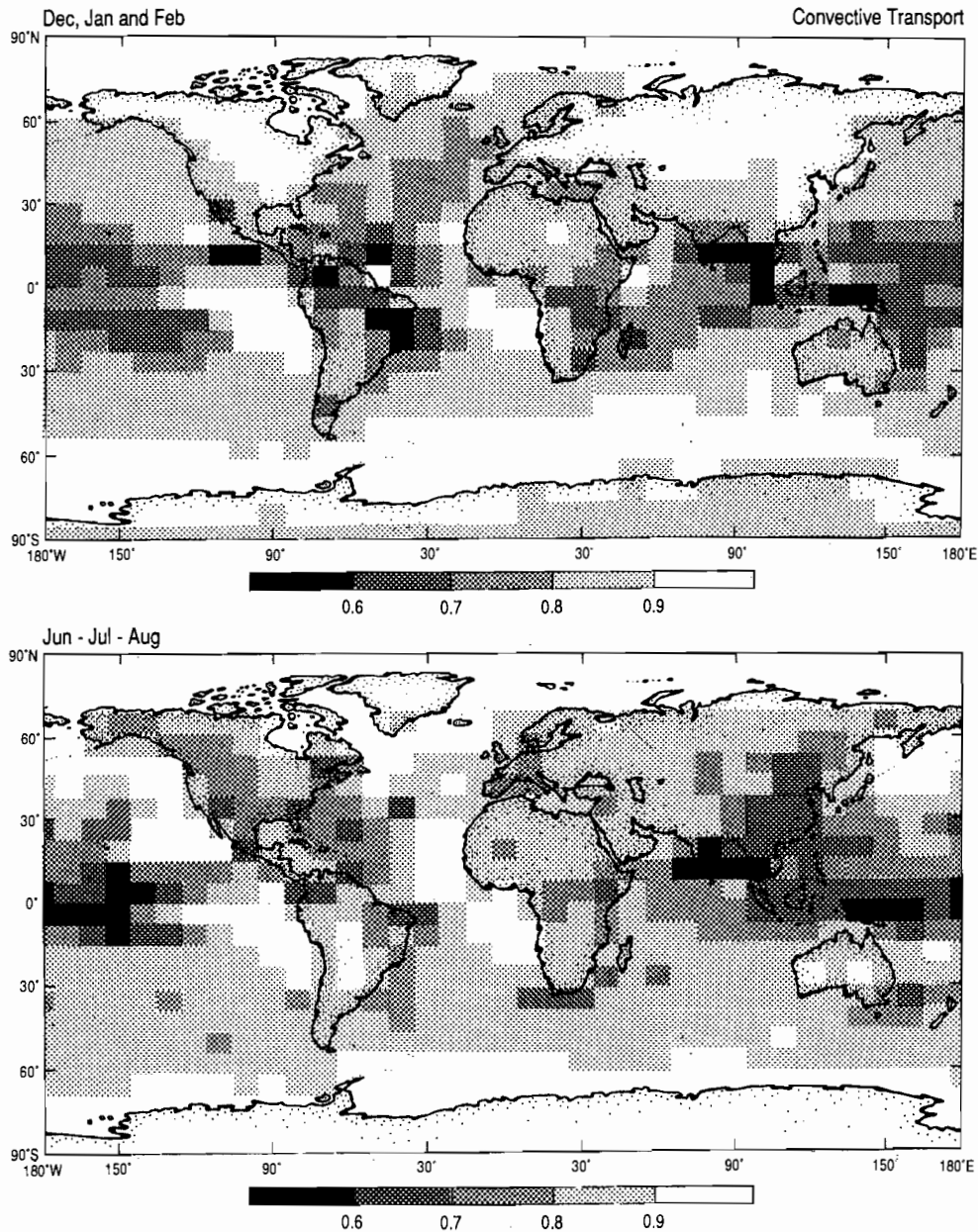

Jun - Jul - Aug

Fig. 2. Vertical model transport occurring solely by convective processes, for winter and summer. Gray shades indicate height of center of tracer mass 24 hours after injection of a unit tracer mass into the lowest model layer in each grid box column. The gray scale is labelled in sigma units; for example, 0.6 denotes a height in pressure units of $p_{top} + 0.6(p_s - p_{top})$ or approximately 594 hPa (see Table 2). Winter refers to the average for December through February, summer to the average for June through August.

after 24 hours, calculated without advective terms and by setting the convective parameter ζ equal to 0.5. It is seen that the effect of vertical convection is most noticeable in tropical regions, where the center of the tracer cloud may be lifted by almost 500 hPa within 24 hours. The convection patterns differ between January and July in association with the seasonally changing tropical circulation. There is also a marked contrast over the northern hemi-sphere continents between the summer and winter season which is directly related to the differing vertical stability of the troposphere.

The model uses a computational time step of 4 hours. In each time step transport by advection is carried out by means of the numerical "slopes scheme," developed by Russell and Lerner [1981]. This scheme, in addition to computing the tracer concentration, also computes the time evolution of the concentration gra-

dient in each grid box. The scheme is comparable in accuracy to a fourth order scheme. Indeed, in the presence of density variations, it is superior to the latter.

Each complete advective step is further subdivided into seven substeps using a spatial leap-frog pattern [Russell and Lerner, 1981]:

> 1 hour in east-west direction,
> 2 hours in north-south direction,
> 1 hour in east-west direction,
> 4 hours in vertical direction,
> 1 hour in east-west direction,
> 2 hours in north-south direction,
> 1 hour in east-west direction.

This arrangement effectively represents a different time step size in the three dimensions, which is forced by the differing typical sizes of the components of the wind vector. In high latitudes, where the longitudinal extent of the grid boxes is reduced, a further subdivision of the advective substep in the east-west direction is made.

After each advective step vertical convection is simulated by applying the transition matrices to the vertical columns as described above.

The use of time varying wind fields, which are updated every 12 hours, does not in principle necessitate any explicit horizontal diffusion since the individual synoptic disturbances are resolved in time and retained in the model. Nevertheless, some horizontal motions are lost when the wind fields are averaged onto the model grid with its rather coarse 7.83° by 10° horizontal resolution. On the other hand the numerical advection scheme inevitably introduces a small amount of diffusion, as has been shown by Russell and Lerner [1981].

Prather et al. [1987] improved the performance of the tracer model based on the GISS wind fields by introducing an additional horizontal diffusion term associated with large convective events. Thereby these authors were able to change the interhemispheric exchange time of any tracer employed in the model. Because of the importance of this exchange time with respect to the north-south distribution of atmospheric CO_2, Keeling et al. [this volume, b] have introduced a horizontal diffusive term into our model in the same way as Prather et al. [1987, Appendix B6], as a sensitivity test.

3.   Model Validation with Radioactive Tracers ^{85}Kr and ^{222}Rn

In order to predict realistically the dispersal of long-lived atmospheric tracers such as CO_2, two basic features of the atmospheric circulation have to be modeled correctly: the large-scale exchange of air between the hemispheres and the mixing intensity in the vertical dimension. The way a model of atmospheric transport incorporates these crucial features may be tested by simulating the dispersal of the tracers krypton-85 and radon-222, since both tracers exhibit fairly simple source configurations at the surface of the earth, and both are removed primarily by radioactive decay. We now discuss simulations of the transport of these two tracers using the three-dimensional model described in the previous section.

The limited existing data on the spatial and temporal distribution of these tracers cannot provide an exhaustive validation of the tran-

sport model, nor be used uniquely to calibrate it. Nevertheless, the model generated distributions of these tracers provide a useful initial visualization of the model's basic transport characteristics.

3.1   Krypton-85

Krypton–85 (^{85}Kr) is a radioactive noble gas which is released in the northern hemisphere as a waste product of nuclear fuel reprocessing; it is removed from the atmosphere primarily by radioactive decay with a mean lifetime, λ_{Kr}, of 15.6 years [Weast, 1966]. Only a negligible fraction enters the oceans. The long lifetime of ^{85}Kr, compared to typical mixing times in the troposphere and the simple pattern of sources, located almost entirely at a few isolated places in the northern hemisphere, makes it an almost ideal atmospheric tracer to study large-scale transport, and in particular interhemispheric exchange processes.

Recently, Jacob et al. [1987] presented the detailed results of a ^{85}Kr simulation study by means of a three-dimensional tracer model. Our present approach is similar to that of Jacob and coworkers. Since we are only interested in a validation of the model with respect to large scale transport, we present and discuss here only briefly the ^{85}Kr simulation experiments.

In order to calculate the large-scale distribution of ^{85}Kr with the transport model we extend a study by Rath [1988] who investigated geographical location and temporal trends of the sources of ^{85}Kr. His ^{85}Kr emission data for the years 1975–1983 are listed in Table 3. The data for the reprocessing plants not located in the Soviet Union were obtained from various statistics of nuclear fuel reprocessing. The source strength of the sole reprocessing plant in the Soviet Union, located in Kyshtym near Sverdlovsk was obtained as the difference between the non-Soviet contribution and the global source emissions as implied from the time trend of the global atmospheric inventory of ^{85}Kr. This global inventory was estimated by means of a two-dimensional model simulation of ^{85}Kr constrained by observations from a series of monitoring stations of the Institute for Atmospheric Radioactivity in Freiburg, Germany. This procedure neglects other possible sources, such as nuclear power plants and nuclear research facilities, the combined contribution of which, however, is estimated to be less than 5 percent of the global emissions [Rath, 1988] (W. Weiss, personal communication).

We started the three-dimensional model simulation run from an initial globally uniform ^{85}Kr concentration of 13.5 pCi m^{-3} for January 1, 1975 [Rath, 1988]. The model was run by successively cycling through the annual set of wind fields while the source emissions were changed for every simulated year since 1975 through 1983 (see Table 3). At every time step the ^{85}Kr concentration was adjusted at every model grid point for the radioactive decay.

Figure 3 shows four meridional profiles of the ^{85}Kr concentration from 1981–1983 as predicted by the model in the surface layer at 30°W. over the Atlantic Ocean. Each profile represents a monthly mean of the predicted daily concentration values. The shaded areas denote the range within one standard deviation of the predicted daily values from the monthly mean. Also shown are concentrations of ^{85}Kr measured on air samples collected on three ship cruises in the Atlantic Ocean [Weiss et al., 1983] (Weiss, personal communication).

TABLE 3. Annual Production of Krypton-85 by Nuclear Fuel Reprocessing Plants, 1975–1983 (in 10^3 Ci yr^{-1})

Plant[a]:	1	2	3	4	5	6	7	8	9[b]
1975	294	24	520	1200	100	657	43	0	1559
1976	250	33	711	1200	92	343	86	0	2067
1977	108	111	448	800	117	669	115	0	2893
1978	291	101	530	700	308	786	34	60	2955
1979	283	0	480	940	280	642	51	0	3535
1980	276	92	580	840	535	825	32	280	3064
1981	212	59	840	1400	310	969	70	110	2691
1982	95	9	515	1190	310	1220	16	190	3103
1983	214	3	698	1129	620	1356	76	90	2442

[a]Plant Locations

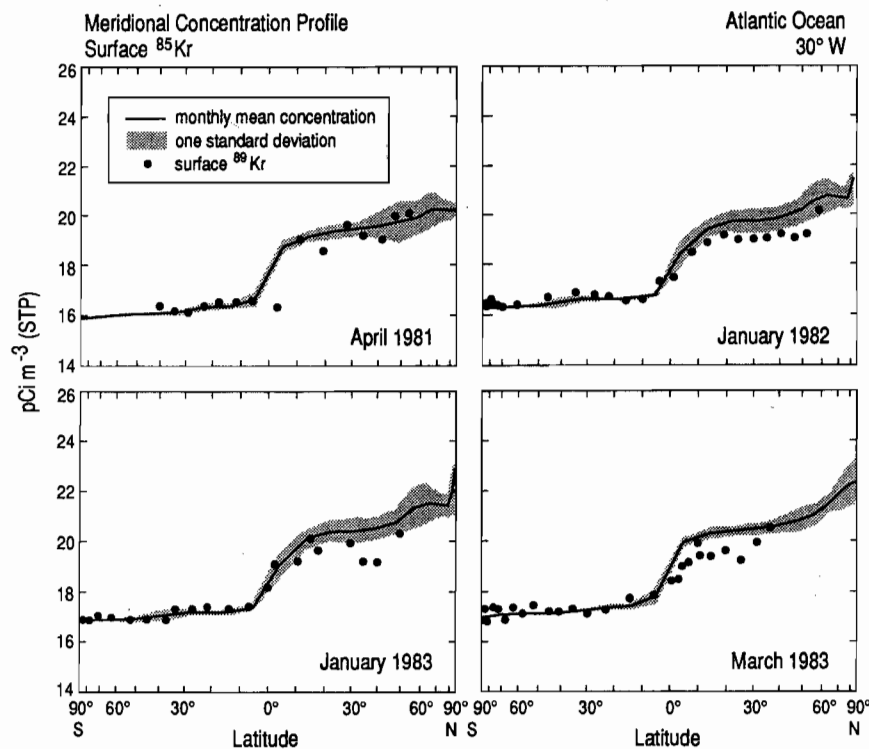|			
1:	Hanford, U.S.A.	46.6°N.,	114.7°W.
2:	Idaho, U.S.A.	43.4°N.,	112.1°W.
3:	Savannah, U.S.A.	33.3°N.,	81.7°W.
4:	Windscale, U.K.	54.6°N.,	3.6°W.
5:	Marcoule, France	44.4°N.,	4.5°E.
6:	La Hague, France	49.0°N.,	0.9°W.
7:	Karlsruhe, F.R.G.	49.0°N.,	8.4°E.
8:	Tokai Mura, Japan	36.5°N.,	140.6°E.
9:	Kyshtym, U.S.S.R.	55.7°N.,	60.6°E.

[b]Estimated by difference (see text).

Fig. 3. Meridional concentration profiles of ^{85}Kr at the surface at 30°W. over the Atlantic Ocean for the four dates as shown, in pCi m^{-3}, referred to standard temperature and pressure (STP). Solid lines indicate monthly mean concentration predicted by the model. Shaded areas define one standard deviation about the mean of the model predicted daily concentration values. Black dots denote measurements of Weiss et al. [1983] and Weiss (personal communication).

The model predicts the structure of the meridional concentration profile rather well, although the region of the Inter-tropical Convergence Zone (ITCZ), which is reflected in the data as a steep concentration jump, is not always found at a location predicted by the model. It is possible that this occasional discrepancy reflects a real difference in atmospheric circulation between the years when the data were obtained and the year interval during 1978 and 1979 as represented by the wind fields used in the model. However, we did not attempt to investigate in detail the wind data for the specific years of the [85]Kr observations.

The interhemispheric exchange time, τ, of the model is calculated from the difference of the [85]Kr inventory in the two hemispheres, $N_N - N_S$, and the net interhemispheric flux of [85]Kr, F_{NS}, according to

$$\tau = \frac{N_N - N_S}{F_{NS}} \quad (3.1)$$

Using annual averages of the quantities in equation (3.1) calculated from our simulation experiment we obtain a value for the interhemispheric exchange time of 1.3 years. This magnitude
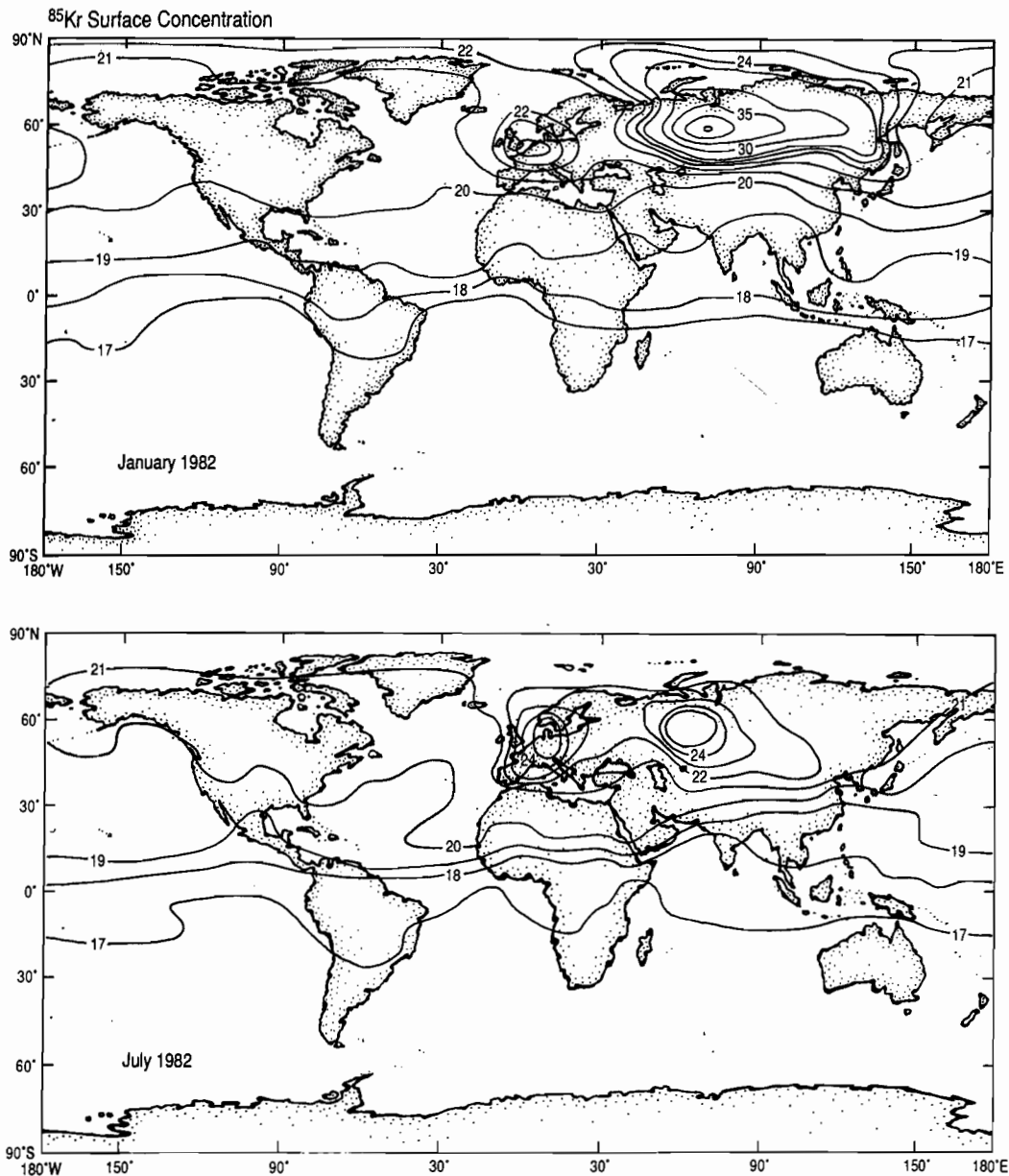

Fig. 4. Monthly mean surface concentration of [85]Kr in the lowest model layer for January and July of 1982, in the same units as in Figure 3. Contour interval is 1 pCi m^{-3} (thick lines) and 5 pCi m^{-3} (thin lines for levels above 25 pCi m^{-3}).

depends slightly on the value chosen for the convection parameter, ζ. Indeed, a second ^{85}Kr model run using a reduced value for ζ of 0.25 instead of the standard case of 0.5 revealed a slightly smaller interhemispheric exchange time of 1.2 years. This result is attributed to the vertical convection process hampering the meridional exchange by advection in the tropical Hadley cells; i.e., a reduction of vertical mixing renders the meridional transport by advective processes more efficient.

Despite the general agreement of model predictions with the observations, we find a tendency of the model to overestimate the measured interhemispheric concentration difference by 10 to 20 percent (see Figure 3). Thus the available data suggest a somewhat faster interhemispheric exchange in reality than as represented in the model. This finding is consistent with the interhemispheric exchange time found by Jacob et al. [1987] of 1.1 years. Implications of this model deficiency for inferring source strengths of carbon dioxide are discussed by Keeling et al. [this volume, b].

Figure 3 shows, also, the large scatter of the predicted daily values north of 30°N., where the section comes close to a major source region. A similar scatter is displayed by the data. On the other hand the model underestimates the variability displayed by the data in the southern hemisphere. This deficiency cannot be explained by measurement errors alone which are on the order of only 1 percent (one standard deviation, see Rath [1988]).

Figure 4 exhibits maps of the calculated ^{85}Kr concentration in the lowermost model layer for the months of January and July 1982. The global increase of 0.25 pCi m^{-3} between January and July has been subtracted from the July picture in order to display the seasonal differences more clearly. The most prominent features displayed in Figure 4 are the high concentrations close to the source regions, especially over the Soviet Union. In these regions the concentration exhibits quite strong seasonal variations with maximum values in the northern hemisphere winter. These seasonal shifts result from the varying vertical stability of the troposphere as discussed in section 2. Measurements of atmospheric ^{85}Kr close to the European source areas have been reported by Weiss et al. [1983] which do exhibit, indeed, a concentration maximum in wintertime.

Further seasonal changes may be seen in the tropical regions reflecting the seasonally changing Hadley cells and, over the Indian Ocean, the reversing Monsoon circulation. This is, for example, seen in Figure 4 by comparing the location of the 18 pCi m^{-3} contour line for January and July. These seasonal shifts in the atmospheric circulation have a profound effect on the atmospheric concentration patterns as discussed in more detail in Heimann et al. [this volume] in connection with the seasonal cycle of CO$_2$ in the tropics.

3.2 Radon-222

Radon-222 (^{222}Rn) is a radioactive noble gas with a mean lifetime of 5.51 days [Weast, 1966]. It is released in significant amounts only at the surface of the continents. Its short lifetime makes it a useful tracer to study the vertical mixing of the troposphere. Unfortunately extensive data on the vertical distribution of ^{222}Rn as a function of season do not yet exist.

In order to examine the behavior of the three-dimensional transport model in the vertical direction, we performed a tracer experiment in which we assume a uniform ^{222}Rn source at the surface
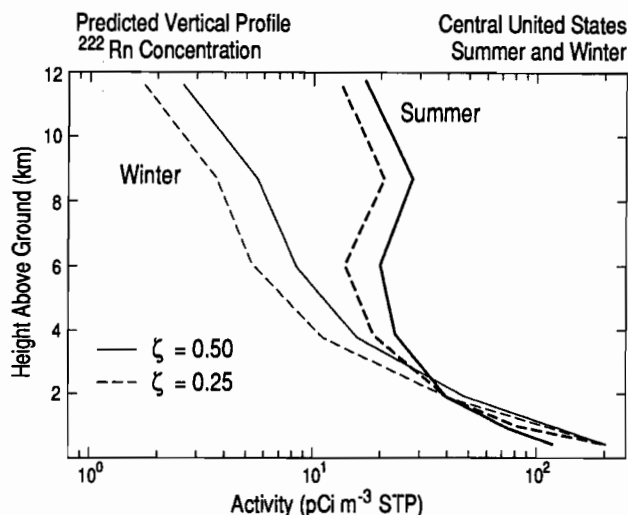

Fig. 5. Predicted vertical profile of the concentration of ^{222}Rn, in pCi m^{-3}, seasonally averaged and referred to standard temperature and pressure (STP), over the central United States for summer and winter. Predictions are shown for convective parameter $\zeta = 0.50$ and 0.25.

over land. Because of the short lifetime of the tracer the model was run for only 13 months of simulation.

Figure 5 shows the model derived vertical distribution over the central United States averaged over the summer and the winter season. The unknown source at the ground was adjusted so that the summer concentration attained a value of 40 pCi m^{-3} at a height of 2 km above ground level, which was reported in a compilation of available ^{222}Rn data by Liu et al. [1984]. The source strength needed to effectuate this distribution was 1.32 atoms cm^2 sec^{-1}, close to the estimates made by Liu et al. [1984] and Turekian et al. [1977].

Figure 5 displays clearly the difference in vertical stability of the troposphere between summer and winter as represented in the model and the data. This atmospheric mixing phenomenon is also evident in the time series of the ^{85}Kr data obtained in western Europe by Weiss et al. [1983].

Also shown in Figure 5 are the model predicted vertical profiles of a model run where the convection parameter, ζ, was set to a value of 0.25. A source strength of 1.28 atoms cm^2 sec^{-1} is needed in this case to match a summer concentration of 40 pCi m^{-3} at 2 km height. It is seen that the change of the factor, ζ, from 0.50 to 0.25 (see equation 2.3) reduces the predicted ^{222}Rn concentrations in the upper troposphere (300–400 hPa) by 20 to 30 percent whereas the values in the lowermost model level (about 960 hPa) are increased by 40 to 60 percent.

A comparison of the compiled vertical ^{222}Rn data of Liu et al. [1984] with the model results using the standard value of the convection parameter ($\zeta = 0.5$) is shown for the summer season in Figure 6 and for the winter season in Figure 7. The shaded areas between dashed lines denote the range of the model predicted daily concentration within one standard deviation from the mean. The vertical attenuation of the summer ^{222}Rn concentration in the troposphere below 7 km (i.e., below a pressure level of about 400

Predicted Vertical Profile   Central United States
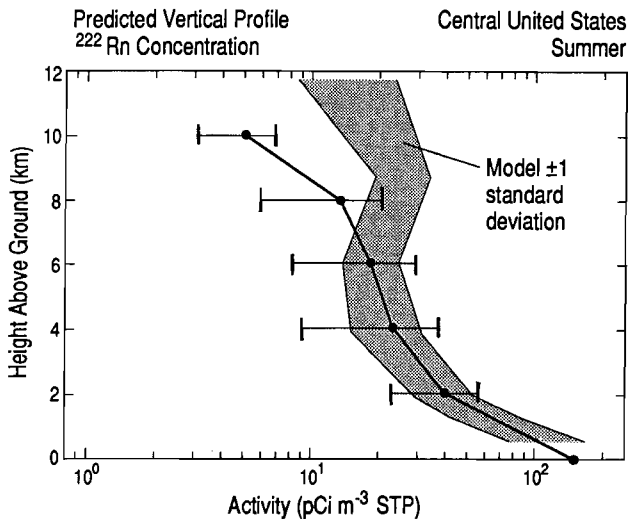^{222}Rn Concentration   Summer

Fig. 6. Concentration of ^{222}Rn over the central United States in the summer season in same units as Figure 5. Black dots and horizontal error bars denote data as compiled by Liu et al. [1984]. The shaded area defines the model predicted range of one standard deviation about the predicted daily concentration values.
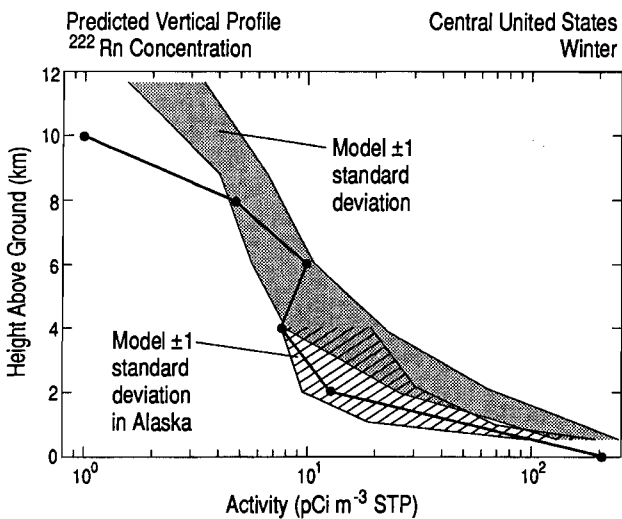
Predicted Vertical Profile   Central United States
^{222}Rn Concentration   Winter

Fig. 7. Concentration of ^{222}Rn as in Figure 6 but in the winter season. The dark shaded area defines the model predicted range of one standard deviation about the predicted daily concentration values over the central United States. The lightly shaded area denotes the same over Alaska.

hPa, see Table 2) is rather well represented by the model, but above 7 km the model overestimates the observations by about a factor of 3. The winter data as compiled by Liu et al. [1984] are much less representative than the summer data since only seven individual measured vertical profiles were used to form an average. Below 700 hPa (about 2.8 km) only five ^{222}Rn profiles were avail-

able, of which four were taken over the Yukon Valley in Alaska. We therefore also show the range of the model predicted winter concentrations over Alaska in Figure 7 (lightly shaded). It is seen how the large vertical stability of the lower troposphere over Alaska in winter reduces the model predicted ^{222}Rn concentration around 2 km height by a factor of 3 as compared to the average over the central United States. No influence of snow cover on the ^{222}Rn emanation rates was provided for in the model runs; its inclusion would further reduce the simulated wintertime concentration in the lower troposphere.

Judging from Figures 6 and 7, we conclude that the three-dimensional transport model simulates the available ^{222}Rn data rather well with $\zeta = 0.5$. However, a rigorous test of the vertical transport characteristics of the model would necessitate a much more representative set of ^{222}Rn concentration measurements as a function of season and location than is currently available.

4.   Simulation of the Atmospheric CO_2 Concentration

This section explains the methodology used to simulate the concentration of atmospheric CO_2 with the three-dimensional transport model, and it presents a description of the individual source components that were used in the model runs.

4.1   Strategy

The present effort to model atmospheric CO_2 is directed at reproducing both its seasonal cycle as a function of latitude and longitude and its nonseasonal spatial distribution, both features averaged over several years. The exchange fluxes of CO_2 between the various carbon reservoirs and the atmosphere are specified as boundary fluxes in the transport model. These fluxes are defined as positive when the net transport is from the surface to the atmosphere and are expressed per unit area of land or ocean, as appropriate. They are broken up into a set of source components, $F_i(\mathbf{x},t)$, i.e., the total (or "composite") source flux, $F_{CMPS}(\mathbf{x},t)$, is expressed as

$$F_{CMPS}(\mathbf{x},t) = \sum_{i=1}^{n} F_i(\mathbf{x},t) \qquad (4.1)$$

As described below in more detail, to carry out our analysis we simulated the CO_2 concentration field with 9 different components, and the atmospheric $^{13}C/^{12}C$ ratio with 11 components, as summarized in Table 4. The model was run successively with only one of the components present as a source for each run. Since the basic model equation (2.1) is linear with respect to the tracer concentration, the results were afterwards combined to obtain the composite solution, $C_{CMPS}(\mathbf{x},t)$

$$C_{CMPS}(\mathbf{x},t) = C_o + \sum_{i=1}^{n} C_i(\mathbf{x},t) \qquad (4.2)$$

where $C_i(\mathbf{x},t)$ is the model solution corresponding to the source flux, $F_i(\mathbf{x},t)$, and is thus the incremental change in concentration of atmospheric CO_2 produced by component i. The constant C_o denotes a background concentration of CO_2, hereafter usually set equal to the mean annual surface concentration at the South Pole.

TABLE 4. CO$_2$ Source Components Used in the Three-Dimensional Atmospheric CO$_2$ Transport Model

1. Seasonal -- locally balanced

    1.   Net primary productivity of the terrestrial biosphere (F_{NPP})

    2.   Heterotrophic respiration of the terrestrial biosphere (F_{RES})

    3.   Air-sea exchange driven by seasonally varying oceanic pCO$_2$ (F_{TDE})

    4.* Temperature dependent isotopic fractionation associated with CO$_2$ exchange at the ocean surface (*F_{TDF})

2. Time independent -- globally balanced

    5.   Equatorial oceanic pCO$_2$ source balanced by equal and uniform oceanic sinks poleward of approximately 16° in each hemisphere (F_{EQU})

    6.   An oceanic source south of approximately 39°S., balanced by a sink in the Atlantic Ocean north of approximately 23°N. (F_{ATL})

3. Seasonally varying or time-independent -- net releases or uptakes

    7.   Industrial CO$_2$ from fossil fuel combustion and cement production (F_{IND})

    8.   Release of CO$_2$ by changes in land use and by deforestation (F_{DES})

    9.   Uptake of CO$_2$ by the terrestrial biosphere in proportion to annual net primary productivity (F_{FER})

    10. Uptake of CO$_2$ by the oceans at a uniform rate per unit area of ice-free ocean surface (F_{UOS})

    11.* Isotopic exchange between the atmosphere and oceans associated with industrial CO$_2$ release and the unbalanced terrestrial biosphere (Carbon-13 Suess effect) (*F_{SUE})

*No concentration dependency.

Table 4 lists the different source components that were used. They fall into three categories:

1. Seasonally varying source components which are locally balanced on annual average, i.e., which, when integrated over 1 year, vanish at every location.

2. Steady sources that are globally balanced, i.e., which do not affect the total CO$_2$ content of the atmosphere.

3. Seasonally varying or steady sources that are not balanced, but represent a net release or uptake of CO$_2$.

The first two categories consist of CO$_2$ fluxes representing the natural exchanges of carbon between the atmosphere and the terrestrial biosphere or the ocean. In the model these fluxes, on an annual basis, are assumed to prevail at a steady state. The third category represents perturbation fluxes of the global carbon cycle which are caused or influenced by human activities. These fluxes include not only industrial CO$_2$ emissions and long-term terrestrial biospheric disturbances, but also perturbations, such as the uptake of CO$_2$ by the ocean and the terrestrial biosphere, induced by the former fluxes.

In constructing these source components as functions of space and time we attempted to make use of as much information *a priori* as was available to us at the time when our study commenced. We have built upon previous investigations to establish the industrial CO$_2$ source (discussed below in subsection 4.2) and the release of CO$_2$ by changes in land use and deforestation (see subsection 4.3.3). Similarly we have constructed net primary productivity of the terrestrial biosphere from remote sensing data (see subsection 4.3.1).

The other natural source components which we chose to include in our model are less reliably known. For these, respiration occurring in the terrestrial biosphere and the exchange of CO$_2$ between the atmosphere and the ocean, we have adopted a method of "integral constraints" in which we prescribe *a priori* only the spatial and temporal structure of each source component based on information derived from previous studies. The global magnitudes of these components, represented by global parameters in the model, are then determined *a posteriori* by comparing the model results to observations of atmospheric CO$_2$ from selected locations.

Even more difficult to establish are the induced perturbation fluxes of CO$_2$. The present three-dimensional transport model does not explicitly treat the internal dynamics of the terrestrial biosphere and the oceans, and therefore cannot portray the long-term evolution of the atmospheric CO$_2$ content. In order to specify the global magnitude of these perturbation fluxes of CO$_2$ and their associated isotopic composition, which are not readily observable, we have accepted the predictions of a global "box diffusion" carbon cycle compartment model [Keeling et al., this volume, a], which was run from preindustrial times to the present so as to match the average atmospheric concentration increase as observed at Mauna Loa Observatory, Hawaii, and the South Pole between the years 1959 and 1982. These fluxes, for the average of the years 1979 and 1980, taken from Table 10 of Keeling et al. [this volume, a], are summarized in Figure 8.

These perturbation fluxes are presumed to vary slowly compared to typical tropospheric mixing times, which are of the order of one to 2 years. We therefore have assumed that a quasi-stationary state prevails in the atmosphere with respect to these fluxes in order to determine their influence on the spatial concentration gradients and to circumvent running the three-dimensional transport model from a preindustrial steady state to the period of interest. Hence such sources were held constant in the model which was then run for 4 years (thereby cycling repeatedly through the wind fields for the 12 months of the Global Weather Experiment), after which the annual change in concentration at every location closely approached the same value. The errors in the generated spatial gradients incurred with this approximation of constancy do not exceed 3 percent in the case of the industrial CO$_2$ source, which increases exponentially with an e-folding time of about 24 years. Errors of this nature resulting from the biospheric perturbation fluxes were even smaller, since the perturbations were assumed to vary even less with time than the industrial CO$_2$ source [Keeling et al., this volume, a]. Limitations of this approach are discussed by Keeling et al. [this volume, b].

A linear trend in CO$_2$ concentration at each grid point was computed from the difference between January 1 of the 4th and 5th year of the runs, and was subtracted from the model predicted con-
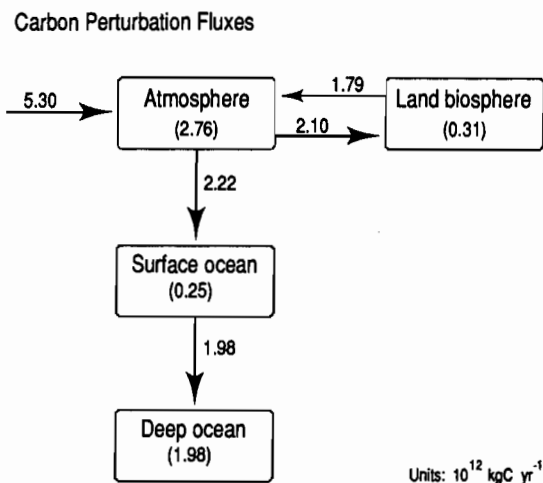
Carbon Perturbation Fluxes

Fig. 8. Summary of the carbon perturbation fluxes, in units of 10^{12} kgC yr^{-1}, approximately for January 1, 1980, as predicted by the box-diffusion model calculation of Keeling et al. [this volume, a]. (The original numbers used in model calculations have been rounded here to the nearest 0.01×10^{12} kgC yr^{-1}.)

centrations to establish the seasonal variation at each location. The annual mean field, based on the 4th year of the run, was computed as the difference from the annual mean found at the South Pole at the surface.

The source components, as described in detail in the following subsections, constitute the input to a standard reference scenario of the CO_2 simulations. For the more uncertain source components, sensitivity tests were conducted afterwards in which alternative source hypotheses were tested and the alternative results were compared to the observations. These tests are discussed in the accompanying articles by Heimann et al. [this volume] and Keeling et al. [this volume, b].

4.2 The Industrial Source Component (F_{IND})

The effect of the CO_2 release by fossil fuel combustion and cement production was simulated on the basis of a map derived from Marland et al. [1985] in which this source was distributed on a 5° by 5° grid over the continents. The originally tabulated data were remapped onto the 7.83° by 10° grid of the three-dimensional model in the same manner as the vegetative index discussed below (see equation (4.4)). In order to produce predictions for different years the model computed atmospheric concentration fields were adjusted by the ratio of the global CO_2 release for the period under consideration to the global release which Marland et al. [1985] computed for 1980 (5.284×10^{12} kgC).

Annual average zonally integrated values are listed in Table 5, prorated to a CO_2 emission rate of 5.300×10^{12} kgC yr^{-1} which is appropriate to a quasi-stationary model calculation for January 1, 1980. This global rate was obtained as the average for 1979 and 1980 according to Rotty [1987a], and is consistent with the rate employed in the compartment model calculations of Keeling et al. [this volume, a].

The production of industrial CO_2 varies with season; according to Rotty [1987b] monthly releases in the northern hemisphere are on average about 18 percent higher in the three winter months than in the summer months. In the southern hemisphere the seasonality is smaller. At each location north of 24°N. we modulated the industrial CO_2 source by the northern hemisphere temporal release pattern and south of 24°S. by the southern hemisphere temporal release pattern as compiled by Rotty [1987b]. We denote the flux as a function of space and time by the symbol, F_{IND}.

4.3 The Terrestrial Biospheric Source Components

The fluxes of CO_2 between the atmosphere and the terrestrial biosphere were divided into a seasonal exchange flux and a perturbation flux. The seasonal exchange flux was further subdivided into a component representing the net primary productivity of the biosphere owing to photosynthesis (denoted F_{NPP}) and a component representing the return flux of CO_2 owing to decomposition of organic material by heterotrophic respiration (F_{RES}). The perturbation flux also was assumed to consist of two components: a flux of carbon resulting from anthropogenic changes in land use (F_{DES}) and a flux representing the effects of stimulated plant growth owing to fertilization (F_{FER}).

Ecologists, at least those writing in the English language, distinguish between plant "productivity" expressed as matter synthesized by plants per unit area and time, and plant "production" expressed without reference to area and usually over the specific time period of 1 year. [see for example, Lieth and Whittaker, 1975, p. 4]. Since no similar distinction is in current usage for the other fluxes which we consider in our model, and since we shall always strive to make clear in the context which units we are using, we dispense with the second term and refer only to "productivity" when discussing the uptake of CO_2 by plants.

4.3.1 Net primary productivity (F_{NPP}). Net primary productivity (NPP) refers to the rate of increase in biomass of plants, typically averaged over a growing season; it is that part of the total or gross productivity of photosynthetic plants that remains after some of the material added to the plants by photosynthesis is utilized in their respiration [loc. cit., p. 4]. In this study, NPP of the land plants was estimated by means of a model for remote sensing of plant growth [Kumar and Monteith, 1981]. According to this model, the rate of fixation of carbon per unit area is proportional to the photosynthetically active solar radiation absorbed by the canopy and is expressed as the product of two independent factors: S, the photosynthetically active solar radiation (PAR) impinging on the surface of the earth, expressed in joules m^{-2}, and f, the fraction of radiation intercepted by the canopy

$$F_{NPP}(\mathbf{x},t) = -e \cdot f(\mathbf{x},t) \cdot S(\mathbf{x},t) \qquad (4.3)$$

The efficiency constant, e, for carbon fixation has been found for various terrestrial plant canopies (mostly crops) to lie between 1.1 and 1.4 gC per megajoule (MJ) of PAR [Monteith, 1977], assuming that the amount of carbon fixed is equal to 55 percent of the dry weight of biomass. We use a value of 1.25 gC per MJ of PAR and assume that the photosynthetically active radiation equals 50 percent of the total solar radiation, i.e., we set e equal to 0.625 gC per MJ of the total incident radiation.

In this approximation, because e is a constant, no allowance is made for circumstances in which the rate of respiration exceeds

gross productivity, for example, when perennial plants near the beginning and end of their growing season may temporarily respire more CO_2 than they incorporate by photosynthesis. Thus, the return flux of CO_2 to the air that is calculated by assuming a steady-state from one year to the next (see subsection 4.3.2 below) is not precisely heterotrophic respiration, i.e., not solely the respiration of non-photosynthetic organisms that utilize photosynthetic plant material.

In ground based field studies the fraction of solar radiation intercepted by the canopy, f, is determined by placing a photometer on the ground beneath the canopy and measuring the fraction, τ, of solar radiation transmitted by the canopy. In practice f is usually taken to be the fraction of incident radiation not transmitted by the canopy, i.e., the radiation either absorbed or reflected to space. In this approximation f is then given by $1 - \tau$. Alternatively it is possible to relate f to the spectral reflectivity properties of the canopy-soil system in the near-infrared and in the visible portion of the spectrum as measured by a radiometer placed in an aircraft or on a satellite. For this purpose previous investigators have used either the simple ratio (SR) between the signals in the near-infrared and in the visible channels or the normalized difference vegetation index (NDVI), defined as the difference of the signals of the near-infrared and of the visible channels divided by the sum of the two channels.

The relation between f and either SR or NDVI is rather complex. It depends on the properties of the canopy-soil system under investigation, on viewing angle of the sensor, and on the zenith angle of the sun. Furthermore, the radiometer measurement typically consists of an instantaneous value from which is sought an estimate of f representative for an entire day. The relation has been investigated empirically in field studies [Kumar and Monteith, 1981, Asrar et al., 1984] and also by means of models of the radiative transfer in the canopy-soil system [Kumar and Monteith, 1981, Sellers 1985].

The model by Kumar and Monteith [1981] predicts an approximately linear relationship between f and the SR. This is consistent with the results reported by Sellers [1985] based on his more comprehensive canopy model.

For the present study we made use of monthly values of the NDVI, computed from the near-infrared (713–986 nm) and the visible red (571–686 nm) channels of the Advanced Very High Resolution Radiometer (AVHRR) flown by the National Oceanic and Atmospheric Administration (NOAA) on their NOAA–7 polar-orbiting satellite [Tarpley et al., 1984; Hayes, 1985]. These data, originally produced by NOAA as weekly global composite data for the individual channels, were made available to us by C. J. Tucker of the Goddard Space Flight Center of the U.S. National Aeronautics and Space Administration (NASA). The NASA laboratory converted daily global-area coverage (GAC) data, obtained from NOAA with a nominal resolution of 4 km at nadir, into NDVI values which were subsequently mapped onto a mercator projection of the globe and composited over each month as described by Tucker et al. [1985]. The technique of compositing consists of selecting at each location the highest NDVI value during the compositing time interval (1 month). This procedure eliminates some of the deteriorating effects of cloud cover and view angle of the sensor [Justice et al., 1985]. On the other hand it reduces the temporal resolution from 1 day of the primary data to approximately 30 days.

The data from November 1983 to October 1984, as furnished to us from NASA, consists of monthly NDVI values averaged over a grid of 4° latitude by 5° longitude. (We would have preferred to use radiometer data for the same period as the wind and air temperature data, December 1978 through November 1979, but such data were not available). We first remapped this index onto the grid of the 7.83° by 10° tracer model by computing land area weighted averages

$$V_k = \frac{\sum_l A_{lk} V_l}{\sum_l A_{lk}} \qquad (4.4)$$

where k denotes the index of a square of the 7.83° by 10° grid, l an index of the 4° by 5° grid. A_{lk} denotes the land area contained in square k and also in square l, and V_k the NDVI of square k and V_l the NDVI of square l. The sums are taken over all 4° by 5° squares, l, contributing to the 7.83° by 10° square k under consideration.

We next converted the NDVI values to simple channel ratios (SR's) and subsequently to estimates of the monthly mean fraction of intercepted radiation f using typical values for the spectral reflectances of soil and leaves. Specifically, we computed f, the fraction of radiation intercepted by the canopy, according to a linearization of the Kumar-Monteith model in which

$$f = a + bZ \qquad (4.5)$$

where Z, the simple channel ratio of the signals from the near-infrared channel to the red channel of the AVHRR instrument, is obtained from the NDVI value, V, by

$$Z = \frac{1 + V}{1 - V} \qquad (4.6)$$

The values of the two constants, a and b, of equation (4.5) were determined by considering two extreme situations.

For bare ground ($f = 0$) we adopted the NDVI value found in the winter months in southern Alaska of 0.025 which corresponds to a channel ratio, Z, of

$$Z (f = 0) = 1.051 \qquad (4.7)$$

Indeed, typical values of the ratio of the reflectances of soil in the two spectral windows considered vary between 0.39/0.30 for light soil and 0.12/0.06 for dark soil, which, when converting to channel ratios, have to be multiplied by a factor of 1/1.48 arising from the ratios of the incident solar radiation in the two spectral windows of the AVHRR channels [Gruber et al., 1983]. Thus light soil as seen by the AVHRR instrument would result in a value of Z of 0.878 and dark soil in a value of Z of 1.35. Our selected value for Z of 1.051 for soil lies well within the range of these estimates.

For full canopy ($f = 1$) we estimated a ratio of 6.854 of the reflectances in the two spectral windows from the theoretical prediction of the Kubelka-Munk theory of scattering in a homogeneous medium as outlined by Kumar and Monteith [equations (2) and (3), pp. 135, 136, 1981]. Thereby we set the transmissivity and the reflectivity of a single leaf to the value 0.4 in the near infrared wave band and to 0.1 in the red spectral region [loc. cit., p.137]. This results in

$$Z (f = 1) = 4.631 \qquad (4.8)$$

after applying the channel ratio factor of 1/1.48. The corresponding NDVI value, V (obtained by inversion of equation 4.6), is 0.65, which is close to the maximum values found in the NDVI fields processed by the NASA laboratory [Justice et al., 1985].

From equations (4.7) and (4.8) we obtain the values of the parameters, a and b, and rewrite equation (4.5) numerically as

$$f = 0.2793\,(Z - 1.051) \qquad (4.9)$$

The determination of the solar radiation (direct and diffuse), S, impinging on the surface of the earth is described in detail in Appendix C. Briefly, we estimated the average monthly insolation from empirical formulas [Holtslag and van Ulden, 1983], taking into account the attenuation by clouds according the parameterization of Kasten and Czeplack [1980]. The fractional cloud cover was estimated from TIROS–N satellite albedo data (January–December 1979) by means of a simple cloud-albedo model of the atmosphere.

The above described procedure results in an estimate of the net primary productivity on a monthly basis. By summation over the 12 months we obtain an estimate of the annual NPP on the grid of the model to apply to the period 1979–1980. Zonally integrated annual values, so obtained, are listed in Table 5. These zonal values sum to a global annual NPP of the terrestrial biosphere of 55.927×10^{12} kgC yr^{-1}.

For model runs we connected the monthly mean values in time with Hermite cubic splines [de Boor, 1978, p.52] at each grid point. In this way we obtained a smooth representation of the source function having precisely the same annual values as the sum of the original monthly values.

A comparison of our estimates of the annual NPP with ground based data [Matthews, 1983] averaged onto the same 7.83° by 10° grid [Fung et al., 1983] is displayed in Figure 9. (Only cells that contain at least 50 percent land are shown.) It is seen how the predicted NPP values, estimated by our procedure are on average somewhat larger than the published values of Fung et al. [1983]. There is a considerable scatter, but no systematic deviation at any particular latitude.

We are aware that our estimate of NPP might be biased at least in three ways. Firstly, the value of the efficiency constant e is uncertain to about 20 percent, and there remains the possibility that it could be different for plants not included in the study of Monteith [1977]. Also, the efficiency varies to some extent with environmental factors such as ambient temperature and available water. We note, however, that all stress factors affecting plant

TABLE 5. Zonally Averaged Source Components (in 10^{12} kg C yr^{-1})

Zonal Index	Approx. Latitude	Area ($\times10^{12}$ m^2) Land	Ice-free Ocean	Industrial CO_2 Release	Net Primary Productivity	Biospheric Destruction	Biospheric Fertilization	Equatorial Source	N. Atl. Sink	Uniform Ocean Sink
24	90N	0.000	0.000	0.0000	0.0000	0.0000	0.0000	0.0000	0.0000	0.0000
23	82N	0.710	0.096	0.0000	0.0000	0.0000	0.0000	−0.0009	−0.0021	−0.0006
22	74N	2.879	1.900	0.0006	−0.1276	0.0010	−0.0048	−0.0171	−0.0450	−0.0126
21	67N	9.922	2.533	0.0297	−1.5238	0.0068	−0.0573	−0.0228	−0.0689	−0.0168
20	59N	10.494	6.812	0.3824	−3.3124	0.0134	−0.1246	−0.0613	−0.1266	−0.0451
19	51N	12.790	9.118	1.3059	−4.9332	0.0144	−0.1856	−0.0820	−0.1154	−0.0603
18	43N	12.225	13.246	1.3349	−4.8083	0.0109	−0.1809	−0.1191	−0.1835	−0.0876
17	35N	12.098	16.375	1.1202	−4.2420	0.0340	−0.1596	−0.1473	−0.2336	−0.1083
16	27N	12.579	18.366	0.5591	−3.5048	0.0764	−0.1318	−0.1652	−0.2249	−0.1215
15	20N	10.544	22.295	0.1799	−2.8202	0.2622	−0.1061	−0.2005	0.0000	−0.1475
14	12N	8.187	25.936	0.0783	−4.0616	0.2092	−0.1528	0.0584	0.0000	−0.1715
13	4N	7.803	26.968	0.0503	−6.2424	0.3269	−0.2348	0.7578	0.0000	−0.1784
12	4S	8.366	26.405	0.0275	−7.0425	0.4492	−0.2649	0.9415	0.0000	−0.1746
11	12S	7.232	26.891	0.0256	−5.3899	0.2300	−0.2027	0.2711	0.0000	−0.1778
10	20S	8.023	24.816	0.0417	−3.9241	0.1401	−0.1476	−0.2160	0.0000	−0.1641
9	27S	6.783	24.162	0.0875	−2.5751	0.0110	−0.0969	−0.2103	0.0000	−0.1598
8	35S	3.150	25.322	0.0669	−1.1457	0.0047	−0.0431	−0.2204	0.0000	−0.1675
7	43S	0.924	24.547	0.0089	−0.2255	0.0006	−0.0085	−0.2137	0.3777	−0.1623
6	51S	0.389	21.592	0.0008	−0.0386	0.0000	−0.0015	−0.1880	0.3322	−0.1428
5	59S	0.008	14.865	0.0000	−0.0092	0.0000	−0.0003	−0.1294	0.2287	−0.0983
4	67S	2.143	3.949	0.0000	0.0000	0.0000	0.0000	−0.0344	0.0608	−0.0261
3	74S	6.202	0.040	0.0000	0.0000	0.0000	0.0000	−0.0003	0.0006	−0.0003
2	82S	4.746	0.000	0.0000	0.0000	0.0000	0.0000	0.0000	0.0000	0.0000
1	90S	0.595	0.000	0.0000	0.0000	0.0000	0.0000	0.0000	0.0000	0.0000
	Totals	148.791	336.233	5.3000	−55.9269	1.7910	−2.1037	0.0000	0.0000	−2.2237

*All components are for the averages of the years 1979–1980 except for the equatorial source component, an adjustable component nominally set to 2.0288×10^{12} kg C yr^{-1} in zones 11–14, and the north Atlantic sink component, also adjustable and nominally set to a hemispheric average of 1×10^{12} kg C yr^{-1}.
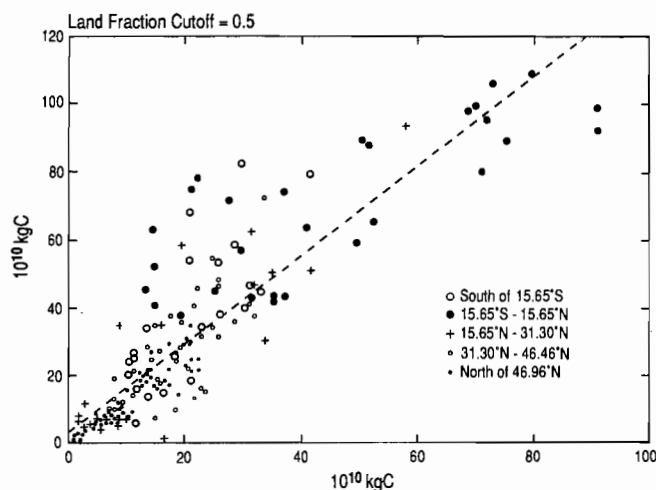
Fig. 9. Comparison of the annual net primary productivity in units of 10^{10} kgC yr^{-1}, as estimated by the model of Kumar and Monteith from remote sensing data (vertical axis, see text) and as compiled by Fung et al. [1983] (horizontal axis). Only cells with more than 50% land surface are included in the figure. The symbols indicate different latitude zones as noted in the figure. The dashed line represents a linear regression curve fit to the data.

growth primarily reduce the intercepted fraction of radiation rather than the efficiency of energy conversion [Kumar and Monteith, 1981]. Secondly, the technique of compositing the vegetation index over one month might not minimize all atmospheric deteriorating effects, particularly in regions of high frequency of cloud cover and in high latitudes due to low sun angles [Justice et al., 1985]. Thirdly, our estimation of insolation might be systematically too high by about 20 percent (see Appendix C).

On the other hand it must be realized that the data used by Fung et al. [1983] represent estimates which were obtained by extrapolating results of individual field studies to averages over the grid cells of the transport model. The agreement obtained, in view of the aforementioned difficulties, is encouraging.

Recently Fung et al. [1987] have reported a study of the atmospheric-biospheric exchange of CO_2 using nearly the same NDVI data that we employed, but extended over a longer period, from April 1982 to January 1985. Their approach differed from ours in that they used the NDVI only to prescribe the seasonal time dependence of terrestrial photosynthesis; the annual integral of NPP was prescribed at every gridpoint of their model based on a study by Matthews [1983]. Furthermore, they did not consider an explicit dependency of NPP on solar radiation. Their estimate of global annual NPP of 47×10^{12} kgC yr^{-1} is close to our estimate of 56×10^{12} kgC yr^{-1}, however, and in view of the relationship displayed in Figure 9, so are their regional estimates of annual NPP.

4.3.2 Respiration (F_{RES}). The flux of CO_2 to the atmosphere by respiration and oxidation within the terrestrial biosphere, principally by heterotrophic respiration occuring in plant detritus and soils, is represented in each grid square of the model by a constant term, and a term dependent on surface air temperature $T(\mathbf{x},t)$, which itself is time dependent

$$F_{RES}(\mathbf{x},t) = F_{R0}(\mathbf{x}) + F_{R1}(\mathbf{x}) \cdot \phi(T(\mathbf{x},t)) \quad (4.10)$$

where

$$\phi(T(\mathbf{x},t)) = \begin{cases} Q_{10}^{(T(\mathbf{x},t)/10)} & \text{if } T(\mathbf{x},t) > T_c \\ 0 & \text{if } T(\mathbf{x},t) \le T_c \end{cases} \quad (4.11)$$

The constant Q_{10} denotes the relative increase of the temperature dependent part of the flux for a 10° centigrade increase in temperature, T. We used monthly mean surface air temperatures extracted from the meteorological fields of the GWE, averaged over each grid square to specify the temperature dependent part of the respiratory flux. The quantity, T_c, denotes a cutoff temperature, below which the temperature dependent respiratory flux vanishes. We set $Q_{10} = 1.5$ and $T_c = -10°C$. Typical Q_{10} values observed in field studies lie between 2 and 3. However, such values are in reference to soil temperature, which exhibits a smaller annual variation as compared to surface air temperature.

The numerical values of the two parameters, F_{R0} and F_{R1}, are not arbitrary as we require that the annually integrated respiratory flux equals the negative of the annual NPP at each grid location. The ratio, F_{R0}/F_{R1} was left as a single adjustable global parameter, which was subsequently determined in a fit of the seasonal variation to the observations as described in section 4.5, below, and in the accompanying article [Heimann et al., this volume]. As an alternative to dividing the respiratory flux into a temperature dependent and a temperature independent part, the value of Q_{10} could have been left as adjustable. However, this would have required a nonlinear fit and correspondingly several additional model runs, which did not appear justified given other uncertainties in the formulation of the biospheric sources and sinks. As an artifact our procedure predicts a small but nonzero respiratory flux of CO_2, if the monthly mean surface air temperature falls below T_c.

The present approach falls far short of a comprehensive description of respiration; it neglects differences between the various biomes on the earth, and it does not take into account the influence of other environmental variables besides temperature such as moisture or the composition of soil or humus. (See, for example, Fung et al., [1987], who employed for each of four classes of biomes a different relationship to describe respiration as a function of temperature.) Nevertheless, temperature represents the dominant factor determining the respiratory flux (for example, see Dörr and Münnich [1987]), and we therefore assume that the seasonal pattern of heterotrophic respiration is captured to first order by the formulation we have adopted.

In practice first the annual integral of the function, $\phi(T(\mathbf{x},t))$, was computed at each location. The model was then run with the source flux

$$\hat{F}_{RES}(\mathbf{x},t) = -\overline{F}_{NPP}(\mathbf{x}) \left[\frac{\phi(T(\mathbf{x},t))}{\int \phi(T(\mathbf{x},t'))dt'} \right] + \overline{F}_{NPP}(\mathbf{x}) \quad (4.12)$$

where $\overline{F}_{NPP}$ denotes the net primary productivity at the particular location averaged over 1 year. For a model run the monthly mean fluxes, computed by equation (4.12) using monthly means of temperature, were smoothly interpolated in time by Hermite cubic splines [de Boor, 1978, p. 51]. Expression (4.12) describes a flux which is locally balanced, i.e., whose integral over 1 year vanishes. (To draw attention to this we place a caret over the symbol for

F_{RES}). Similarly, the model run involving NPP as described in the previous section was actually performed with a locally balanced source function given by

$$\hat{F}_{NPP}(\mathbf{x},t) = F_{NPP}(\mathbf{x},t) - \bar{F}_{NPP}(\mathbf{x}) \qquad (4.13)$$

The combined seasonal exchange flux between the biosphere and the atmosphere is then specified as

$$F_{NPP}(\mathbf{x},t) + F_{RES}(\mathbf{x},t) = \hat{F}_{NPP}(\mathbf{x},t) + v_{RES}\,\hat{F}_{RES}(\mathbf{x},t) \qquad (4.14)$$

$$= F_{NPP}(\mathbf{x},t) + (v_{RES} - 1)\bar{F}_{NPP}(\mathbf{x})$$

$$- v_{RES}\bar{F}_{NPP}(\mathbf{x})\frac{\phi(T(\mathbf{x},t))}{\int\phi(T(\mathbf{x},t'))dt'} \qquad (4.15)$$

In equation (4.14) v_{RES} denotes the adjustable global parameter, introduced as a factor multiplying $\hat{F}_{RES}$. It is seen that the respiratory part appearing in equation (4.15) has the same structure as equation (4.10) where the constants, F_{R0} and F_{R1}, of equation (4.10) are reexpressed as

$$F_{R0}(\mathbf{x}) = \bar{F}_{NPP}(\mathbf{x})(v_{RES} - 1) \qquad (4.16)$$

and

$$F_{R1}(\mathbf{x}) = -\bar{F}_{NPP}(\mathbf{x})\frac{v_{RES}}{\int\phi(T(\mathbf{x},t'))dt'} \qquad (4.17)$$

The concentration field $C_{SBE}(\mathbf{x},t)$ generated by the seasonal exchange fluxes with the terrestrial biosphere is thus given by

$$C_{SBE}(\mathbf{x},t) = \hat{C}_{NPP}(\mathbf{x},t) + v_{RES}\,\hat{C}_{RES}(\mathbf{x},t) \qquad (4.18)$$

where $\hat{C}_{NPP}$ and $\hat{C}_{RES}$ denote the model generated concentration fields resulting from the individually locally balanced source components, $\hat{F}_{NPP}$ and $\hat{F}_{RES}$, respectively. The subscript SBE denotes "seasonal biospheric exchange".

4.3.3 Biospheric destruction (F_{DES}). Fluxes of carbon resulting from changes in land use and from deforestation have been established by Houghton et al. [1983, 1987]. From the second reference we have adopted a global release rate of 1.791×10^{12} kgC yr^{-1} in 1980, broken down into 12 different regions of the world. As a first approximation we distributed this source within each region proportional to the annual net primary productivity. No information was available about seasonal CO_2 release patterns, hence the source was assumed to be constant during the course of 1 year. Zonally integrated annual rates are listed in Table 5. The fluxes are assumed to apply to the average of 1979–1980 as in the case of the other fluxes. Additional details of how we established this source component are given in Appendix E.

4.3.4 Biospheric fertilization (F_{FER}). The effect of stimulated plant growth owing to increased levels of atmospheric CO_2, or other causes, is included in the model as a time independent sink distributed proportionally to the annual NPP distribution, i.e.,

$$F_{FER}(\mathbf{x}) = \eta\,\bar{F}_{NPP}(\mathbf{x}) \qquad (4.19)$$

The global strength of this sink, and thus the proportionality constant, η, is set according to the prediction of the compartment model, as indicated by Keeling et al. [this volume, a, Table 12] (there designated as a "biospheric CO_2-stimulated uptake").

The fertilization sink might more realistically have been specified to be proportional to the seasonally varying net primary productivity F_{NPP}. The latter, however, is about 20 times greater in magnitude than the fertilization sink. Hence the approximation by the time invariant representation according to equation (4.19) does not appreciably affect the model generated seasonal concentration variations. On the other hand, because F_{FER} is not uniform spatially, it influences the mean annual distribution of atmospheric CO_2. It is this effect of stimulated plant growth which is modeled and discussed by Keeling et al. [this volume, b]. Zonally integrated annual rates for the average of the period 1979–1980 are listed in Table 5 and further described in Appendix E.

4.4   The Oceanic CO_2 Source Components

The gas exchange flux, F_{ex}, between the oceans and the atmosphere at a given location and time is modelled by the expression

$$F_{ex} = k_{ex}\,(pCO_{2\,sea} - pCO_{2\,air}) \qquad (4.20)$$

where F_{ex} denotes the exchange flux in units of carbon mass per unit of time and area, $pCO_{2\,sea}$ the partial pressure of CO_2 (pCO_2) corresponding to equilibrium with inorganic carbon in the surface layer of the oceans (sea), and $pCO_{2\,air}$ the partial pressure of CO_2 in the overlying atmosphere (air). Afterwards, as discussed below, both partial pressures are approximated by their corresponding CO_2 mixing ratios (concentrations) in parts per million of dry air by volume (ppm), thus neglecting the relatively insignificant influences on $pCO_{2\,sea}$ and $pCO_{2\,air}$ of departures in barometric pressure and water vapor from globally averaged mean annual values.

In the standard model run the gas exchange coefficient, k_{ex}, is assumed to be constant in space and time; its value was set to correspond to a global atmospheric residence time of 7.87 years with respect to the gross air-sea flux. This exchange time is equivalent to a gas exchange rate of 17.99 mol m^{-2} yr^{-1} at an atmospheric CO_2 mixing ratio of 290 ppm, and is therefore in agreement with the gas exchange rate derived by Siegenthaler [1983, Table 2] on the basis of a compartment model, without a polar oceanic outcrop, calibrated with preindustrial radiocarbon.

Coefficient k_{ex}, as shown by Siegenthaler [1983, equation (3)] (with a_c equal to zero), is related to the atmospheric residence time, k_{am}^{-1}, by the expression

$$k_{ex} = k_{am}\frac{1}{A_{oc}}\frac{N_{ao}}{p_{ao}} \qquad (4.21)$$

where A_{oc} denotes the global surface area of the oceans, and N_{ao} the mass of carbon in the atmosphere, corresponding to a prescribed CO_2 partial pressure, p_{ao}.

So that the dynamic behavior of the three-dimensional transport model to a global perturbation affecting atmospheric CO_2 is essentially the same as that of the compartment model of Keeling et al. [this volume, a], we substitute for the full area of the oceans (3.62 $\times 10^{14}$ m^2 according to Siegenthaler [1983]) that portion not covered by ice, i.e., we set

$$A_{oc} = 3.36233 \times 10^{14}\ \text{m}^2 \qquad (4.22)$$

Further, we reduce N_{ao} from the value of 615.6×10^{12} kgC atm^{-1} of Siegenthaler [1983] to the value pertaining to the atmosphere below the 10 hPa pressure level, because the three-dimensional model's vertical domain extends only up to a height of 10 hPa.

Also, we account for the presence of water vapor in the global atmosphere, assumed to be 0.33 percent of moist air, to establish the CO$_2$ partial pressure, p_{ao} as was done by Keeling et al. [this volume, a, Table 8, Footnote 1]. Thus we set

$$\frac{N_{ao}}{p_{ao}} = \frac{609.13 \times 10^{12} \text{ kgC}}{289.04 \times 10^{-6} \text{ atm}} \tag{4.23}$$

With these values, and with k_{am}^{-1} equal to 7.87 yr, we obtain

$$k_{ex} = 7.9641 \times 10^2 \text{ kgC m}^{-2} \text{ yr}^{-1} \text{ atm}^{-1} \tag{4.24}$$

Assumed to apply to water at 20°C. and 35‰ salinity, the transfer velocity, k_{ex}/K_o, is 5.47 m day^{-1}, where we adopt for the solubility coefficient, K_o, the value of Weiss [1974, p. 209] of 33.22 × moles m^{-3} atm^{-1}, and for the atomic weight of carbon, 12.011 g mole^{-1} [cf. Bacastow and Björkström, 1981, equation (2.21)].

The value of p_{ao} in equation (4.23) is equivalent to a mixing ratio of CO$_2$ in dry air of 290.00 ppm [Keeling et al., this volume, a, Table 8]. Since observations of CO$_2$ in both air and water are normally expressed as mixing ratios, it is convenient to reexpress k_{ex} in terms of ppm, i.e., we compute

$$k_{ex} = k_{am} \frac{1}{A_{oc}} \frac{N_{ao}}{C_{ao}} \tag{4.25}$$

where C_{ao} denotes a CO$_2$ mixing ratio in dry air of 290.00 ppm. From equation (4.25) we obtain

$$k_{ex} = 7.9377 \times 10^{-4} \text{ kgC m}^{-2} \text{ yr}^{-1} \text{ ppm}^{-1}$$
$$= 2.1747 \times 10^{-6} \text{ kgC m}^{-2} \text{ day}^{-1} \text{ ppm}^{-1} \tag{4.26}$$
$$= 1.8106 \times 10^{-4} \text{ moles m}^{-2} \text{ day}^{-1} \text{ ppm}^{-1}$$

The magnitude of k_{ex} is known at best to plus or minus 20 percent, thus introducing a considerable uncertainty into the calculation of gas exchange.

We invoke an assumption that the gas exchange rate is invariant both because of uncertain knowledge of the correct temporal and spatial variability of k_{ex} and because we do not wish to produce an oceanic model which at the outset is excessively difficult to interpret. We must cope with large uncertainties in knowledge of the variability of $pCO_{2\,sea}$, and we must distinguish terrestrial biospheric influences on the observed atmospheric CO$_2$ distribution, before we can reasonably interpret model predictions of air-sea exchange. We therefore prefer to postpone to a later study consideration of the kinetics of oceanic gas exchange. However, in a sensitivity model run the effects of a variable exchange coefficient upon the model predicted CO$_2$ concentration and stable carbon isotope ratio are investigated, as explained by Keeling et al. [this volume, b].

We approximate the atmospheric partial pressure $pCO_{2\,air}$ in equation (4.20) by a constant, thus ascribing all spatial and temporal variability of the air-sea exchange flux to the partial pressure $pCO_{2\,sea}$ in the oceanic surface layer. This approximation, without introducing significant errors into the model predictions, decouples the air-sea exchange flux from the atmospheric concentration field which is computed by the model. The approximation has two computational advantages. Firstly, $pCO_{2\,sea}$ may be decomposed into a linear combination of independent components, as described below. Secondly, considerable computer time is saved since without this approximation a new time constant of 7.87 yr is introduced into the model equation, necessitating the simulation of 20 years or more in order to achieve a quasi-stationary state. (We comment on the effects of neglecting variations in $pCO_{2\,air}$ with respect to seasonality of the carbon cycle in the next subsection. Keeling et al. [this volume, subsection 4.2.5] discuss the effect of this neglect on the simulated mean annual cycle.)

The difference, $pCO_{2\,sea} - pCO_{2\,air}$, was decomposed into a seasonal component, two stationary components, and a perturbation component representing the uptake of industrial CO$_2$ by the oceans and adjustments by the oceans to terrestrial biospheric imbalances. Each of these components is described below in more detail.

The effect of the seasonally varying extent of sea ice (specified according to Alexander and Mobley [1976]), assumed to be impermeable to the CO$_2$ gas, was included. In all cases that we consider, its influence on the generated atmospheric concentration patterns was found to be negligible because the regions involved are small in extent and were assumed to exhibit only modest partial pressure differences between the air and the sea.

4.4.1 Seasonal variations of CO$_2$ partial pressure in surface waters (F_{TDE}). In the temperate and polar latitudes, substantial seasonal variations occur in the partial pressure of CO$_2$ in the surface waters of the oceans ($pCO_{2\,sea}$). Only part of these variations is caused by the annual changes in temperature that shift the equilibrium of the carbonate system in sea water. Additionally, $pCO_{2\,sea}$ is influenced by variations of the depth of the mixed layer, rate of upwelling or mixing with subsurface waters, horizontal advection of waters with different origin and photosynthesis of the marine biosphere. We have addressed only the temperature dependent exchange (TDE) in our model, but modified this dependency to account in part for biological activity.

In the absence of high organic productivity the relatively slow exchange of CO$_2$ between air and sea and the buffered chemical state of sea water prevent large variations in the amounts of dissolved inorganic carbon from occurring in the surface layer of the oceans over the course of one season if the layer is thicker than about 30 meters [Tans, 1978; Kamber, 1980; Weiss et al., 1982]. Therefore, in order to specify the CO$_2$ flux arising from warming and cooling, we make the simplification that $pCO_{2\,sea}$ as a function of time is dependent solely on that variation which arises from temperature variations at a constant concentration of dissolved inorganic carbon and at constant alkalinity.

The effect of the carbonate chemistry of sea water is calculated from the relationship given by Weiss et al. [1982, p. 511, equation 1] between $pCO_{2\,sea}$ (assumed to be equal to the fugacity, f_{CO_2}) and temperature, T, in degrees centigrade

$$\frac{d}{dT} ln(f_{CO_2}) = 0.03107 - 2.785 \times 10^{-4} T \tag{4.27}$$
$$- 1.839 \times 10^{-3} ln (f_{CO_2})$$

where *ln* denotes the natural logarithm.

In high latitudes the marine biosphere to a large extent cancels or even overrides the effect of temperature on $pCO_{2\,sea}$, since photosynthetic activity is highest when light supply is at a maximum, if ample nutrients are available [Fogg, 1975]. In order to allow at least partially for this effect we reduce the temperature driven variation of $pCO_{2\,sea}$ linearly to zero in the zone between 35.22° and 50.87° latitude in each hemisphere, and we assume that no seasonal changes of $pCO_{2\,sea}$ occur poleward of 50.87° in each hemi-

sphere. This reduction in temperature driven variation has the consequence that the effective $pCO_{2\,sea}$ signals modeled for the waters in the high latitudes of the two hemispheres are different owing to the large annual signal of $pCO_{2\,air}$ (on the order of 15 ppm peak to peak at 70°N.) in the northern hemisphere compared to the southern (about 1 ppm). In effect, we assume a substantial signal in $pCO_{2\,sea}$ in the northern hemisphere oceans, synchronous with atmospheric CO_2 variations, and a much smaller, synchronous signal of $pCO_{2\,sea}$ in the southern latitudes. The signal in the north is perhaps more correct than the small signal in the south, but observational data with good seasonal coverings are far too few to prove adequately our assumptions, since an overriding influence of marine biological activity is suggested by the limited oceanographic data which we have studied. The effect of these on the predicted atmospheric CO_2 concentration is not large, however, owing to the small areas of polar oceans in each hemisphere (especially in the north), relative to the areas of the subtropical gyres where the modeled $pCO_{2\,sea}$ signal, induced solely by temperature, is probably realistic. We await an opportunity to make use of new, more extensive, direct observations of the seasonal variability of $pCO_{2\,sea}$ to improve on this formulation [Takahashi et al., 1985, 1986, and 1988; Peng et al. 1987].

The coastal upwelling areas off the western coasts of Africa and South America were treated as special cases. Here the seasonal variations in surface water temperature are largely caused by changes in the rate of upwelling of cooler water. A computation of the oscillation of $pCO_{2\,sea}$ from the temperature effect alone does not take into account that the upwelling water is enriched in CO_2 relative to surface waters [Broecker and Peng, 1982, p.160]. This effect is likely to produce a rise in $pCO_{2\,sea}$ with cooler temperatures, contrary to the aforementioned temperature effect. Additionally the marine biosphere presumably has an important influence, because upwelling waters are enriched in nutrients. Lacking observational evidence, we reduce the variations of $pCO_{2\,sea}$ in these regions to the values computed in the subtropical gyres 2 grid units (20° longitude) further offshore.

Since we are here only interested in the seasonal variation, we adjusted the mean $pCO_{2\,sea}$ at each location so that the time-integrated flux over 1 year vanishes everywhere.

4.4.2 Stationary components (F_{EQU} and F_{ATL}). The surface waters of the oceans exhibit large spatial variations in CO_2 partial pressure ($pCO_{2\,sea}$) annually averaged [see, for example, Keeling, 1968; Takahashi et al., 1983]. These variations presumably reflect nearly stationary natural oceanic fluxes of CO_2, and thus produce spatial gradients in atmospheric CO_2 which do not vary strongly from year to year, in contrast to the steadily increasing gradients produced by industrial CO_2. These $pCO_{2\,sea}$ variations are represented in the model as the sum of two global source components.

Based on the observations reported by Keeling [1968] and from the FGGE expedition in the central Pacific Ocean ([Weiss et al., 1982] as shown by Keeling and Heimann [1986, Figure 10]) we constructed a fairly crude map of the stationary difference in CO_2 partial pressure between the oceans and the atmosphere in the equatorial region between 15.65°S. and 15.65°N. appropriate to the year 1980 (upper panel of Figure 10). The average difference, $pCO_{2\,sea} - pCO_{2\,air}$, for this zone and consistent with this map, is 24.16 ppm. We assume that the CO_2 flux out of the oceans in this equatorial region in each hemisphere exactly balances fluxes into

the oceans poleward of 15.65°. A uniform deficit in $pCO_{2\,sea}$ is postulated for each of these sink regions: −11.38 ppm in the northern hemisphere, −11.01 ppm in the southern. With the exchange coefficient, k_{ex}, assigned the nominal value given by equation (4.26), the flux released in the tropics was computed to be 2.0288×10^{12} kgC yr^{-1}, of which 40.23 percent occurs in the northern hemisphere, the remainder in the southern. The global distribution of these fluxes we call the "equatorial oceanic source" component, denoted by F_{EQU}. Because $pCO_{2\,sea}$ in the equatorial region to derive this component was estimated from recent observations influenced by the uptake of industrial CO_2 and possibly as well by perturbations of the terrestrial biosphere, this component does not strictly represent natural oceanic conditions. Keeling et al. [this volume, a] make allowances for recent perturbations in $pCO_{2\,sea}$ in connection with their analysis of the mean annual distribution of atmospheric CO_2, using a compartment model.

The simulated mean annual meridional concentration gradient cannot be reconciled with the observational data, as shown by Keeling et al. [this volume, b], without an additional CO_2 flux of the order of 1×10^{12} kgC yr^{-1} through the atmosphere from the southern into the northern hemisphere. Such a flux was implemented in the model with an additional oceanic source-sink couple, F_{ATL} comprising a source region south of 39.13°S. and a corresponding sink north of 23.48°N. in the Atlantic Ocean. We excluded the North Pacific Ocean as a sink owing to the lack of evidence of deep water formation in that ocean compared with the North Atlantic [see, for example, von Arx, 1974, Chapter 7]. With a nominal source strength of 1×10^{12} kgC yr^{-1}, the North Atlantic Ocean has a uniform deficit in $pCO_{2\,sea}$ of −40.58 ppm and the southern oceans an excess of 19.46 ppm (lower panel of Figure 10). The justification for this source component is further discussed by Keeling et al. [this volume, b].

The model was run separately with each of these two source-sink components, using the nominal value for the exchange coefficient, k_{ex}, as given by equation (4.26) and a nominal value of 1×10^{12} kgC yr^{-1} for the strength of the North Atlantic Sink. In forming the composite model-generated concentration field the contribution from each of the two components was weighted by a factor (v_{EQU}, v_{ATL}, respectively), which was determined from atmospheric CO_2 observations (see section 4.5 below and Keeling et al. [this volume, b]). These adjustments may be interpreted as uncertainties in specifying either k_{ex} or $pCO_{2\,sea}$.

To distinguish between the nominal and adjusted component fields we write

$$C_{EQU}(\mathbf{x},t) = v_{EQU}\,\hat{C}_{EQU}(\mathbf{x},t) \tag{4.28}$$

$$C_{ATL}(\mathbf{x},t) = v_{ATL}\,\hat{C}_{ATL}(\mathbf{x},t) \tag{4.29}$$

where $\hat{C}_{EQU}(\mathbf{x},t)$ and $\hat{C}_{ATL}(\mathbf{x},t)$ denote the nominal fields. Similarly $\hat{F}_{EQU}(\mathbf{x})$ and $\hat{F}_{ATL}(\mathbf{x})$ will henceforth denote, respectively, the stationary fluxes which generate these nominal fields. Zonally integrated values of $\hat{F}_{EQU}(\mathbf{x})$ and $\hat{F}_{ATL}(\mathbf{x})$ are listed in Table 5. The concentration fields are variable, as indicated, even though the fluxes are constant in time, because of the redistribution by atmospheric transport over land and ice covered areas, and because of temporal and spatial variability in the atmospheric circulation.

4.4.3 Uniform uptake of CO_2 by the oceans (F_{UOS}). A substantial fraction of the industrial CO_2 injected into the atmosphere is taken up by the oceans [Baes, 1982, p. 189]. We therefore
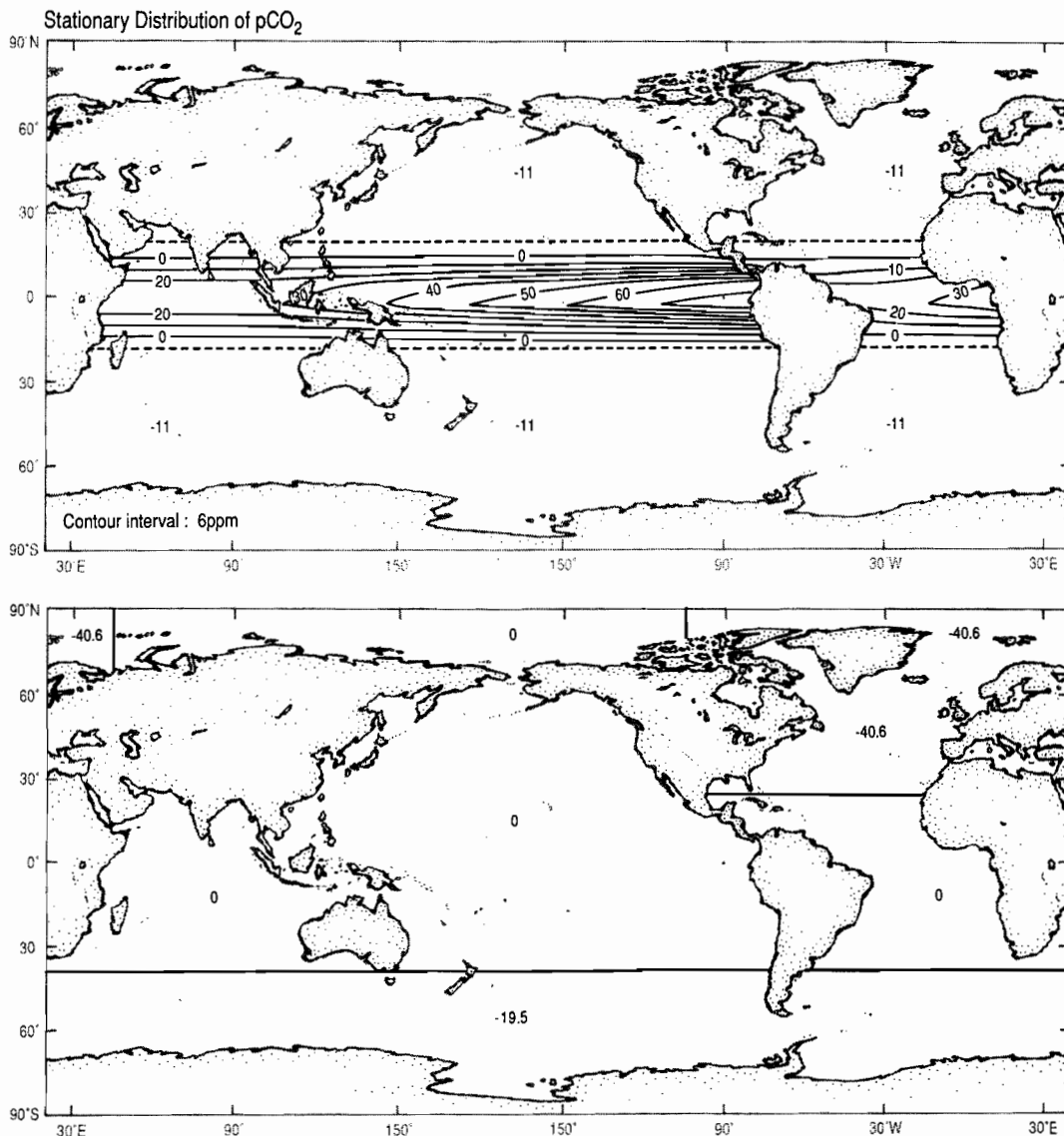
Stationary Distribution of pCO_2

Fig. 10. Stationary distribution of the CO_2 partial pressure difference, $pCO_{2\,sea} - pCO_{2\,air}$, associated with the adjustable oceanic source components, in units of ppm (approximately equal to microatmospheres). Upper panel: equatorial source component, F_{EQU}. Lower panel: North atlantic sink component, F_{ATL}.

included a source function, which for simplicity is taken as a constant flux uniformly distributed over the part of the oceans not covered with ice. The globally integrated magnitude of this uniform oceanic sink (UOS) is specified according to the compartment model result of Keeling et al. [this volume, a, Table 12] (sum of surface and deep oceanic uptake rates). It also includes the considerably smaller oceanic adjustment to biospheric destruction and fertilization. With an exchange coefficient, k_{ex}, as specified by equation (4.26), a global average difference in $pCO_{2\,sea} - pCO_{2\,air}$ of -3.7609 ppm is needed to effectuate each 10^{12} kgC yr^{-1} of this flux (for example, a difference of -8.36 ppm is needed in the period 1979–1980).

To determine the concentration field, C_{UOS}, associated with the uptake of CO_2, we first set the CO_2 partial pressure difference in equation (4.20) equal to 3.7609 ppm, corresponding to a globally integrated sea to air flux of 10^{12} kgC yr^{-1}, and ran the three-dimensional model with

$$F_{UEX}(\mathbf{x},t) = k_{ex} \cdot 3.7609 \text{ ppm} \qquad (4.30)$$

where UEX denotes "uniform (oceanic) exchange".

The flux, positive out of water, is constant over the part of the ocean not covered by ice, but zero elsewhere, and hence it varies with both time and location, as indicated. Then, to compute C_{UOS},

we multiplied the concentration field C_{UEX}, generated by F_{UEX}, by the appropriate constant factor, v_{UOS}, where

$$C_{UOS}(\mathbf{x},t) = v_{UOS}\, C_{UEX}(\mathbf{x},t) \qquad (4.31)$$

to achieve the CO_2 sink prescribed by the compartment model for the particular year under investigation. For example, for the period 1979–1980, $v_{UOS} = -2.2237$. Zonally integrated values of the flux for the average of the period 1979–1980 are listed in Table 5. Monthly averages of the seasonally varying fluxes are too numerous to show. They are illustrated by Heimann et al. [this volume].

At the time we commenced our study we lacked reliable information for considering the regional distribution of this perturbation flux. Recently, Maier-Reimer and Hasselmann [1987] have presented a first attempt to map the spatial structure of this flux by means of a global three-dimensional oceanic tracer transport model. According to their model, the most prominent regions of oceanic uptake of CO_2 lie in the zones of equatorial upwelling and at high latitudes where deeper water masses come in contact with surface waters. If this model correctly identifies the major regions of uptake, the errors which we incur by prescribing a uniform uptake of industrial CO_2 are to a considerable degree compensated for by the stationary oceanic source components, F_{EQU} and F_{ATL}, described above in subsection 4.4.2, because the broadly defined regions introduced into our model by these two source components tend to coincide with the patterns of oceanic uptake indicated by the model of Maier-Reimer and Hasselman. In effect the inferred magnitudes of these two stationary oceanic fluxes may be interpreted as being partially caused by this perturbation flux. This possibility is further discussed by Keeling et al., [this volume, b].

4.5 Fit of the Three Global Source Parameters

In the specification of the various source components, discussed above, three global adjustment parameters were introduced. These were to be subsequently determined by a least squares fit of the model-predicted atmospheric concentration fields to atmospheric CO_2 observations, listed by Keeling et al. [this volume, a].

One of the global parameters, v_{RES} is associated with seasonal sources (cf. equation 4.18), hence its value was set by fitting the function

$$S_C(C_{CMPS}) = v_{RES}S_C(\hat{C}_{RES}) + \sum_{i=1}^{n} S_C(C_i) \qquad (4.32)$$

to the observed seasonal variation at a selected set of monitoring stations. The linear operator $S_C(\_)$, stands for a quantitative measure of the seasonal variation: we use the eight coefficients of the first four harmonics corresponding to the base period of one year to specify $S_C(\_)$. The sum in equation (4.32) is taken over all components except $\hat{C}_{RES}$. Details of the fitting procedure are presented in Appendix D.

Similarly, let $M_C(\_)$ denote the linear operator which extracts the mean annual concentration field relative to the concentration at the South Pole on the surface. The other two global parameters, v_{EQU} and v_{ATL}, were then determined together with the atmospheric background concentration C_o by fitting

$$M_C(C_{CMPS}) = C_o + v_{EQU}M(\hat{C}_{EQU}) + v_{ATL}M_C(\hat{C}_{ATL}) + \sum_{i=1}^{n} M_C(C_i)$$
$$(4.33)$$

(see equations (4.28) and (4.29)) to the mean annual atmospheric CO_2 concentration observed at the surface along a meridional section in the central Pacific Ocean [see subsection 4.4.2, above].

The two fits are not independent, since the stationary sources involving the parameters v_{EQU} and v_{ATL} also generate a small seasonal signal because of the time varying transport terms of the model. The converse is also true: the seasonal sources generate, on annual average, nonuniform concentration distributions [Heimann et al., this volume]. Because of this interdependence between the two fits we used an iterative procedure to determine the free parameters. However, the interdependence was found to be very small; a satisfactory convergence was found after two iterations.

4.6 Summary of the Global Source Components

In Table 6 are listed annual averages of the globally integrated fluxes associated with each of the individual source components of the three-dimensional transport model described above. These global source strengths are prescribed for 1 January of each of the four years (1962, 1968, 1980, and 1984) for which meridional profiles

TABLE 6. Strengths of Source Components (in 10^{12} kg C yr^{-1})

Subscript		Annual Average for Historic Period			
Symbol	Definition	1962	1968	1980	1984
IND	Global industrial CO_2 release	2.6555	3.5075	5.3000	5.1920
NPP	Global net primary productivity of land plants	−49.4953	−51.6205	−55.9269	−57.4928
RES	Global respiration of land plants	49.4953	51.6205	55.9269	57.4928
DES	Global terrestrial biospheric destruction	1.6927	1.7288	1.7910	1.8086
FER	Global terrestrial biospheric fertilization	−1.4250	−1.6018	−2.1037	−2.2688
TDE	Seasonal CO_2 uptake and release by the oceans	Constant value of 0.0			
EQU	Equatorial CO_2 release; high latitude uptake	Nominal value* of ±2.0288			
ATL	North Atlantic CO_2 uptake; release south of 40°S.	Nominal value* of ∓1.0000			
UOS	Uniform oceanic net sink for industrial CO_2	−1.3851	−1.6179	−2.2237	−2.2970
SUE	Flux to generate field, C_{SUE}, associated with Suess Effect			89.5743	90.8134

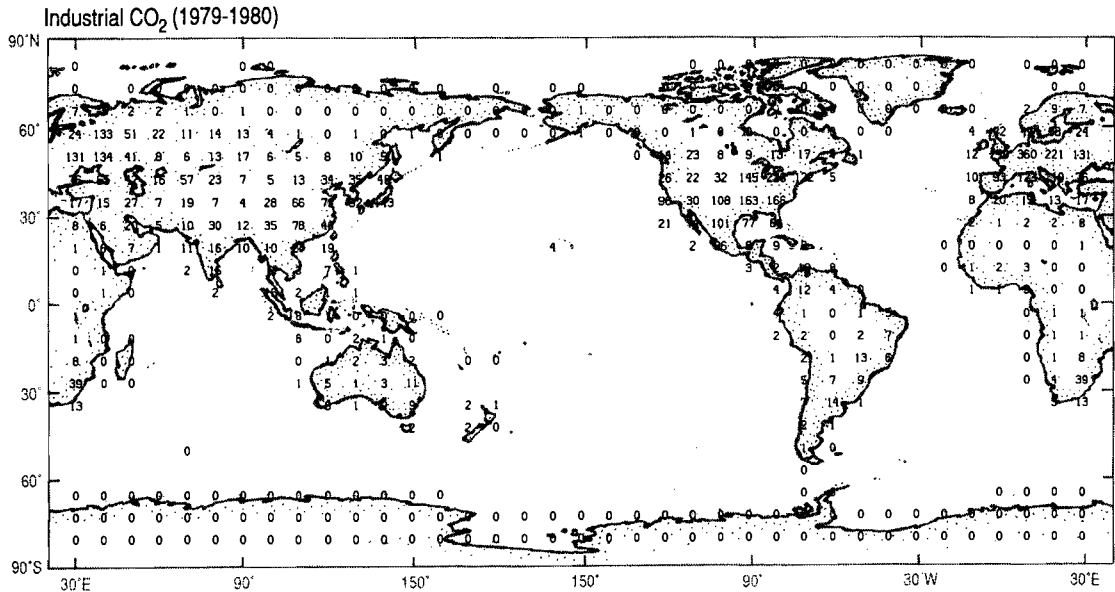*See text

Industrial CO_2 (1979-1980)

Fig. 11. Distribution of the source component for industrial CO_2, F_{IND}, in 1979–1980, in units of 10^9 kgC yr^{-1}, for each grid box of the three-dimensional model. Entries at 30°E. are shown twice, here and in the succeeding figures.

of the mean annual CO_2 data are computed by the model by Keeling et al. [this volume, b].

The distributions of the source components, expressed as fluxes averaged over each grid box of the model for the model year 1979–1980, are shown in Figures 11 to 17. In the case of net primary productivity the actual annual integrals $\bar{F}_{NPP}(x)$ are shown. The annual integral of respiration, having the same magnitude as net primary productivity but opposite sign, is not shown. The North Atlantic component is nominally set equal to 1×10^{12} kgC

yr^{-1} in each hemisphere. The zonal averages for each component sum to the corresponding entries in Table 5.

Four of the components, F_{IND}, F_{FER}, F_{DES}, and F_{UOS}, have different globally integrated values for each of these dates as prescribed by the compartment model of Keeling et al. [this volume, a]. Since the data for industrial CO_2 production are provided as calendar year averages [loc. cit., Table 7], this flux was computed as the average of the global production for the specified year and the preceding year. For the other three components of

Net Primary Productivity (1979-1980)
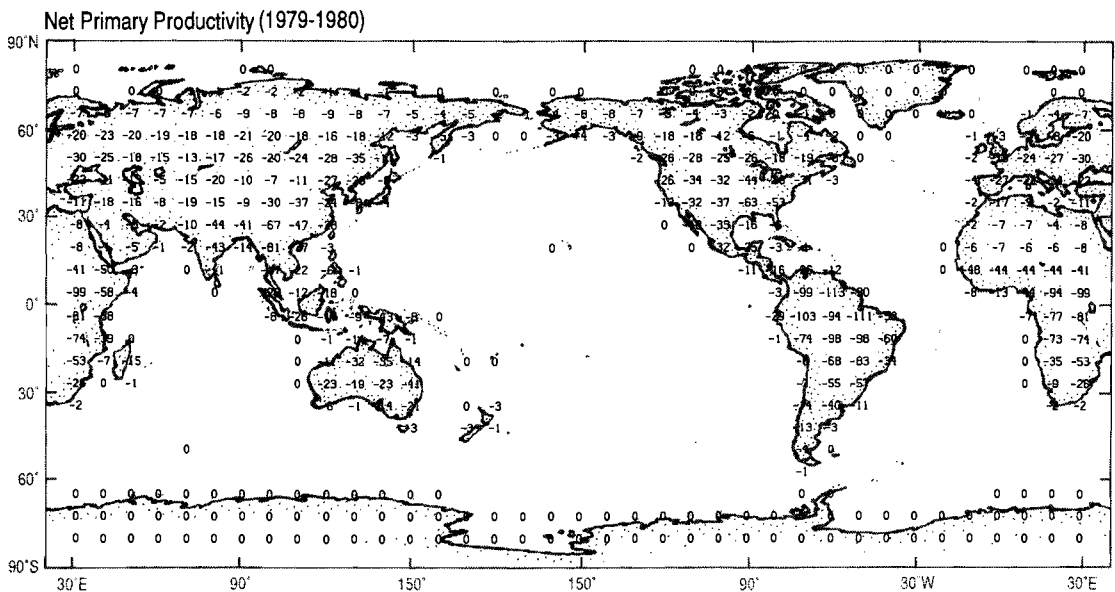
Fig. 12. Distribution of the source component for annual net primary productivity, F_{NPP}, in 1979–1980, in units of 10^{10} kgC yr^{-1}, for each grid box of the three-dimensional model.

Biosphere Destruction (1979-1980)
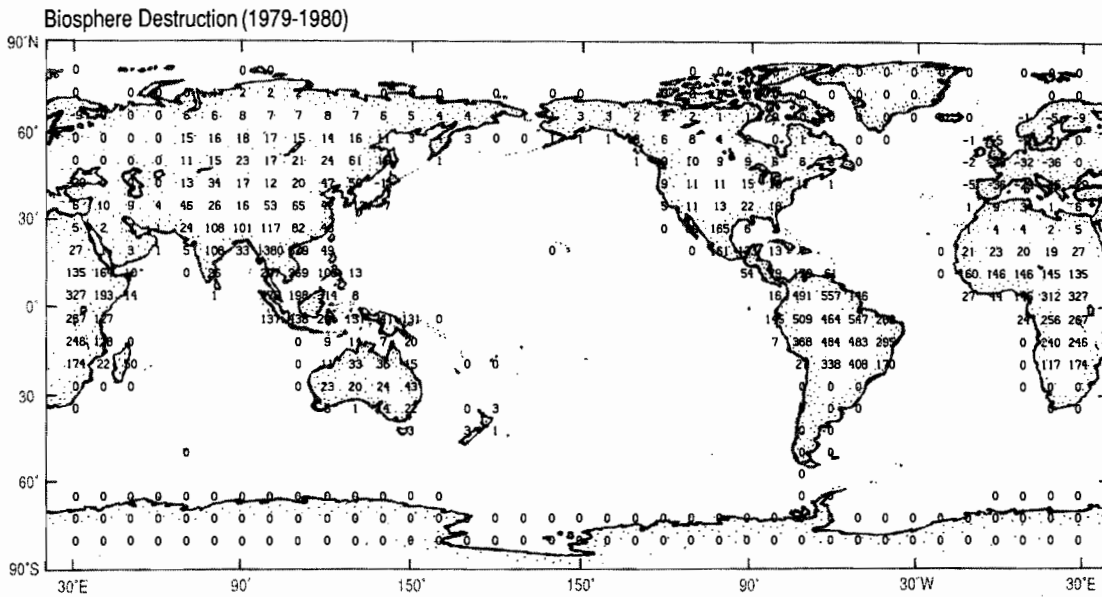
Fig. 13. Distribution of the source component for biospheric destruction, F_{DES}, (CO_2 release to the atmosphere by land use changes and deforestation) in 1979–1980, in units of 10^8 kgC yr^{-1}, for each grid box of the three-dimensional model.

this group of four, annual fluxes determined by the compartment model [loc. cit., Table 12) were likewise averaged over the same two year intervals. The components F_{NPP} and F_{RES} for 1962, 1968, and 1984 were adjusted with respect to 1980 as described by Keeling et al. [this volume, a, subsection 2.4].

The seasonal oceanic flux, F_{TDE}, integrates locally, and hence also globally, to zero. The equatorial flux, F_{EQU}, was estimated from direct observations of oceanic pCO_2, and the flux associated with the Atlantic ocean, F_{ATL}, was nominally set as discussed directly above. Both F_{EQU} and F_{ATL} are adjusted afterwards by

spatially constant scaling factors to effect a global least squares fit of the mean annual concentration field of the model to the atmospheric CO_2 observations. The values found by fitting are listed by Keeling et al. [this volume, b, Tables 1 and 2].

5. Simulations of the $^{13}C/^{12}C$ Ratio of CO_2

5.1 Method

This section describes the procedures that we have used to compile the isotopic ratio fields used to simulate the $^{13}C/^{12}C$ ratio of

Biosphere Fertilization (1979-1980)
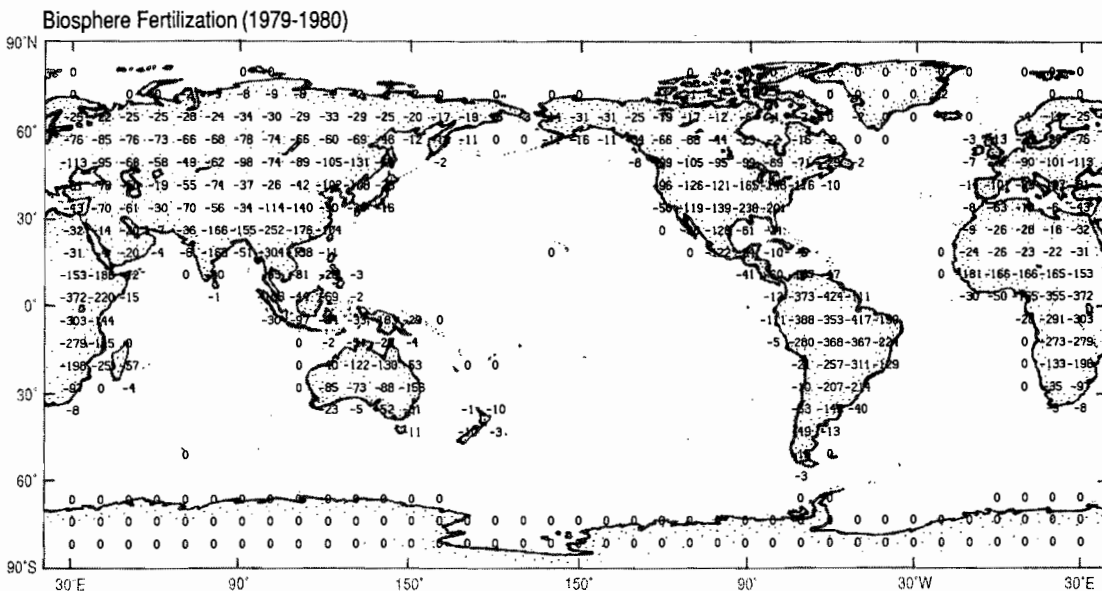
Fig. 14. Same as Figure 13, but for biospheric fertilization, F_{FER}.
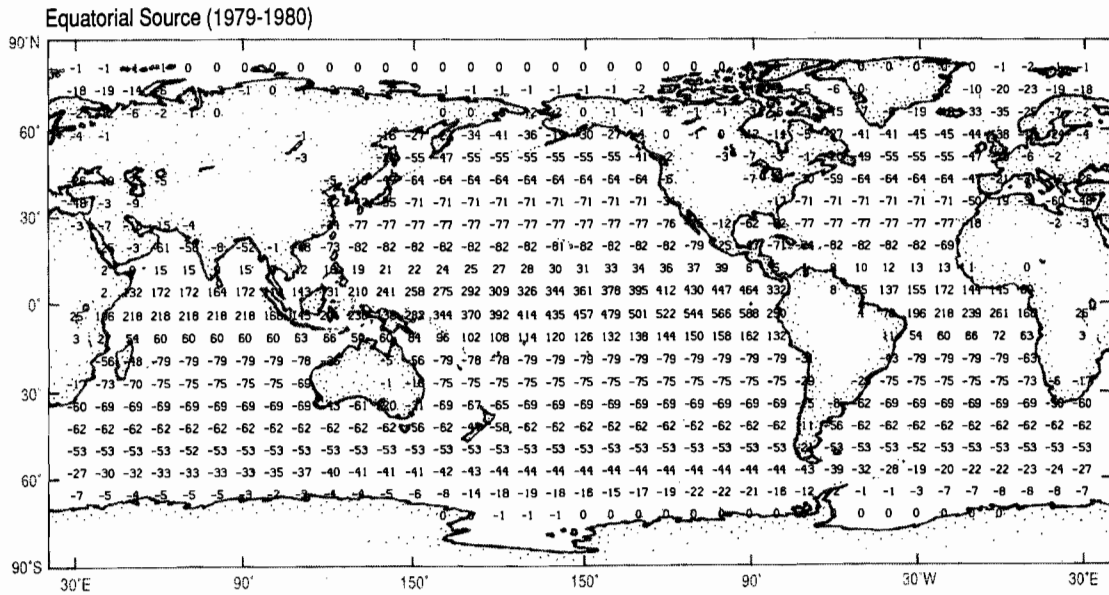
Fig. 15. Distribution of the source component for the release of CO$_2$ from equatorial ocean water and its reabsorption at higher latitudes, F_{EQU}, in units of 10^8 kgC yr^{-1}, for each grid box of the three-dimensional model.

atmospheric CO$_2$ with the three-dimensional model. We have endeavored to present a formulation which is general enough to be used in conjunction with any time and space varying fluxes of the carbon cycle, so as possibly to be useful in future studies when improved models of carbon transport become available. Our formulation is thus considerably more detailed than those of Pearman and Hyson [1986] and Gillette and Box [1986] who have recently modeled the distribution of ^{13}CO$_2$ using two-dimensional transport models.

The transport of ^{13}CO$_2$ is governed by an equation analogous to equation (2.1) for CO$_2$, here recognized as the sum of ^{12}CO$_2$ and ^{13}CO$_2$,

$$\frac{d}{dt}\left[\rho(\mathbf{x},t)\,^*C(\mathbf{x},t)\right] = \,^*Q(\mathbf{x},t) \tag{5.1}$$

where $^*C(\mathbf{x},t)$ denotes the concentration of the rare species ^{13}CO$_2$, and where the source term for ^{13}CO$_2$, $^*Q(\mathbf{x},t)$, is set everywhere
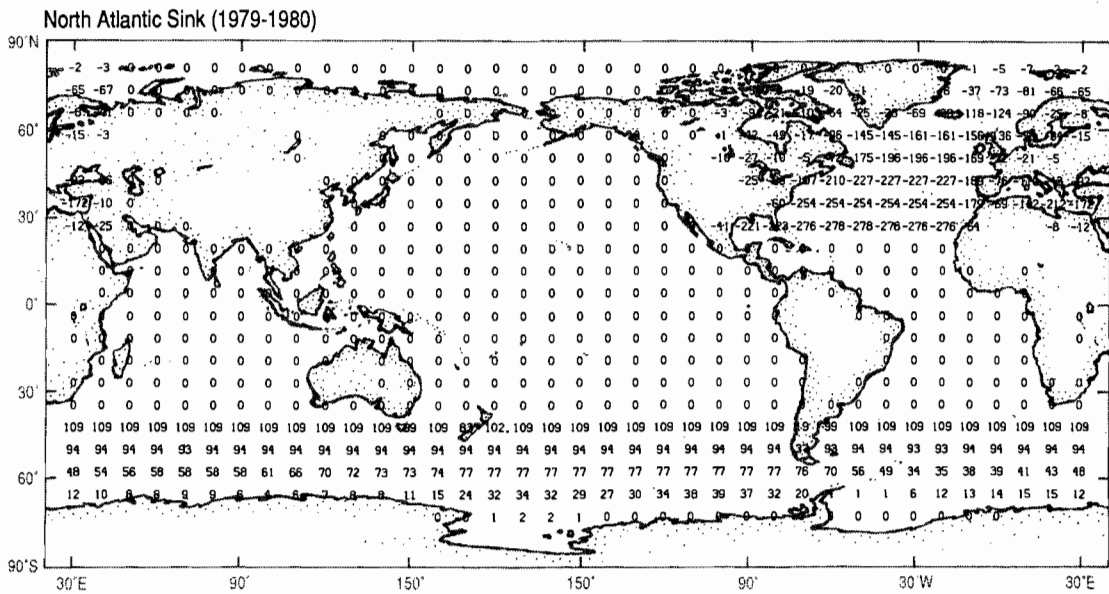
Fig. 16. Same as Figure 15 but for the absorption of CO$_2$ in the North Atlantic Ocean, balanced by a release in the southern oceans, F_{ATL}.

Uniform Ocean Sink (1979-1980)
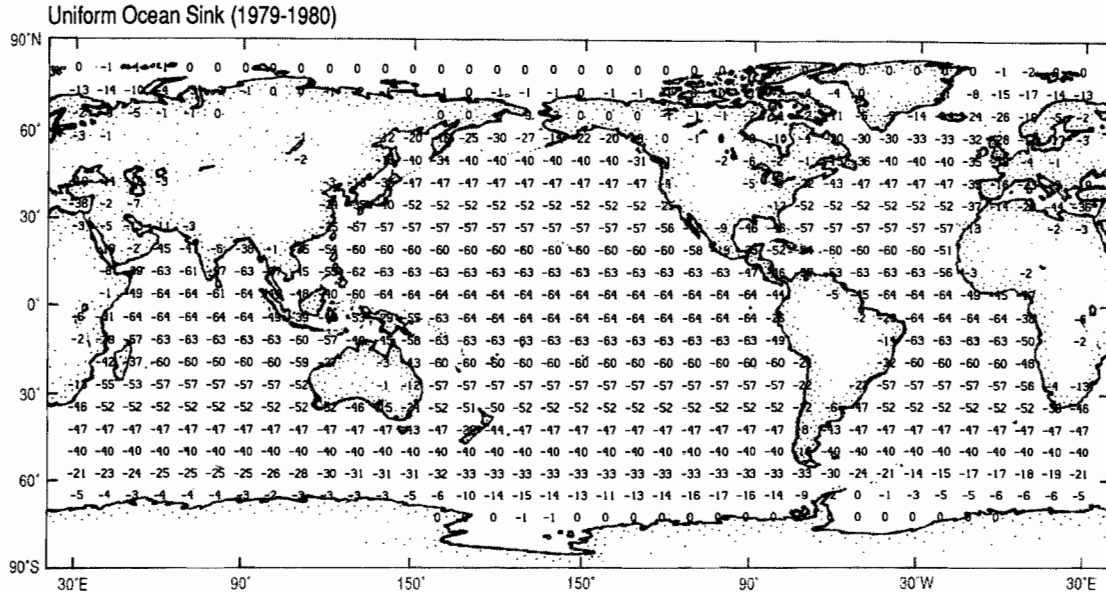
Fig. 17. Same as Figure 15, but for the removal of industrial CO_2 from the air in 1979–1980 assumed to be at a constant rate per unit area, F_{UOS}, in units of 10^8 kgC yr^{-1}.

equal to zero as was the corresponding term, $Q(\mathbf{x},t)$ for CO_2 (see section 2). The boundary flux of $^{13}CO_2$ at the surface of the earth we denote as $^*F_{CMPS}$. This flux, which is expressed as a sum of components, $^*F_i$, is analogous to the composite CO_2 boundary flux, F_{CMPS}, in equation (4.1). The solution of (5.1), denoted by $^*C_{CMPS}$, is then given by

$$^*C_{CMPS}(\mathbf{x},t) = {}^*C_o + \sum_{i=1}^{n} {}^*C_i(\mathbf{x},t) \qquad (5.2)$$

where $^*C_i$ are the solutions of equation (5.1) corresponding to the particular rare isotopic boundary fluxes, $^*F_i$. The term, $^*C_o$, denotes the constant background concentration of $^{13}CO_2$, corresponding to the background concentration, C_o, for the sum of $^{12}CO_2$ and $^{13}CO_2$.

Stable carbon isotope ratios are commonly expressed by a reduced ratio $^{13}\delta$ defined as

$$^{13}\delta = r/r_s - 1 \qquad (5.3)$$

where r and r_s denote the $^{13}C/^{12}C$ ratio of the sample and of a standard respectively. As in the preceding paper, [Keeling et al., this volume, a] we adopt the value $r_s = 0.0112372$ for standard PDB as established by Mook and Grootes [1973, p. 296]. Henceforth in this article, and succeeding companion articles, we omit the left superscript 13 on δ.

The transformation of equations in $^*C$ to the δ system is simplified if we first express isotopic ratios in terms of the sum of carbon-12 and carbon-13. For this purpose we introduce the quantities

$$R = {}^*C/C = r/(1+r) \qquad (5.4)$$

$$R_s = r_s/(1+r_s) = 0.01111232854 \qquad (5.5)$$

$$R_o = {}^*C_o/C_o \qquad (5.6)$$

$$R_i = {}^*C_i/C_i \qquad (5.7)$$

$$\delta' = R/R_s - 1 \qquad (5.8)$$

the latter with specific values δ_o', δ_i', and δ_{CMPS}', corresponding to R_o, R_i, and R_{CMPS}, respectively.

In the three-dimensional transport model the composite $^{13}C/(^{12}C + ^{13}C)$ field of atmospheric CO_2 arising from the sum of the contributions of all of the component sources is obtained by dividing equation (5.2) by (4.2) to yield the ratio, R_{CMPS}. Thus at any specified time and location

$$R_{CMPS} = \frac{{}^*C_o + \sum_{i=1}^{n} {}^*C_i}{C_o + \sum_{i=1}^{n} C_i} = \frac{(\delta_o' + 1)C_oR_s + \sum_{i=1}^{n} (\delta_i' + 1)C_iR_s}{C_o + \sum_{i=1}^{n} C_i}$$

$$= R_s \left[\frac{\delta_o'C_o + \sum_{i=1}^{n} \delta_i'C_i}{C_{CMPS}} + 1 \right] \qquad (5.9)$$

Since from equation (5.8) it follows that

$$R_{CMPS} = (\delta_{CMPS}' + 1) R_s \qquad (5.10)$$

the last form of writing equation (5.9) is equivalent to

$$\delta_{CMPS}' C_{CMPS} = \delta_o' C_o + \sum_{i=1}^{n} \delta_i' C_i \qquad (5.11)$$

Thus the product of δ' and CO_2 concentration, C, exactly obeys the additivity rule of equation (3.2) of the preceding article [Keeling et al., this volume, a].

Equation (5.11) allows the calculation of the isotopic composition of the composite solution, $\delta_{CMPS}'(\mathbf{x},t)$, from the fields generated by the individual source components, $\delta_i'(\mathbf{x},t)$, related to the $^*C_i(\mathbf{x},t)$ via equations (5.7) and (5.8).

The relation between the δ' and the δ values is given by

$$\delta' = \frac{\delta}{1 + r_s(1+\delta)} \qquad (5.12)$$

which follows directly from the definitions (5.3) to (5.8). Because $|R_s\delta| \ll 1$, equation (5.12) may be rearranged and expanded

$$\delta' = \delta \cdot \frac{R_s}{r_s} \cdot \frac{1}{1 + R_s\delta} \qquad (5.13)$$

$$= \delta \cdot \frac{R_s}{r_s} \cdot \left\{ 1 - R_s\delta + R_s^2\delta^2 - \cdots \right\} \qquad (5.14)$$

The second term in the sum on the right of equation (5.14), $R_s\delta$, is on the order of 10^{-4} since, as shown below, the isotopic compositions of all sources considered are so close to the PDB standard that their δ values do not exceed 30‰. The higher order terms are still smaller. We therefore assume that δ is proportional to δ', and we approximate equation (5.11) by

$$\delta_{CMPS} C_{CMPS} = \delta_o C_o + \sum_{i=1}^{n} \delta_i C_i \qquad (5.15)$$

Multiplying both sides of equation (4.2) by δ_o, subtracting this relation from equation (5.15), and then dividing both sides of the resulting equation by C_{CMPS}, we form the difference equation

$$\delta_{CMPS}(\mathbf{x},t) - \delta_o = \sum_{i=1}^{n} \Delta\delta_i(\mathbf{x},t) \qquad (5.16)$$

where by definition

$$\Delta\delta_i(\mathbf{x},t) = \frac{(\delta_i(\mathbf{x},t) - \delta_o)C_i(\mathbf{x},t)}{C_{CMPS}(\mathbf{x},t)} \qquad (5.17)$$

and where we have indicated by $(\mathbf{x},t)$ which quantities represent scalar fields depending on space and time.

The increment, $\Delta\delta_i(\mathbf{x},t)$, denotes the shift in isotopic ratio of atmospheric CO_2 corresponding to the incremental change in concentration $C_i(\mathbf{x},t)$. The constant, δ_o, denotes the reduced isotopic ratio corresponding to the constant background concentrations $^*C_o$ and C_o defined by equations (5.2) and (4.2), respectively. The isotopic increment, $\Delta\delta_i(\mathbf{x},t)$, is thus proportional to the difference in isotopic ratio $\delta_i(\mathbf{x},t)$ of component i from a constant reference ratio, and its deviation respects the additivity rule mentioned after equation (5.11).

5.2   Isotopic Contribution from the Industrial Source Component

The isotopic composition of CO_2 gas released by fossil fuel combustion and cement production in our calculations was assigned a value of

$$\delta_{IND} = -27.28‰ \qquad (5.18)$$

based on the estimate of Tans [1981, p. 128]. This value is assumed to be spatially constant since we have no information on any geographic variations. We also assume that it does not vary with time because the small variations which would be inferred with respect to variations in the proportions of different types of fuels burned in different years are negligible, and we have no information on how the isotopic ratios of these fuels might have changed between 1980 and 1984. With these assumptions,

$\delta_{IND}(\mathbf{x},t)$ in (5.16) reduces to a constant, and the isotopic contribution from the industrial source is given by

$$\Delta\delta_{IND}(\mathbf{x},t) = (\delta_{IND} - \delta_o)\frac{C_{IND}(\mathbf{x},t)}{C_{CMPS}(\mathbf{x},t)} \qquad (5.19)$$

5.3   Isotopic Contributions from the Biospheric Source Components

The isotopic compositions of the fluxes of CO_2 between the atmosphere and the terrestrial biosphere are assumed to be uniform in space, but to vary globally from year to year as prescribed by the compartment model of Keeling et al. [this volume, a]. In the two isotopic simulations which we consider they are prescribed by the mean δ value in each reservoir for the first of January of 1980 and 1984. They also depend on certain fractionation factors, α_i, as employed in the compartment model [Keeling et al., this volume, a, Tables 8 and 12]. Specifically, we use the following values

$$\delta_{PHO} = \alpha_{ab}(1 + \delta_a) - 1 = -25.5282‰ \text{ in } 1980$$
$$= -25.5866‰ \text{ in } 1984$$
$$(5.20)$$

for the isotopic composition of terrestrial biospheric CO_2 uptake by photosynthesis and

$$\delta_{BIO} = \alpha_{ba}(1 + \delta_b) - 1 = -24.9296‰ \text{ in } 1980$$
$$= -24.9864‰ \text{ in } 1984$$
$$(5.21)$$

for the isotopic composition of terrestrial biospheric CO_2 release.

5.3.1   Net primary productivity. The isotopic contribution resulting from NPP at any location or time is prescribed in the three-dimensional model by

$$\Delta\delta_{NPP}(\mathbf{x},t) = (\delta_{PHO} - \delta_o)\frac{C_{NPP}(\mathbf{x},t)}{C_{CMPS}(\mathbf{x},t)} \qquad (5.22)$$

5.3.2   Respiration. In the case of the respiration of the terrestrial biosphere, the compartment model of Keeling et al. [this volume, a] considers only the exchange of long-lived carbon, with the global flux, averaged over 1 year and set equal to 24.624×10^{12} kg yr^{-1}. This estimate derives from a study by SCEP [1970, p. 161] in which the global organic biospheric carbon pool is divided into short and long-lived fractions on the basis of estimated residence times and of a global NPP of 56×10^{12} kgC yr^{-1}, also averaged over 1 year.

To be consistent in modeling the isotopic composition of respiratory carbon with the compartment model predictions, we take the respiratory flux through the global short-lived pool to be $56.00 - 24.624 = 31.376 \times 10^{12}$ kgC yr^{-1}, although in computing fluxes we use the slightly different total flux estimate from remote sensing data of 55.927×10^{12} kgC yr^{-1}, as discussed in section (4.3.1). We assume that the short-lived carbon has exactly the isotopic ratio of carbon transferred to the biosphere according to equation (5.20) by photosynthesis, whereas the long-lived carbon has the ratio prescribed by equation (5.21) and is thus displaced from dynamic isotopic equilibrium owing to the input of industrial carbon to the carbon cycle (the "carbon-13 Suess effect" [Keeling, 1979]).

We further assume that the carbon released by both the short and long-lived biospheric carbon pools is not isotopically fractionated ($\alpha_{ba} = 1$). Hence the average δ value of the respiratory flux is given by

$$\delta_{RES} = (1 - \mu)\delta_{PHO} + \mu\,\delta_{BIO} \qquad (5.23)$$

$$= -25.2650\permil \text{ in 1980}$$

$$= -25.3227\permil \text{ in 1984}$$

where μ denotes the long-lived fraction of the global carbon pool (= 24.624/56.0). The isotopic contribution to the atmospheric δ-field is given by

$$\Delta\delta_{RES}(\mathbf{x},t) = (\delta_{RES} - \delta_o)\,\frac{C_{RES}(\mathbf{x},t)}{C_{CMPS}(\mathbf{x},t)} \qquad (5.24)$$

5.3.3 Biospheric destruction and fertilization. The isotopic contributions resulting from the fluxes owing to biospheric destruction and fertilization are computed by assuming the same isotopic compositions for uptake and release of CO_2 by the terrestrial biosphere as for photosynthesis and respiration respectively, hence

$$\Delta\delta_{DES}(\mathbf{x},t) = (\delta_{RES} - \delta_o)\,\frac{C_{DES}(\mathbf{x},t)}{C_{CMPS}(\mathbf{x},t)} \qquad (5.25)$$

and

$$\Delta\delta_{FER}(\mathbf{x},t) = (\delta_{PHO} - \delta_o)\,\frac{C_{FER}(\mathbf{x},t)}{C_{CMPS}(\mathbf{x},t)} \qquad (5.26)$$

5.4 Isotopic Contributions Arising from CO_2 Exchange with the Oceans

The exchange flux of $^{13}CO_2$ between the oceans and the atmosphere at a given location and time is modeled by an expression similar to equation (4.20). It may be written as

$$^*F_{ex} = \alpha'_{ma}R_mF_{ma} - \alpha'_{am}R_aF_{am} \qquad (5.27)$$

(see, for example, Siegenthaler and Münnich [1981]). Here

$$F_{ma} = k_{ex}\,pCO_{2\,sea} \qquad (5.28)$$

$$F_{am} = k_{ex}\,pCO_{2\,air} \qquad (5.29)$$

denote the fluxes of $^{12}C + ^{13}C$ from the ocean surface layer to the atmosphere and from the atmosphere to the surface layer, respectively, and R_a and R_m denote the $^{13}C/(^{12}C + ^{13}C)$ ratios of CO_2 in the atmosphere and of dissolved inorganic carbon in the surface oceans, respectively. The fractionation factors are expressed in the δ' system (see Table 8 of Keeling et al. [this volume, a]). In general all quantities in equation (5.27) vary with time and location.

The first term in equation (5.27) expresses the flux of $^{13}CO_2$ from the oceanic surface to the air. The $^{13}C/(^{12}C + ^{13}C)$ ratio, $R_{sea\,to\,air}$, of the corresponding full flux, F_{ma} is the product of R_m and the kinetic fractionation factor α'_{ma}, i.e.,

$$R_{sea\,to\,air} = \alpha'_{ma}R_m \qquad (5.30)$$

To transform this equation, and afterwards equation (5.27), to the δ system we replace the $^{13}C/(^{12}C + ^{13}C)$ ratios in equation (5.30) by respective $^{13}C/^{12}C$ ratios according to equation (5.4). The $^{13}C/^{12}C$ ratio corresponding to $R_{sea\,to\,air}$, is

$$r_{sea\,to\,air} = \alpha_{ma}\,r_m \qquad (5.31)$$

Hence

$$\alpha'_{ma}R_m = \frac{\alpha_{ma}\,r_m}{(1 + r_{sea\,to\,air})} \qquad (5.32)$$

Similarly, for the flux of $^{13}CO_2$ from the air to the sea

$$\alpha'_{am}R_a = \frac{\alpha_{am}\,r_a}{(1 + r_{air\,to\,sea})} \qquad (5.33)$$

where $r_{air\,to\,sea}$ denotes the $^{13}C/^{12}C$ ratio of F_{am}. The ratios $r_{sea\,to\,air}$ and $r_{air\,to\,sea}$ differ from the standard ratio, r_s, by no more than $10\permil$. Thus these ratios may be replaced in the denominators of equations (5.32) and (5.33) by r_s to the same approximations as equation (5.15). Substitution of equations (5.32) and (5.33) into equation (5.27), after invoking this approximation, results in the expression

$$^*F_{ex} = (\alpha_{ma}r_mF_{ma} - \alpha_{am}r_aF_{am})/(1 + r_s) \qquad (5.34)$$

or, in view of equation (5.5)

$$^*F_{ex} = (\alpha_{ma}r_mF_{ma} - \alpha_{am}r_aF_{am})(R_s/r_s) \qquad (5.35)$$

To resolve this flux into previously identified source components, we first relate the separate fluxes F_{am} and F_{ma} to the respective CO_2 partial pressures via equations (5.28) and (5.29). We thus obtain the expression

$$^*F_{ex} = k_{ex}(R_s/r_s)(\alpha_{ma}r_mpCO_{2\,sea} - \alpha_{am}r_apCO_{2\,air}) \quad (5.36)$$

Next we investigate the nature of the fractionation process involved in air-sea exchange.

The kinetic fractionation factor, α_{ma}, is the product of the equilibrium fractionation factor, α_{DIC}, of dissolved CO_2 with respect to total dissolved inorganic carbon, DIC (equal to CO_2 + HCO_3^- + CO_3^{2-}), multiplied by the ratio of the transfer velocities of $^{13}CO_2$, w^*, and of CO_2, w

$$\alpha_{ma} = \alpha_{DIC}\,\frac{^*w}{w} \qquad (5.37)$$

The other kinetic fractionation factor, α_{am}, is given by the product of the equilibrium fractionation factor of dissolved CO_2 with respect to gaseous CO_2, α_β, together with the ratio of the transfer velocities of $^{13}CO_2$ and CO_2 [Siegenthaler and Münnich, 1981, p. 250]. Thus

$$\alpha_{am} = \alpha_\beta\,\frac{^*w}{w} \qquad (5.38)$$

A small additional effect related to the reaction of dissolved CO_2 with OH^- is included [Siegenthaler and Münnich, 1981, p. 255].

The $^{13}C/^{12}C$ equilibrium fractionation factor of gaseous CO_2 with respect to total dissolved inorganic carbon is defined as the ratio α_{ma}/α_{am}, hence taking into account equations 5.37 and 5.38

$$\alpha_{eq} = \frac{\alpha_{ma}}{\alpha_{am}} = \frac{\alpha_{DIC}}{\alpha_\beta} \qquad (5.39)$$

The temperature dependency of the equilibrium fractionation of gaseous CO_2 with respect to dissolved HCO_3^-, α_b, has been measured by Mook et al. [1974, p. 175]:

$$\alpha_b = 1.02389 - \frac{9.483}{T + 273.15} \qquad (5.40)$$

where the temperature, T, is given in degrees centigrade. Since total dissolved inorganic carbon consists of about 85 percent HCO_3^-, and the fractionation factors for the remaining inorganic carbon species are nearly the same as for HCO_3^-, we neglect the small influences of these on the isotopic equilibrium and equate α_b with α_{eq} [see Keeling et al., this volume, a, Table 8].

Considerable simplification results if we next make several approximations. First, we neglect the unknown but presumably small temperature dependencies of the transfer velocity ratio, $*w/w$, and equilibrium fractionation, α_β, of dissolved CO_2 with respect to gaseous CO_2, on the grounds that these fractionations are too slight to exhibit a strong temperature dependency compared to that of α_{DIC}. Thus we will henceforth assume that α_{am} is a constant whereas α_{ma} varies with location and time in accordance with variations implied by equation (5.40), where the temperature, T, is specified by the same field employed in the model to compute $pCO_{2\,sea}$. We adopt for α_{am} the constant value adopted in the compartment model calculations as listed in Table 7.

We further assume constant values for r_a and r_m in equation (5.36). These we obtain from compartment model predictions of δ_a and δ_m [Keeling et al., this volume, a, Table 12] via equation (5.3). This approximation is reasonable because the $^{13}C/^{12}C$ ratio of atmospheric CO_2 on annual average varies regionally by at most a few tenths of a per mil [Keeling et al., this volume, a]. Similarly the $^{13}C/^{12}C$ ratio of inorganic carbon in the surface ocean water exhibits variations on the order of 0.5‰ [Kroopnik et al., 1977], whereas the equilibrium fractionation factor, α_{eq}, changes by more than 3‰ between 0° and 30°C. We also neglect any time or space variations in k_{ex} as was done for CO_2 (cf. equation 4.20).

Thus we assume that equation (5.36) has the explicit time and space dependency

$$*F_{ex}(\mathbf{x},t) =$$

$$k_{ex}(R_s/r_s)\alpha_{am}(\alpha_{eq}(\mathbf{x},t)r_m pCO_{2\,sea}(\mathbf{x},t) - r_a pCO_{2\,air}(\mathbf{x},t)) \quad (5.41)$$

where we have replaced α_{ma} by $\alpha_{am}\alpha_{eq}$ according to equation (5.39).

To resolve the flux, $*F_{ex}$, into components, we introduce a globally and annually averaged equilibrium fractionation factor $\langle\alpha_{eq}\rangle$ of gaseous CO_2 with respect to total dissolved inorganic carbon. From the temperature fields of Alexander and Mobley [1976] and equation (5.40) we calculate that $\langle\overline{\alpha_{eq}}\rangle = 0.991445$. Next we divide the $^{13}CO_2$ exchange flux into three parts as follows. The first part we prescribe to reflect the temperature dependent fraction (TDF) of the isotopic equilibrium between CO_2 in air and sea water, i.e.,

$$*F_{TDF}(\mathbf{x},t) = k_{ex}(R_s/r_s)\alpha_{am}r_m pCO_{2\,sea}(\mathbf{x},t)(\alpha_{eq}(\mathbf{x},t) - \langle\overline{\alpha}_{eq}\rangle)$$

$$(5.42)$$

The remaining part of the flux we will further divide into two parts in order to separate the dependencies of this remainder on the air to sea differences in isotopic ratio and partial pressure.

With regard to the isotopic difference, since we assume that the isotopic ratios r_a and r_m are constant, the isotopic field of atmospheric CO_2 is influenced only by a departure from global isotopic equilibrium brought about by perturbations to the carbon cycle. The principal perturbation is produced by industrial CO_2, but biospheric destruction and fertilization also contribute. Since these perturbations are already allowed for in assigning magnitudes to r_a

and r_m for specific times, the contribution of this component to $*F_{ex}$ is evidently

$$*F_{SUE}(\mathbf{x},t) = k_{ex}(R_s/r_s)\alpha_{am}pCO_{2\,air}(\mathbf{x},t)(\langle\overline{\alpha_{eq}}\rangle r_m - r_a) \quad (5.43)$$

where, to obtain this expression, equation (5.42) is first subtracted from equation (5.41) and then, in the resulting equation, $pCO_{2\,sea}(\mathbf{x},t)$ is set equal to $pCO_{2\,air}(\mathbf{x},t)$ to remove the influence of the partial pressure gradient from the expression. We label this flux "SUE" since the perturbation involved is sometimes called the "carbon-13 Suess effect".

The part of the flux not included in the sum of $*F_{TDF}$ and $*F_{SUE}$ is evidently

$$*F_{OCD}(\mathbf{x},t) = k_{ex}(R_s/r_s)\alpha_{am}\langle\overline{\alpha_{eq}}\rangle r_m(pCO_{2\,sea}(\mathbf{x},t) - pCO_{2\,air}(\mathbf{x},t))$$

$$(5.44)$$

which we label "OCD" to indicate that it is "oceanic concentration dependent."

As can be seen, this part of the flux depends on the difference in CO_2 partial pressure, $pCO_{2\,sea}(\mathbf{x},t) - pCO_{2\,air}(\mathbf{x},t)$, and thus is proportional to the CO_2 gas exchange flux F_{ex} defined by equation (4.20). This flux is due to the sum of all of the oceanic source components defined in subsection 4.4, i.e.,

$$F_{ex}(\mathbf{x},t) = F_{TDE}(\mathbf{x},t) + F_{EQU}(\mathbf{x}) + F_{ATL}(\mathbf{x}) + F_{UOS}(\mathbf{x}) \quad (5.45)$$

Hence the corresponding isotopic flux is

$$*F_{OCD}(\mathbf{x},t) = *F_{TDE}(\mathbf{x},t) + *F_{EQU}(\mathbf{x}) + *F_{ATL}(\mathbf{x}) + *F_{UOS}(\mathbf{x}) \quad (5.46)$$

Thus we are able to separate the composite isotopic flux, $*F_{ex}$, into a sum of distinct components, two of which, $*F_{TDF}$ and $*F_{SUE}$, are expressed with the restriction that no associated net air-sea flux of CO_2 takes place and the others, expressed as a series in equation (5.46), correspond to total stable carbon components previously defined.

To compute the contribution of the isotopic exchanges having no associated net CO_2 flux to the composite isotopic field, δ_{CMPS}, requires a modification to equation (5.16), since this equation is valid only if there is a change in CO_2 concentration, C_i, associated with each isotopic contribution, $\Delta\delta_i$. First, we write in place of equation (5.9)

$$R_{CMPS} = \frac{*C_o + \sum_{i=1}^{n} *C_i + *C_{iso}}{C_o + \sum_{i=1}^{n} C_i} \quad (5.47)$$

where n sums over the number of modeled isotopic exchanges for which there is an associated change in concentration, and $*C_{iso}$ denotes the increase in ^{13}C associated with the sum of the fluxes $*F_{TDF}$ and $*F_{SUE}$. After performing the arithmetic operations as before, we derive for $\delta_{CMPS}(\mathbf{x},t)$ the following expression in place of equation (5.16)

$$\delta_{CMPS}(\mathbf{x},t) - \delta_o = \sum_{i=1}^{n} \Delta\delta_i(\mathbf{x},t) + \frac{*C_{iso}(\mathbf{x},t)}{C_{CMPS}(\mathbf{x},t)R_s} \quad (5.48)$$

We now denote the carbon-13 increases in atmospheric CO_2 associated with $*F_{TDF}$ and $*F_{SUE}$ as $*C_{TDF}$ and $*C_{SUE}$, respectively. From the linearity of model equation (5.1) it follows that

$$*C_{iso}(\mathbf{x},t) = *C_{TDF}(\mathbf{x},t) + *C_{SUE}(\mathbf{x},t) \quad (5.49)$$

The flux, $^*F_{TDF}$, varies in time and space but is globally balanced. In order to simulate its effect on the atmospheric $^{13}C/^{12}C$ ratio, a separate three-dimensional transport model run was performed from which we obtained the corresponding atmospheric $^{13}CO_2$ concentration field. As a further simplification in this run we ignored the relatively small variations in $^*F_{TDF}$ which result from variations in the oceanic CO_2 partial pressure by approximating $pCO_{2\,sea}(x,t)$ in terms of a constant globally and annually averaged value for the partial pressure in air, $<p\overline{CO}_{2\,air}>$, as given by the compartment model of Keeling et al. [this volume, a] (336.88 ppm in 1980, and of 341.54 ppm in 1984, both for January 1). In this way we disassociate this component from the adjustable and interannually variable oceanic source components which determine the model representation of $pCO_{2\,sea}$ without introducing significant error into the computation. Then, assuming uniform atmospheric and surface oceanic background isotopic ratios, r_a and r_m as noted above, we directly calculate the contribution to the composite atmospheric field δ_{CMPS} by

$$\Delta\delta_{TDF}(\mathbf{x},t) = \frac{^*C_{TDF}(\mathbf{x},t)}{C_{CMPS}(\mathbf{x},t)\,R_s} \qquad (5.50)$$

where $^*C_{TDF}(\mathbf{x},t)$ is generated by the flux

$$^*F_{TDF}(\mathbf{x},t) = k_{ex}R_s\alpha_{am}(1+\delta_m)<p\overline{CO}_{2\,air}>(\alpha_{eq}(\mathbf{x},t)-<\overline{\alpha}_{eq}>)$$
$$(5.51)$$

and where r_m/r_s in equation (5.42) is replaced by $(1+\delta_m)$ in accordance with equation (5.3). The corresponding expression for the flux associated with the carbon-13 Suess effect is

$$^*F_{SUE}(\mathbf{x},t) = k_{ex}R_s\alpha_{am}<p\overline{CO}_{2\,air}>(<\overline{\alpha}_{eq}>(1+\delta_m)-(1+\delta_a))$$
$$(5.52)$$

where we replaced the variable, $pCO_{2\,air}(\mathbf{x},t)$, by its global annual average, $<p\overline{CO}_{2\,air}>$, to be consistent with the approximation used to compute the oceanic fluxes of CO_2.

Since all of the terms in equation (5.52) are assumed to be constant, this equation represents a flux uniformly distributed over the ocean surface. Hence its atmospheric $^{13}CO_2$ concentration field is proportional to the CO_2 component C_{UEX} used to compute the oceanic uptake of industrial CO_2 via equation (4.30), which has the same source structure. Since C_{UEX} was defined as a source to the atmosphere and was computed for a globally and annually averaged CO_2 partial pressure difference

$$<p\overline{CO}_{2\,sea}> - <p\overline{CO}_{2\,air}> = 3.7609\ \text{ppm} \qquad (5.53)$$

(see equations 4.20 and 4.30), whereas the Suess effect arises from isotopic exchange involving the entire amount of CO_2 in the atmosphere, the incremental change in concentration, C_{SUE}, associated with the Suess effect is given by the expression

$$C_{SUE}(\mathbf{x},t) = \frac{<p\overline{CO}_{2\,air}>}{3.7609\ \text{ppm}}\ C_{UEX}(\mathbf{x},t) \qquad (5.54)$$

It follows that

$$\Delta\delta_{SUE}(\mathbf{x},t) = \alpha_{am}(<\overline{\alpha}_{eq}>(1+\delta_m)-(1+\delta_a))\frac{C_{SUE}(\mathbf{x},t)}{C_{CMPS}(\mathbf{x},t)} \qquad (5.55)$$

where $<p\overline{CO}_{2\,air}>$, δ_a, and δ_m are set equal to the predictions of the box diffusion model for the appropriate year, and the fractiona-

tion factor α_{am} is a constant as discussed after equation (5.40). The equilibrium factor $<\overline{\alpha}_{eq}>$ (see Table 7) is assigned a value as explained after equation (5.41).

Specifically, we compute the following values for the reduced isotopic ratio of the CO_2 released by the oceans

$$\delta_{SUE} = \alpha_{am}(<\overline{\alpha}_{eq}>(1+\delta_m)-(1+\delta_a))+\delta_a \qquad (5.56)$$
$$= -6.9328\%o\ \text{in 1980}$$
$$= -6.9872\%o\ \text{in 1984}$$

The remaining isotopic flux, $^*F_{OCD}(\mathbf{x},t)$, since it is proportional to a sum of components affecting the CO_2 concentration, is readily computed in the manner of the isotopic components involving net CO_2 exchanges. In accordance with equation (5.44) the reduced isotopic ratio of the CO_2 emitted or absorbed by ocean water, expressed as a global annual average, is

$$\delta_{OCD} = \alpha_{am}<\overline{\alpha}_{eq}>(1+\delta_m)-1 \qquad (5.57)$$
$$= -8.7192\%o\ \text{in 1980}$$
$$= -8.7736\%o\ \text{in 1984}$$

As in the case of the carbon-13 Suess effect we replace the quantity $pCO_{2\,air}(\mathbf{x},t)$ by the globally and annually averaged value, $<p\overline{CO}_{2\,air}>$. The isotopic contribution of this flux to the composite isotopic field is thus prescribed by

$$\Delta\delta_{OCD}(\mathbf{x},t) = (\delta_{OCD}-\delta_o)\frac{C_{OCD}(\mathbf{x},t)}{C_{CMPS}(\mathbf{x},t)} \qquad (5.58)$$

where (cf. equation 5.45)

$$C_{OCD}(\mathbf{x},t) = C_{TDE}(\mathbf{x},t)+C_{EQU}(\mathbf{x},t)+C_{ATL}(\mathbf{x},t)+C_{UOS}(\mathbf{x},t) \qquad (5.59)$$

The isotopic term, $\Delta\delta_{OCD}$, contributes so marginally to the isotopic field of atmospheric CO_2 [Keeling et al. this volume, b] that we will consider only the summed contribution of the individual components specified in equation (5.59). Heimann et al. [this volume] disregard altogether the very small contribution to the seasonal variation in $^{13}C/^{12}C$ ratio of atmospheric CO_2 arising from these terms.

5.5 Summary

In summary we obtain, in accordance with equation (5.48), the composite $^{13}C/^{12}C$ ratio field, $\delta_{CMPS}(\mathbf{x},t)$, in terms of isotopic contributions, $\Delta\delta_i(\mathbf{x},t)$, and the background ratio, δ_o, explicitly written for the eight components as

$$\delta_{CMPS} = \Delta\delta_{IND}+\Delta\delta_{NPP}+\Delta\delta_{RES}+\Delta\delta_{FER}+\Delta\delta_{DES}$$
$$+\Delta\delta_{TDF}+\Delta\delta_{SUE}+\Delta\delta_{OCD}+\delta_o \qquad (5.60)$$

where all terms except δ_o depend on $\mathbf{x}$ and t, and where $\Delta\delta_{OCD}$ is a composite of the four individual oceanic components of equation (5.59). As explained in the preceding sections, all isotopic contributions were computed directly from appropriate CO_2 component fields except $\Delta\delta_{TDF}$, which necessitated a separate transport model run.

The numerical values assigned to the constant isotopic parameters are listed in Table 7. The computational equations for the $\Delta\delta_i$ are summarized in Table 8. Here we explicitly set the background isotopic ratio, δ_o, equal to the ratio δ_a for the atmosphere as

TABLE 7. Isotopic Parameters to Compute Source-Sink
Functions of the Three-Dimensional Model

Symbol	Definition	Value
α_{ab}	$^{13}C/^{12}C$ fractionation factor for CO_2 uptake by the local biosphere	0.9818731
α_{ba}	$^{13}C/^{12}C$ fractionation factor for CO_2 release by the terrestrial biosphere	1.0000000
α_{am}	$^{13}C/^{12}C$ fractionation factor for CO_2 uptake by the surface ocean water	0.9982000
α_{ma}	$^{13}C/^{12}C$ fractionation factor for CO_2 evasion from surface ocean water	0.9896604
$<\bar{\alpha}_{eq}>$	globally and annually averaged equilibrium fractionation factor of gaseous CO_2 with respect to total dissolved inorganic carbon	0.991445
r_s	$^{13}C/^{12}C$ ratio of isotopic standard PDB	0.0112372
δ_a	δ value of atmospheric CO_2 for January 1, 1980, 1984, respectively (‰)	−7.5379, −7.5974
δ_b	δ value of carbon in the long-lived terrestrial biosphere for January 1, 1980, 1984, respectively (‰)	−24.9296, −24.9864
δ_m	δ value of dissolved inorganic carbon in surface ocean water for January 1, 1980, 1984, respectively (‰)	1.6373/1.5824
δ_{IND}	δ value of fossil fuel carbon (‰)	−27.2800

TABLE 8. Formulas for Computing Isotopic
Contributions of Individual Source Components
(in ‰) for a Specific Location

For 1980:

$\Delta\delta_{IND} = (-27.28 + 7.5379) \, C_{IND}/C_{CMPS}$

$\Delta\delta_{NPP} = (-25.5282 + 7.5379) \, C_{NPP}/C_{CMPS}$

$\Delta\delta_{RES} = (-25.2650 + 7.5379) \, C_{RES}/C_{CMPS}$

$\Delta\delta_{DES} = (-25.2650 + 7.5379) \, C_{DES}/C_{CMPS}$

$\Delta\delta_{FER} = (-25.5282 + 7.5379) \, C_{FER}/C_{CMPS}$

$\Delta\delta_{TDF}$: special computer run

$\Delta\delta_{SUE} = (-6.9328 + 7.5379) \, C_{SUE}/C_{CMPS}$

$\Delta\delta_{OCD} = (-8.7192 + 7.5379) \, C_{OCD}/C_{CMPS}$

For 1984:

$\Delta\delta_{IND} = (-27.28 + 7.5974) \, C_{IND}/C_{CMPS}$

$\Delta\delta_{NPP} = (-25.5866 + 7.5974) \, C_{NPP}/C_{CMPS}$

$\Delta\delta_{RES} = (-25.3227 + 7.5974) \, C_{RES}/C_{CMPS}$

$\Delta\delta_{DES} = (-25.3227 + 7.5974) \, C_{DES}/C_{CMPS}$

$\Delta\delta_{FER} = (-25.5866 + 7.5974) \, C_{FER}/C_{CMPS}$

$\Delta\delta_{TDF}$: same as for 1980

$\Delta\delta_{SUE} = (-6.9872 + 7.5974) \, C_{SUE}/C_{CMPS}$

$\Delta\delta_{OCD} = (-8.7736 + 7.5974) \, C_{OCD}/C_{CMPS}$

Note

The component scaling factors discussed by Keeling et al. [this volume, b] are equivalent to the ratios $\Delta\delta_i/C_i$, and thus can be readily compared by dividing the sum or difference in parentheses by C_{CMPS}, for each component.

prescribed by the compartment model [Keeling et al., this volume, a, Table 12] for the specific year to which the calculation pertains, i.e.,

$$\delta_o = \delta_a \qquad (5.61)$$

$$= -7.5379 \text{ in } 1980$$

$$= -7.5974 \text{ in } 1984$$

Thus we assume that δ_a is the reduced ratio for the South Pole (see equation 5.2), an assumption which is nearly but not exactly correct. Afterwards, however, the value of δ_o is redetermined more realistically, as described by Keeling et al. [this volume, b], by a least squares fit to all appropriate observational data.

6.   Concluding Remarks

Following upon an analysis of observed atmospheric CO_2 data by Keeling et al. [this volume, a], we have developed a framework for using these data to interpret the global carbon cycle. Our basic approach has been to adapt the GISS three-dimensional tracer transport model developed by Russell and Lerner [1981], Hansen et al. [1983], and Fung et al. [1983] to predict CO_2 concentrations, taking into account observed wind fields of the atmosphere together with estimates of the sources and sinks of atmospheric CO_2. We have explained how we formulated this model, but we defer to two additional articles [Heimann et al. and Keeling et al., this volume, b] its use to interpret CO_2 observations and the justification for some of the major assumptions underlying its formulation. Thus our major conclusions are more appropriately stated in these subsequent articles. Here we will only remark on the performance of the model and provide a summary of our methodology for constructing the sources and sinks of atmospheric CO_2.

The three-dimensional atmospheric transport model employed in the present study is subject to several limitations which must be kept in mind:

1. The model lacks an explicitly formulated boundary layer.
2. The wind fields used were derived from observations over a single year during the Global Weather Experiment (GWE) of 1978–1979.
3. The model has a rather coarse horizontal resolution (7.83° latitude by 10.00° longitude).
4. Vertical convection is kept constant at each location during each month.

Depending on the time scale of interest, these limitations affect model predictions of tracer concentration distributions differently.

Over land, predictions of concentration variations on time scales shorter than a month are generally beyond the capabilities of the model. Here, the real boundary layer changes diurnally and its thickness depends critically on the locally prevailing stability of the lower troposphere and on the balance of the energy fluxes at the ground surface. Neither of these processes is included in the present transport model, except as a monthly averaged mixing effect arising from the convection formulation. Over the oceans these limitations of the model are less serious, because the boundary layer is in general more uniform and stationary than over land. Furthermore, the oceanic sources and sinks of CO_2 are widespread and relatively weak compared to continental sources and therefore do not greatly influence the CO_2 concentration in the overlying air on short time scales. Indeed, the model permits a coarse assessment of synoptic time scale variations of the atmospheric CO_2 concentration at oceanic stations, as described by Heimann et al. [this volume].

On longer time scales the lack of representativeness of the GWE wind fields constitutes one of the major limitations of the present model version. Even though the GWE data set represents probably the most complete and accurate description of the state of the global atmosphere to date, there exist nevertheless important spatial and temporal gaps in the observing systems, most notably in the tropical regions and over the southern hemisphere oceans [Bengtsson et al., 1982]. Also, there is some evidence that the GWE period of 1978–1979 is not typical of a climatic average year of the atmospheric circulation, especially in the southern hemisphere [Trenberth, 1984].

Because the atmospheric CO_2 observing stations on land used in our study are spaced relatively far apart, it can be anticipated that the coarse horizontal resolution of the model will not appear to be a serious limitation when comparing model simulations to data at these stations. The more closely spaced data from ships during the FGGE Shuttle of 1979–1980, also used in our study, however, do show discrepancies which may reflect the coarseness of the grid spacing, as discussed by Keeling et al. [this volume, b].

The limitations in assuming vertical convection to be constant during each month rule out simulations of subgridscale vertical transport on a synoptic scale, and thus probably degrade the predictions at Mauna Loa Observatory and at Ocean Station P, discussed by Heimann et al. [this volume]. The use of results from a general circulation model rather than actual weather observations to establish monthly averages of vertical convection probably further degrades the simulations on all time scales. We await a better transport model to resolve these questions.

For the model directly to predict atmospheric CO_2 concentrations, the sources and sinks of CO_2 at the earth's surface must be fully specified. Our direct knowledge of oceanic and biospheric exchange fluxes with the atmosphere is insufficient, however, to expect realistic predictions of atmospheric CO_2 concentrations without improving the specification of these fluxes on the basis of the agreement of model predictions with the observed CO_2 fields. But this use of adjustments to the fluxes cannot be carried so far as to invert the model to predict boundary fluxes from the atmospheric CO_2 distribution. Our observational data are far too sparse to specify adequately the three-dimensional CO_2 field.

We have adopted a compromise which we term the method of "integral constraints." For poorly known components of exchanges we have specified spatial and temporal variations, to the extent that the available independent data allow, but we have left as adjustable ("tunable") either the global annual average integral of the component's surface flux or some global measure of its seasonal amplitude.

To facilitate this approach we have broken the problem into parts. We have separately specified fluxes involving the oceans and terrestrial biosphere, and we have distinguished between seasonally varying and annual mean fluxes. We have further distinguished processes for which we could find more or less specific data to help us determine rates of exchange. Thus, for example, we separately computed the flux field owing to net primary productivity (NPP) of plants because satellite data for the greenness of the land permit us to estimate NPP everywhere over land.

Our first need for an adjustable model parameter arises because we could not find a similarly specific measure of the respiratory flux of plants, their detritus, and soils. We therefore sought an indirect factor to assist in predicting its spatial and temporal variation. We noted that it is strongly dependent on temperature, and we designated this dependency via a mathematical formula in which we have provided a single adjustable factor to describe how strong this dependency is. This factor is set to produce an optimal prediction of the seasonal cycle atmospheric CO_2 via a least squares fitting procedure. This prediction, however, must take into account all components of exchange since all, to some extent, contribute to the seasonal variations of atmospheric CO_2. To our advantage most of these components can be anticipated to produce variations too small to impact the fit significantly. Indeed only with respect to the seasonal variation in atmospheric CO_2 generated by the CO_2 partial pressure of sea water ($pCO_{2\,sea}$) are we apprehensive that uncertainties in our specification of this source component may significantly degrade our optimal prediction.

Furthermore, we take advantage of the ability of the model to distinguish regional differences in the carbon cycle, in an attempt to minimize this problem of a competing oceanic flux. In the temperate and polar regions of the northern hemisphere the oceanic CO_2 exchange component should have the least effect on the seasonal cycle of atmospheric CO_2 because of the large fraction of land relative to ocean and the strong seasonality of land plant activity. We therefore propose to use only northern hemisphere stations to determine the unknown global parameter in the specification of the respiration. Our estimate of the temperature dependence of respiration thus discriminates against possible evidence from equatorial stations, but near the equator temperature variations are expected to be small so that the use of a possibly biased scaling factor should not be a serious drawback. A further test of our approach can be made *a posteriori*: we may test whether the seasonal variations found by the model for oceanic

processes, indeed, are small enough not to interfere with our fit for respiration.

We have provided that two additional source components be adjustable. Both involve oceanic CO_2 and mainly influence the mean annual atmospheric CO_2 field. These components are so poorly known that no attempts at direct specifications are likely to be better than even the crudest of inverse calculations. But, to avoid a fully inverted computation, we have left to be fit only very broad regional averages of the mean annual CO_2 exchange associated with each component. We have distinguished tropical exchange from extratropical, and we have allowed that the exchange at high latitudes in the northern hemisphere differs from that in the southern hemisphere irrespective of the distribution of tropical exchange.

To establish regional patterns of fluxes within the areas being separately adjusted, we have employed the limited available observational data on the mean annual distribution of $pCO_{2\,sea}$. Near the equator in the Pacific Ocean, where data are most abundant, we have specified in some detail the mean annual pattern, including an obvious asymmetry with respect to the equator. On the basis of sparse supporting data elsewhere, we have afterwards specified similar zonal patterns for the other tropical oceans. Outside of the equatorial region only very crude estimates of the zonal distribution of $pCO_{2\,sea}$ are available owing to the unknown extent of seasonal variations. Within individual ocean basins we have made no attempt to specify any patterns at all, being content to obtain average rates of CO_2 exchange by adjustments to the observational data for atmospheric CO_2.

We cannot expect these broadly defined specifications to produce precise predictions of atmospheric CO_2 or to represent beyond doubt the true rates of exchange at the ocean surface. Our approach is only a first step. But it may be possible to make improvements later on. Our method of specifying patterns from whatever data are available, and then prorating these patterns via adjustable global scaling factors, is a method capable of providing improved predictions as better independent data became available. Significant improvements, however, probably require not only a better determination of $pCO_{2\,sea}$ for all seasons and over all major

oceanic basins but also a more correct determination of the rates of CO_2 gas exchange with respect to time and space, a problem further addressed by Keeling et al. [this volume, b].

In the case of the respiratory component of the terrestrial biosphere, in which we attempt to fix a universal time-independent temperature sensitivity parameter, a single fit to observational data was made, choosing data for near the year 1980 [see Heimann and Keeling, this volume]. In the case of the oceanic components, in which the fitting is directly related to establishing regionally integrated fluxes, we allow for interannual variability. This entails [see Keeling et al. this volume, b] making separate fits for each of the historic periods in which Keeling et al. [this volume, a] provide nearly full latitudinal coverage of the mean annual CO_2 field.

We have developed a methodology to compute the reduced $^{13}C/^{12}C$ ratio, δ, of atmospheric CO_2, as well as the concentration, as a function of time and location. Although a direct isotopic calculation is possible by repeating, for the rare species $^{13}CO_2$, the computations already made for the sum of the rare and abundant species which make up CO_2 gas, we gain insight into the complicated, even partly counter-intuitive, interplay of the isotopic and concentration fields by resolving the δ field into the same components already derived for the concentration field. In all but one instance in which a purely isotopic, temperature-dependent fractionation requires a separate computer run, we are able, with only minor simplifications of the exact relationships, to define isotopic component fields which differ from their counterparts for concentration only by constant factors. This methodology not only saves effort in making computations, but also allows use of the results already obtained for components of the concentration field to be the starting point for assessing the differing contributions of these components to the related isotopic field.

We have thus described procedures for defining carbon source components and for introducing these components into the three-dimensional atmospheric tracer transport model. Two succeeding articles discuss how well the model predictions match the observational data. The outcome for seasonal predictions is discussed by Heimann et al. [this volume], and for mean annual predictions by Keeling et al. [this volume, b].

Appendices

Appendix A. Interpolation and Integration of the GWE Wind Fields onto the Tracer Model Grid

The tracer model requires the specification of the air mass fluxes across the box boundaries of the tracer model grid. Only the horizontal fluxes are required, the vertical fluxes are then calculated from the principle of conservation of mass. The air mass flux F_x in the eastern direction crossing the vertical meridional face of a box is given by

$$F_x = \int\limits_{y_1}^{y_2} \int\limits_{z_1}^{z_2} \rho \, u \, dz \, dy \qquad (A.1)$$

where ρ denotes the density of air and u the wind component in eastward direction. The integration is performed over the vertical extent of the box from z_1 to z_2 and over the meridional extent from y_1 to y_2. Introducing reduced pressure (sigma) variables in the vertical leads to

$$F_x = -\frac{(p_s - p_t)}{g} \int\limits_{y_1}^{y_2} \int\limits_{\sigma_1}^{\sigma_2} u \, d\sigma \, dy \qquad (A.2)$$

where we use the hydrostatic approximation

$$\frac{dp}{dz} = -\rho g \qquad (A.3)$$

and the definition of σ

$$\sigma = \frac{p - p_t}{p_s - p_t} \qquad (A.4)$$

Here p_s denotes the surface pressure, p_t the pressure at the top of the atmosphere (we take $p_t = 10$ hPa) and g the acceleration of gravity. The mass fluxes in the meridional direction are given by an equation analogous to (A.2).

The wind fields and geopotential data of the GWE (ECMWF level III–b data) are available on a grid with 1.875° by 1.875° horizontal resolution and 15 pressure levels in the vertical dimension. They were produced by a four-dimensional data-assimilation system developed at the European Center for Medium Range Weather Forecasts [Bengtsson et al., 1982].

The calculation of the mass fluxes using equation (A.2) was performed as follows. First, the wind and geopotential data were reduced by a factor of 4 in order to make the data processing work manageable on our computer system. This was achieved by selecting only every other grid point in the longitudinal and the meridional direction. Secondly, at each grid location the surface pressure was determined by linear interpolation or extrapolation. The geopotential of the surface of the earth was thereby specified using the 1° by 1° Scripps topography [Gates and Nelson, 1973]. Thirdly, the vertical integral over σ in (A.2) was evaluated at each retained GWE grid location, using the trapezoidal rule. Finally the integral in the meridional direction was computed with the trapezoidal rule using linear interpolation in the zonal direction.

After obtaining the meridional and zonal mass fluxes, the average surface pressure in each box of the tracer model grid was calculated from the surface pressure values estimated at the GWE grid locations using bilinear interpolation.

Appendix B. Correction of the Wind Fields for Conservation of Mass

The continuity for air mass, expressed with σ coordinates in the vertical (see eq. A.4) requires that

$$\frac{\partial p_s}{\partial t} + \int\limits_0^1 \nabla \cdot (p_s - p_t)v \, d\sigma = 0 \qquad (B.1)$$

i.e., that the rate of change of the surface pressure matches the vertically integrated air mass convergence.

The mass flux fields as derived with the method described in Appendix A did not entirely conserve mass in the vertical air column. It was found that there existed on average a root mean square air mass imbalance of 4 percent per 12 hours (the time interval for which the GWE wind fields are available). A correction had to be added which was derived as follows.

Denoting by $\mathbf{F}$ the vertically integrated mass flux field

$$\mathbf{F} = g^{-1}(p_s - p_t) \int\limits_0^1 \mathbf{v} \, d\sigma \qquad (B.2)$$

and by M, the vertically integrated air mass per unit area

$$M = g^{-1}(p_s - p_t) \qquad (B.3)$$

equation (B.1) is reexpressed as

$$\frac{\partial M}{\partial t} = -\nabla \cdot \mathbf{F} \qquad (B.4)$$

We now set

$$\mathbf{F} = \mathbf{F}_{obs} + \mathbf{F}_{cor} \qquad (B.5)$$

where $\mathbf{F}_{obs}$ denotes the vertically integrated mass flux estimated from the GWE fields and $\mathbf{F}_{cor}$ denotes a correction to be found so that equation (B.4) is fulfilled. Inserting (B.5) into (B.4) we obtain an equation for $\mathbf{F}_{cor}$

$$\nabla \cdot \mathbf{F}_{cor} = -\nabla \cdot \mathbf{F}_{obs} - \frac{\partial M}{\partial t} \qquad (B.6)$$

Clearly $\mathbf{F}_{cor}$ should contain no rotational part, hence it may be expressed as the gradient of a scalar potential Θ

$$\mathbf{F}_{cor} = \nabla \Theta \qquad (B.7)$$

and equation (B.6) results in

$$\nabla^2 \Theta = -\nabla \cdot \mathbf{F}_{obs} - \frac{\partial M}{\partial t} \qquad (B.8)$$

This Poisson equation for Θ has to be solved on the sphere where the right hand side of (B.8) is calculated from the GWE data. The appropriate boundary conditions are that the meridional component of the gradient of Θ vanish at the poles and that Θ be periodic in the zonal (east-west) direction.

We solved the discrete version of equation (B.8) on the tracer model grid using two-dimensional discrete Fourier transforms and calculated the vertically integrated mass flux correction $\mathbf{F}_{cor}$ from equation (B.7). The correction was then distributed uniformly in the vertical.

Appendix C.   Estimation of Monthly Insolation

The monthly insolation, S, expressed in J m^{-2}, was used to compute the net primary production (NPP, see subsection 4.3.1). It was calculated from the daily insolation S_d, estimated with the following formula [Holtslag and Van Ulden, 1983]

$$S = \int_{t_1}^{t_2} (a_1 \sin(\phi(\lambda,\psi;t)) + a_2)(1 + b_1 N^{b_2}) dt \qquad (C.1)$$

Here t_1 and t_2 denote the time of sunrise and sunset at a specific location, respectively, $\phi(\lambda,\psi;t)$ the elevation of the sun, where λ denotes the longitude, ψ the latitude, and N the total cloud cover, expressed as a fraction between 0 and 1. The first factor of the integrand in (C.1) estimates the solar radiation (direct and diffuse) at the surface of the earth for clear sky conditions, and the second factor represents an attenuation factor owing to the presence of clouds. We use the following values for the four empirical parameters that appear in equation (C.1) [Holtslag and Van Ulden, 1983]

$$a_1 = 90 \text{ W m}^{-2}$$
$$a_2 = 30 \text{ W m}^{-2}$$
$$b_1 = 0.75$$
$$b_2 = .4$$

The solar elevation ϕ, which is a function of longitude, λ, latitude, ψ, and time, t, is computed using astronomical formulas.

No global cloud cover data with appropriate seasonal and geographical resolution were readily available. However, we had access to daily albedo data, obtained from the visible channel of the AVHRR instrument on the TIROS–N satellite in 1979 [Gruber and Krueger, 1984]. In order to estimate N from these data we used the following simple albedo model.

The atmosphere is divided into three layers as shown schematically in Figure C.1. The middle layer consists of a cloud deck with a fractional extent that we equate to the total cloud cover fraction, N. The clouds are assumed to possess a uniform reflectivity r_c but no absorptivity. Hence reflectivity, ρ_2, and transmissivity, τ_2, of the middle layer are given by
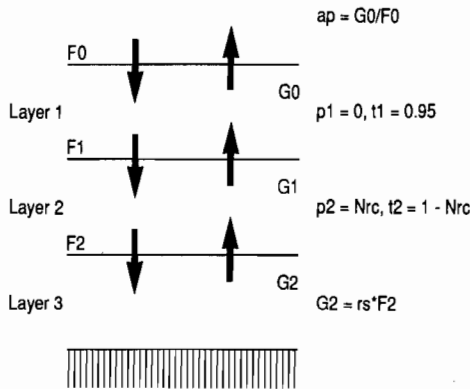

Fig. C.1. Schematic structure of the 3-layer albedo model used to estimate fractional cloud cover from observed satellite albedo data. The symbols are explained in the text. The equations pertain to the specific layers where they appear in the figure.

$$\rho_2 = N r_c \qquad (C.2)$$
$$\tau_2 = 1 - N r_c \qquad (C.3)$$

The layer above the cloud is assumed to possess a transmissivity τ_1 but no reflectivity. The optical properties of layer 3, located below the cloud deck, and of the surface are combined into the single effective reflectivity r_s^*. We use a two-stream approximation of the radiative transfer, thereby denoting the downward fluxes of radiation by F and the upward fluxes by G.

The fluxes (F_{i-1}, G_{i-1}) at the top of layer i are related to the fluxes (F_i, G_i) at the bottom of the layer by the matrix equation

$$\begin{bmatrix} F_{i-1} \\ G_{i-1} \end{bmatrix} = \frac{1}{\tau_i} \begin{bmatrix} 1 & -\rho_i \\ \rho_i & \tau_i^2 - \rho_i^2 \end{bmatrix} \begin{bmatrix} F_i \\ G_i \end{bmatrix} \qquad (C.4)$$

where τ_i denotes the transmissivity and ρ_i the reflectivity of the layer.

The albedo a_p as measured by the radiometer of the satellite, is defined as the ratio of the fluxes at the top of the atmosphere, F_0 and G_0

$$a_p = \frac{G_0}{F_0} \qquad (C.5)$$

Using equation (C.4) for the first and the second layer, thereby inserting the appropriate reflectivities and transmissivities as indicated in Figure C.1, we reexpress the albedo as

$$a_p = \tau_1^2 \left[\frac{\rho_2 + r_s^* - 2\rho_2 r_s^*}{1 - \rho_2 r_s^*} \right] \qquad (C.6)$$

This equation is solved for ρ_2, thus expressing the cloud fraction N as a function of the albedo, a_p, and the effective reflectivity r_s^*, of the combined layer 3 and the surface.

Daily albedo measurements were available on a global mercator array with a resolution of 2.5° by 2.5° latitude and longitude. By linear interpolation we remapped these data onto a 4° by 5° grid which was aligned parallel to the grid of the transport model.

At each location the monthly minimal value of a_p was selected and assumed to represent almost cloud free conditions in the area. Thus by setting ρ_2 equal to zero in equation (C.6), we computed r_s^*. This latter quantity was then assumed to remain constant during the whole month at the particular location, which allows the calculation of ρ_2 and hence N for each day of the month. Subsequently the monthly average of the daily attenuation factor was computed and, using equation (C.1), we evaluated the monthly average of the daily insolation, thereby averaging the contributions from the four grid points of the 4° by 5° grid lying within each 8° by 10° grid square of the transport model.

As an example, Figure C.2 shows isolines of the global radiation at the surface for the month of June as estimated by the procedure outlined above. Figure C.2 may be compared with a map of the same quantity published by Raschke and Preuss [1979, Figure 4] obtained for the month of June 1969 from radiometer data of the Nimbus 3 satellite. Both fields agree well in terms of their structure, but our values appear to be systematically larger by about 20 percent. Two reasons may explain this discrepancy. Firstly, it is well known that air- and space-borne cloud detection methods usually result in lower cloud amounts than recorded by ground observers, primarily because of different viewing geometry

June Global Radiation
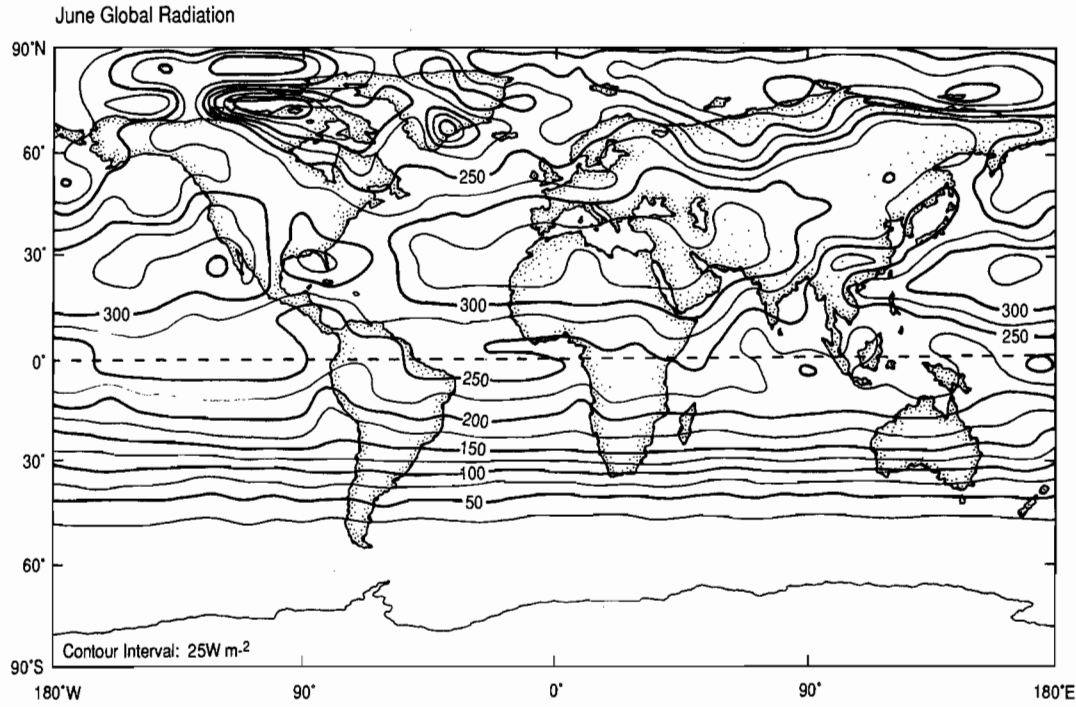
Fig. C.2. Estimated global radiation (in Wm^{-2}) at the surface of the earth for the month of June.

[Hughes, 1984]. Indeed, a comparison of our zonal mean cloud cover fraction with the climatology based on ground measurements by Berlyand and Strokina [see Hughes, 1984] shows that our data are systematically lower by about 20 percent. A similar finding has been reported by Raschke and Preuss [1979]. The empirical constants in the cloud attenuation factor of equation (C.1) were determined using ground based values of cloud cover [Kasten and Czeplack, 1980]. Therefore the use of equation (C.1) with cloud cover fractions derived from satellite data is not entirely consistent. Secondly, our method very likely tends to underestimate cloud cover because of the error prone assumption that the monthly minimal albedo represents cloudfree conditions.

Appendix D. Fit of the Respiratory Flux to the Observations

The following derivation explains the method used in fitting the respiration component to the observed concentrations at the four key stations. The observations $C_{obs}(\mathbf{x}_j, t)$, after subtraction of the long-term trend are given by a finite harmonic series of order m (we used $m = 4$)

$$C_{obs}(\mathbf{x}_j, t) = \sum_{k=1}^{m} [a_k(\mathbf{x}_j) \sin \omega_k t + b_k(\mathbf{x}_j) \cos \omega_k t] \quad (D.1)$$

where $\mathbf{x}_j$ stands for the location of station j ($j = 1,..., l$; we used four stations, hence $l = 4$), t denotes time in years, ω_k denotes the angular velocity ($= 2 k \pi$), and m denotes the number of harmonics. A similar representation holds for each of the i different model components ($i = 1,..., n$; we used nine components, hence $n = 9$)

$$C_i(\mathbf{x}_j, t) = \sum_{k=1}^{m} [a_{ik}(\mathbf{x}_j) \sin \omega_k t + b_{ik}(\mathbf{x}_j) \cos \omega_k t] \quad (D.2)$$

In general the linear combination of the first r of these components C_i are to be fit to the observations, C_{obs}. (In practice we fitted only 1 component, hence $r = 1$). Firstly, we subtract the contributions of the fixed components $i = r + 1, \ldots, n$ from the observations by defining:

$$C^*(\mathbf{x}_j, t) = C_{obs}(\mathbf{x}_j, t) - \sum_{i=r+1}^{n} C_i(\mathbf{x}_j, t) \quad (D.3)$$

Secondly we find the coefficients λ_i, $i = 1,...,r$ by minimizing the quantity S^2:

$$S^2 = \sum_{j=1}^{l} \int_0^T \left[C^*(\mathbf{x}_j, t) - \sum_{i=1}^{r} \lambda_i C_i(\mathbf{x}_j, t) \right]^2 dt \quad (D.4)$$

The time integral is taken over the base period of 1 year, i.e., $T = 1$. Upon inserting (D.1), (D.2) and (D.3) into (D.4) we obtain:

$$S^2 = \frac{T}{2} \sum_{j=1}^{l} \sum_{k=1}^{m} \left[\left[a_k^*(\mathbf{x}_j) - \sum_{i=1}^{r} \lambda_i a_{ik}(\mathbf{x}_j) \right]^2 + \left[b_k^*(\mathbf{x}_j) - \sum_{i=1}^{r} \lambda_i b_{ik}(\mathbf{x}_j) \right]^2 \right] \quad (D.5)$$

Here we have used the orthogonality of the harmonic functions i.e.,

$$\int_0^T \sin \omega_k t \, \sin \omega_{k'} t \, dt = \frac{T}{2} \delta_{kk'} \quad (D.6)$$

$$\int_0^T \cos\omega_k t \cos\omega_{k'} t \, dt = \frac{T}{2}\delta_{kk'} \qquad (D.7)$$

where $\delta_{kk'}$ is equal to 1 if $k = k'$ and otherwise is equal to zero.

$$\int_0^T \sin\omega_k t \cos\omega_{k'} t \, dt = 0 \qquad (D.8)$$

Equation (D.5) corresponds to the standard multiple linear regression problem where the coefficients λ_i are to be found such that S^2 attains a minimum. The adjusted observations are the $m \cdot l$ harmonic coefficients $a_k^*(\mathbf{x}_j)$ and $b_k^*(\mathbf{x}_j)$ and the components that are fitted are the harmonic coefficients $a_{ik}(\mathbf{x}_j)$ and $b_{ik}(\mathbf{x}_j)$ of the model components $i = 1,...,r$. Since estimates of the standard deviation ($\sigma_{kja}, \sigma_{kjb}$) of the observed harmonic coefficients at each station are available, appropriate weights are introduced by multiplying each squared term in expression (D.5) by σ_{kja}^{-2} and σ_{kjb}^{-2}, respectively.

Appendix E. Construction of the Model Source Components of Biospheric Destruction and Fertilization

Here we amplify the short discussions in subsections 4.3.3 and 4.3.4 of the main text regarding how these two nonseasonal components were established from available information. The constructions were made more complicated by the use of various unpublished updates of information that we obtained from other investigators.

We originally obtained estimates of terrestrial biospheric destruction for selected geographic regions from R. A. Houghton by private communication. These estimates reflected work in progress

TABLE E.1. Net flux of carbon in 1980 (in 10^9 kgC yr^{-1}) from land-use changes and deforestation

Region	Code No.	Net Flux	Notes
USA and Canada	1	24	1
Europe	2	−28	2
USSR			
West	3	0	2
East	4	35	2
Japan and Korea	5	−3	2
China	6	69	2
North Africa and Middle East	7	7	2
Australia and New Zealand	8	28	2
Tropical America	9	665	3
Tropical Africa	10	373	3
Tropical Asia			
Indian subcontinent	11	45	4
Southeast Asia	12	576	5
Total		1791	

Notes
1. From Table 1 of Houghton et al. [1987], reduced by 1×10^9 kg to achieve a global total of 1791×10^9 kg
2. Copied directly from Table 1 of loc. cit.
3. Copied directly from Table 4 of loc. cit.
4. Sum of fluxes for Bangladesh, Bhutan, India, Nepal, Pakistan, and Sri Lanka as listed in Table 4 of loc. cit.
5. Sum of fluxes for the remaining countries listed as tropical Asia in Table 4 of loc. cit.
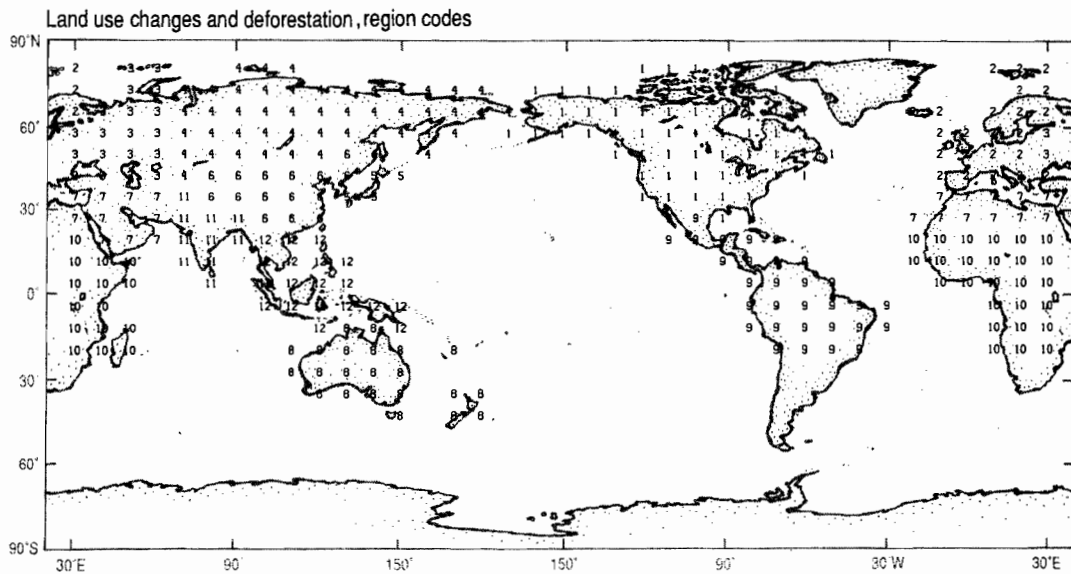

Fig. E.1. Grid locations of twelve regions for which the CO$_2$ flux from land-use changes and deforestation were calculated. The numbers identify the regions according to the code numbers listed in Table E.1. Numbers placed over water refer only to the land portion of the respective grid locations.

which later resulted in the publication by Houghton et al. [1987]. The global estimate of destruction by Houghton et al. [1987] was 1×10^9 kg of carbon higher than an earlier unpublished estimate by Houghton which Keeling et al. [this volume, a] used as an input to the box diffusion model. Since the results of this compartment model define the global source strengths of many of the three-dimensional model source components, and we did not wish to readjust these components to reflect a negligible change in the global total of destruction, we have retained the earlier estimate by making a minor adjustment to the published data, as indicated in Table E.1. The model grid locations that we assigned for each region are shown in Figure E.1.

Within each region the source component for destruction is distributed in proportion to net primary productivity (NPP) on an annual basis, from monthly averages of NPP obtained in the manner described in subsection 4.3.1. For two regions, tropical Africa and tropical South America, the distributions initially were made over all of both continents, not just the tropical portions. Because this broadened distribution has only a very minor impact on the predicted seasonal cycle of atmospheric CO_2, Heimann et al. [this volume] have retained model outputs calculated with this broader distribution, whereas Keeling et al. [this volume, b] use the more correct distribution, shown in Figure 13, to investigate the mean annual fields of atmospheric CO_2.

Annual averages of NPP, used in establishing the distributions of both biospheric destruction and fertilization, were derived from monthly averages of the normalized difference vegetative index (NDVI). We received several versions of these indices [C. J. Tucker, private communication] reflecting updates of remote sensing data carried out by the National Aeronautic and Space Administration (NASA). By an oversight, different versions of the indices were initially used to compute monthly averaged NPP (for component F_{NPP}) and annual NPP as a basis for distributing biospheric destruction and fertilization (components, F_{DES} and F_{FER}). The two versions differ only slightly: the former predicts that 36.4 percent of the annual flux occurs in the southern hemisphere, the latter 37.3 percent. Since the influence of substituting between these differing versions of NDVI is negligible when computing the seasonal cycle of atmospheric CO_2 produced by destruction and fertilization, Heimann et al. [this volume] have retained the initially computed results for these source components, whereas Keeling et al. [this volume, b] employ the former version for all components, as summarized in Figures 12, 13, and 14 and in Table 5.

References

Alexander, R. C., and Mobley, R. L., Monthly average sea surface temperatures and ice pack limits on a 1 deg global grid, *Monthly Weather Review*, v. 104, p. 143–148, 1976.

Asrar, G., Fuchs, M., Kanemasu, E. T., and Hatfield, J. L., Estimating absorbed photosynthetic radiation and leaf area index from spectral reflectance in wheat, *Agronomy Journal*, v. 76, p. 300–306, 1984.

Bacastow, R. B., and Björkström, A., Comparison of Ocean Models, in *SCOPE 16: Carbon Cycle Modelling*, edited by B. Bolin, p. 29–79, John Wiley and Sons, Chichester, 1981.

Baes, C. F., Jr., Effects of ocean chemistry and biology on atmospheric carbon dioxide, in *Carbon Dioxide Review: 1982*, edited by W. C. Clark, p. 189–204, Oxford University Press, 1982.

Bengtsson, L., Kanamitsu, M., Kallberg, P., and Uppala, S., FGGE 4-dimensional data assimilation at ECMWF. *American Meteorological Society Bulletin*, v. 63, p. 29–43, 1982.

Bolin B., Keeling, C. D., Bacastow, R. B., Björkström, A., and Siegenthaler, U., Carbon cycle modelling, in *SCOPE 16: Carbon Cycle Modelling*, edited by B. Bolin, p. 1–28, John Wiley and Sons, Chichester, 1981.

Broecker W. S., and Peng, T. -H., *Tracers in the Sea*, 690 p., Eldigio Press, Columbia University, New York, 1982.

de Boor, C., *A Practical Guide to Splines*, 392 p., Springer, New York, 1978.

Dörr, H., and Münnich, K. O., Annual variation in soil respiration in selected areas of the temperate zone, *Tellus*, v. 39B, p. 114–121, 1987.

Fogg, G. E., Primary productivity, in *Chemical Oceanography*, edited by J. P. Riley and G. Skirrow, 2nd Edition, v. 2, p. 385–453, Academic Press, London, 1975.

Fung, I. Y., Analysis of the seasonal and geographic patterns of atmospheric CO_2 distributions with a three-dimensional model, in *The Changing Carbon Cycle: A Global Analysis*, edited by J. R. Trabalka and D. E. Reichle, p. 459–473, Springer-Verlag, New York, 1986.

Fung, I., Prentice, K., Matthews, E., Lerner, J., and Russell, G., Three-dimensional tracer model study of atmospheric CO_2: Response to seasonal exchanges with the terrestrial biosphere, *Journal of Geophysical Research*, v. 88, p. 1281–1294, 1983.

Fung, I. Y., Tucker, C. J., and Prentice, K. C., Application of advanced very high resolution radiometer vegetation index to study atmosphere-biosphere exchange of CO_2, *Journal of Geophysical Research*, v. 92, p. 2999-3015, 1987.

Gates, W. L., and Nelson, A. B., A new (revised) tabulation of the Scripps topography on a 1° global grid. Part I: Terrain heights,

Report R–1276–1–ARPA, 132 p., Rand Corporation, 1700 Main Street, Santa Monica, CA, 40406, 1975.

Gillette, D. A., and Box, E. O., Modeling seasonal changes of atmospheric carbon dioxide and carbon 13, *Journal of Geophysical Research,* v. 91, p. 5287–5304, 1986.

Gruber, A., and Krueger, A. F., The status of the NOAA outgoing longwave radiation data set, *Bulletin American Meteorological Society,* v. 65, p. 958–962, 1984.

Gruber, A., Ruff, I., and Earnest, C., Determination of the planetary radiation budget from TIROS-N satellites, *NOAA Technical Report NESDIS 3,* 12 p., U.S. Department of Commerce, NOAA/NESDIS, Washington, DC, 1983.

Hansen, J., Russell, G., Rind, D., Stone, P., Lacis, A., Lebedeff, S., Ruedy, R., and Travis, L., Efficient three-dimensional global models for climate studies: Models I and II, *Monthly Weather Review,* v. 111, p. 609–662, 1983.

Hayes, L., The current use of TIROS-N series of meteorological satellites for land-cover studies, *International Journal of Remote Sensing,* v. 6, p. 35–45, 1985.

Heimann, M., Keeling, C. D., and Fung, I. Y., Simulating the atmospheric carbon dioxide distribution with a three-dimensional tracer model, in *The Changing Carbon Cycle: A Global Analysis* edited by J. R. Trabalka and D. E. Reichle, p. 16–49, Springer-Verlag, New York, 1986.

Heimann, M., Keeling, C. D., and Tucker, C. J., A three-dimensional model of atmospheric CO$_2$ transport based on observed winds: 3. Seasonal cycle and synoptic time scale variations, in *Aspects of Climate Variability in the Pacific and the Western Americas,* edited by D. H. Peterson, this volume, American Geophysical Union, Washington, DC, 1989.

Hollingsworth, A., Lorenc, A. C., Tracton, M. S., Arpe, K., Cats, G., Uppala, S., and Kallberg, P., The response of numerical weather prediction systems to FGGE II-B data. Part I: Analyses. *Quarterly Journal of the Royal Meteorological Society,* v. 111, p. 1–66, 1985.

Holton, J., *An Introduction to Dynamic Meteorology,* 391 p., Academic Press, New York, 1979.

Holtslag, A. A. M., and Van Ulden, A. P., A simple scheme for daytime estimates of the surface fluxes from routine weather data, *Journal of Climate and Applied Meteorology,* v. 22, p. 517–529, 1983.

Houghton, R. A., Hobbie, J. E., Melillo, J. M., Moore, B., Peterson, B. J., Shaver, G. R., and Woodwell, G. M., Changes in the carbon content of terrestrial biota and soils between 1860 and 1980: A net release of CO$_2$ to the atmosphere, *Ecological Monographs,* v. 53, p. 235–262, 1983.

Houghton, R. A., Boone, R. D., Fruci, J. R., Hobbie, J. E., Melillo, J. M., Palm, C. A., Peterson, B. J., Shaver, G. R., Woodwell, G. M., Moore, B., Skole, D. L., and Myers, N., The flux of carbon from terrestrial ecosystems to the atmosphere in 1980 due to changes in land use: Geographic distribution of the global flux, *Tellus,* v. 39B, p. 122–139, 1987.

Hughes, N. A., Global cloud climatologies: A historical review, *Journal of Climate and Applied Meteorology,* v. 23, p. 724–751, 1984.

Jacob, D. J., Prather, M. J., Wofsy, S.C., and McElroy, M. B., Atmospheric distribution of [85]Kr simulated with a general circulation model, *Journal of Geophysical Research,* v. 92, p. 6614–6626, 1987.

Julian, P. R., Comments on the ECMWF IIIb analysis data set. *GWE Newsletter No. 1,* 15–17, 1983.

Justice, C. O., Townshend, J. R. G., Holben, B. N., and Tucker, C. J., Analysis of the phenology of global vegetation using meteorological satellite data, *International Journal of Remote Sensing,* v. 6, p. 1271–1318, 1985.

Kamber, D., Modellierung der Variationen von CO$_2$ und $\delta^{13}C$ in Nord- und Suedhemisphaere, Diploma Thesis, 64 p., University of Bern, Switzerland, 1980.

Kasten, F., and Czeplak, G., Solar and terrestrial radiation dependent on the amount and type of cloud, *Solar Energy,* v. 24, p. 177–189, 1980.

Keeling, C.D., Carbon dioxide in surface ocean waters: 4. Global distribution, *Journal of Geophysical Research,* v. 73, p. 4543–4553, 1968.

Keeling, C. D., The Suess effect: [13]Carbon – [14]Carbon Interrelations, *Environment International,* v. 2, p. 229–300, 1979.

Keeling, C. D., and Heimann, M., Meridional eddy diffusion model of the transport of atmospheric carbon dioxide: 2. Mean annual carbon cycle. *Journal of Geophysical Research,* v. 91, p. 7782–7796, 1986.

Keeling, C. D., Harris, T. B. and Wilkins, E. M., Concentration of atmospheric carbon dioxide at 500 and 700 millibars. *Journal of Geophysical Research,* v. 73, 4511–4528, 1986.

Keeling, C. D., Bacastow, R. B., Carter, A. F., Piper, S. C., Whorf, T. P., Heimann, M., Mook, W. G., and Roeloffzen, H., A three-dimensional model of atmospheric CO$_2$ transport based on observed winds: 1. Analysis of observational data, in *Aspects of Climate Variability in the Pacific and the Western Americas,* edited by D. H. Peterson, this volume, American Geophysical Union, Washington, DC, 1989a.

Keeling, C. D., Piper, S. C., and Heimann, M., A three-dimensional model of atmospheric CO$_2$ transport based on observed winds: 4. Mean annual gradients and interannual variations, in *Aspects of Climate Variability in the Pacific and the Western Americas,* edited by D. H. Peterson, this volume, American Geophysical Union, Washington, DC, 1989b.

Kroopnick, P. M., Margolis, S. V., and Wong, C. S., $\delta^{13}C$ Variations in marine carbonate sediments as indicators of the CO$_2$ balance between the atmosphere and oceans, in *The Fate of Fossil Fuel CO$_2$ in the Oceans,* edited by N. R. Andersen and A. Malahoff, p. 295–321, Plenum Press, New York, 1977.

Kumar, M., and Monteith, J. L., Remote sensing of crop growth, in *Plants and the Daylight Spectrum,* edited by H. Smith, p. 133–144, Academic Press, New York, 1981.

Lambert, S. J., List of known or suspected problems with the ECMWF analyses of FGGE data. *GWE Newsletter No. 1,* 15, 1983.

Lieth, H., and Whittaker, R. H., *Primary Productivity of the Biosphere,* 339 p., Springer-Verlag, New York, 1975.

Liu, S. C., McAfee, J. R., and Cicerone, R. J., Radon 222 and tropospheric vertical transport, *Journal of Geophysical Research,* v. 89, p. 7291–7297, 1984.

Maier-Reimer, E., and Hasselmann, K. Transport and storage in the ocean – An inorganic ocean-circulation carbon cycle model, *Climate Dynamics 2,* 63–90, 1987.

Marland, G., Rotty, R. M., and Treat, N. L., CO$_2$ from fossil fuel burning: Global distribution of emissions, *Tellus,* v. 37B, p. 243–258, 1985.

Matthews, E., Global vegetation and land use: New high-resolution data bases for climate studies, *Journal of Climate and Applied Meteorology*, v. 22, p. 474–487, 1983.

Monteith, J. L., Climate and the efficiency of crop production in Britain, *Royal Society of London, Philosophical Transaction, Series B*, v. 281, p. 277–294, 1977.

Mook, W. G., and Grootes, P. M., A measuring procedure and corrections for the high precision mass spectrometric analysis of the stable isotopes of carbon, nitrogen and oxygen, *International Journal of Mass Spectrometry and Ion Processes*, v. 12, p. 273–298, 1973.

Mook, W. G., Bommerson, J. C., and Staverman, W. H., Carbon isotope fractionation between dissolved bicarbonate and gaseous carbon dioxide, *Earth and Planetary Science Letters*, v. 22, p. 169–176, 1974.

Pearman, G. I., and Hyson, P., Global transport and inter-reservoir exchange of carbon dioxide with particular reference to stable isotopic distributions, *Journal of Atmospheric Chemistry*, v. 4, p. 81–124, 1986.

Peng, T.-H., Takahashi, T., Broecker, W. S., and Olafsson, J., Seasonal variability of carbon dioxide, nutrients and oxygen in the northern North Atlantic surface water: Observations and a model, *Tellus*, v. 39B, p. 439–458, 1987.

Prather, M. J., McElroy, M. B., Wofsy, S. C., Russel, G., and Rind, D., Chemistry of the global troposphere: fluorocarbons as tracers of air motion, *Journal of Geophysical Research*, v. 91, p. 6671–6681, 1987.

Raschke, E., and Preuss, H. J., The determination of the solar radiation budget at the earth's surface from satellite measurements, *Meteorologische Rundschau*, v. 32, p. 18–28, 1979.

Rath, H. K., Simulation der globalen ^{85}Kr und ^{14}CO$_2$ Verteilung mit Hilfe eines zeitabhängigen zweidimensionalen Modelles der Atmosphäre, Thesis, University of Heidelberg, 1988.

Rotty, R. M., A look at 1983 CO2 emissions from fossil fuels, *Tellus*, v. 39B, p. 203–208, 1987a.

Rotty, R. M., Estimates of seasonal variation in fossil fuel CO$_2$ emissions, *Tellus*, v. 39B, p. 184–202, 1987b.

Russell, G. L., and Lerner, J. A., A new finite-differencing scheme for the tracer transport equation, *Journal of Applied Meteorology*, v. 20, p. 1483–1498, 1981.

SCEP (Study of Critical Environmental Problems), *Man's Impact on the Global Environment*, Carroll L. Wilson, SCEP Director, 819 p., MIT Press, Cambridge, MA, 1970.

Sellers, P. J., Canopy reflectance, photosynthesis and transpiration, *International Journal of Remote Sensing*, v. 6, p. 1335–1372, 1985.

Siegenthaler, U., Uptake of excess CO$_2$ by an outcrop-diffusion model of the ocean, *Journal of Geophysical Research*, v. 88, p. 3599–3608, 1983.

Siegenthaler, U., and Münnich, K. O., ^{13}C/^{12}C fractionation during CO$_2$ transfer from air to sea, in *SCOPE 16: Carbon Cycle Modelling*, edited by B. Bolin, p. 249–258, John Wiley and Sons, Chichester, 1981.

Takahashi, T., Chipman, D., and Volk, T., Geographical, seasonal and secular variations of the partial pressure of CO$_2$ in surface waters of the North Atlantic Ocean: The results of the North Atlantic TTO program, in *Proceedings: Carbon Dioxide Research Conference: Carbon Dioxide, Science, and Consensus*, p. II.123–II.145, U.S. Department of Energy,

CONF–820970, available from National Technical Information Service, Springfield, VA, U.S.A., 1983.

Takahashi, T., Olafsson, J., Broecker, W. S., Goddard, J., Chipman, D. W., and White, J., Seasonal variability of the carbon-nutrient chemistry in the ocean areas west and north of Iceland, *Rit Fiskideildar*, v. 9, p. 20–36, 1985.

Takahashi, T., Goddard, J., Sutherland, S. C., Chipman, D. W., and Breeze, C. C., Seasonal and geographic variability of carbon dioxide sink/source in the oceanic areas: Observations in the north and equatorial Pacific Ocean, 1984–1986 and global summary, *Final Technical Report for MM 19X–89675C*, 66 p., Lamont-Doherty Geological Observatory, Palisades, NY, 1986.

Takahashi, T., Goddard, J., Sutherland, S. C., Mathieu, G., and Chipman, D. W., Assessment of carbon dioxide sink/source in the north Pacific Ocean: Seasonal, and geographic variability, 1986–1987, *Progress Report for Contract 19X–89675C*, 66 p., Lamont-Doherty Geological Observatory, Palisades, NY, 1988.

Tans, P., Carbon 13 and carbon 14 in trees and the atmospheric CO$_2$ increase, PhD Thesis, 99 p., University of Groningen, The Netherlands, 1978.

Tans, P., ^{13}C/^{12}C of industrial CO$_2$, in *SCOPE 16: Carbon Cycle Modelling*, edited by B. Bolin, p. 127–129, John Wiley and Sons, Chichester, 1981.

Tarpley, J. D., Schneider, S. R., and Money, R. L., Global vegetation indices from the NOAA-7 meteorological satellite, *Journal of Climate and Applied Meteorology*, v. 23, p. 491–494, 1984.

Trenberth, K. E., Interannual variability of the Southern Hemisphere circulation: Representativeness of the year of the Global Weather Experiment, *Monthly Weather Review*, v. 112, p. 108–123, 1984.

Trenberth, K. E., The role of eddies in maintaining the Westerlies in the Southern Hemisphere winter. *Journal of Atmospheric Science*, v. 44, 1498–1508, 1987.

Trenberth, K. E., ECMWF global analyses 1979–1986: Circulation statistics and data evaluation. National Center of Atmospheric Research Technical Note NCAR/TN–300+STR, 94 pp., 1988.

Tucker, C. J., Townshend, J. R. G., and Goff, T. E., African land-cover classification using satellite data, *Science*, v. 227, p. 369–375, 1985.

Turekian, K. K., Nozaki, Y., and Benninger, L. K., Geochemistry of atmospheric radon and radon products. *Annual Review of Earth and Planetary Sciences*, v. 5, 227 p., 1977.

von Arx, W. S., *An Introduction to Physical Oceanography*, 422 p., Addison-Wesley Publishing Company, Reading, MA, 1974.

von Hippel, F., and Levi, B. G., Controlling the source, *Report PU/CEES 167*, 38 p., Princeton University 1984.

Weast, R. C., (Editor-in-chief), *Handbook of Chemistry and Physics*, 47th Edition, p. 34–55, Chemical Rubber Co., Cleveland, 1966.

Weiss, R. F., Carbon dioxide in water and sea water: The solubility of a non-ideal gas, *Marine Chemistry*, v. 2, p. 203–215, 1974.

Weiss, R. F., Jahnke, R. A., and Keeling, C. D., Seasonal effects of temperature and salinity on the partial pressure of CO$_2$ in seawater, *Nature*, v. 300, p. 511–513, 1982.

Weiss, W., Sittkus, A., Stockburger, H., and Sartorius, H., Large-scale atmospheric mixing derived from meridional profiles of krypton 85, *Journal of Geophysical Research*, v. 88, p. 8574–8578, 1983.